1 Magmatic evolution of the Campi Flegrei and Procida

2 Volcanic Fields, Italy, based on interpretation of data

3 from well-constrained melt inclusions

- 4 Rosario Esposito¹, Kimberly Badescu¹, Matthew Steele-MacInnis², Claudia Cannatelli³,
- 5 Benedetto De Vivo⁴, Annamaria Lima⁵, Robert J. Bodnar⁶, Craig E. Manning¹
- Department of Earth, Planetary and Space Science, UCLA, Los Angeles, CA
 90095-1567 USA email: r.esposito@epss.edu.edu
- 2 Department of Earth and Atmospheric Sciences, University of Alberta,
 Edmonton, Alberta Canada T6G 2E3
- 3Department of Geology and Andean Geothermal Center of Excellence (CEGA),
 Universidad de Chile, Santiago, Chile
- Università telematica Pegaso, Piazza Trieste e Trento 48, 80132 Napoli &
 Benecon Scarl, Via S. Maria di Costantinopoli 104, 80138, Napoli
 - ⁵Dipartimento di Scienze della Terra, delle Risorse e dell'Ambiente, Università di Napoli Federico II, *Via Cintia snc, 80126 Napoli, Italy*
- ⁶Fluids Research Laboratory, Department of Geosciences, Virginia Tech,
 Blacksburg, VA 24061 USA

Abstract

One of the main goals of studying melt inclusions (MI) is to constrain the pre-eruptive physical and chemical processes that have occurred in a magma reservoir at the micro-scale. Recently, several studies that focused on magmatic differentiation of volcanic systems produced detailed interpretations based on data from MI trapped at different times and locations in the plumbing system. Ideally, MI data should be collected and tested following the melt inclusion assemblage (MIA) protocol that consists of studying and analyzing groups of MI that were trapped at the same time, and, thus, at the same chemical and physical conditions. However, the rarity of MIA in juvenile volcanic phenocrysts precludes this methodology in many cases, leading to uncertainty concerning the validity of the MI as recorders of pre-eruptive conditions.

In this study, we focused on MI from the Campi Flegrei (CF) and Procida Island (PI) volcanic systems in southern Italy, including data from this study and data from the literature. The database included MI hosted in sanidine, clinopyroxene, plagioclase, biotite and olivine, and, thus, represents melts trapped at various stages in the overall differentiation process. We developed a protocol to select the most reliable MI from a dataset associated with a single magmatic system. As a first step we compare MI data with bulk rock data for the same magmatic system. This comparison reveals that most MI show major element compositions that fall within or close to the range for bulk rocks — these MI are considered to be "normal". Some MI show anomalous compositions and are not representative of the melt in equilibrium with the phenocryst host and were excluded from the data set. In the second step we selected only bubble-free MI from the previously identified "normal" MI to interpret the volatile evolution. In the third step we compare compositions of the "normal" bubble-free MI to compositions predicted by rhyolite-MELTS simulations, assuming a variety of initial conditions.

Comparison of data obtained from basaltic-trachybasaltic MI with rhyolite-MELTS predictions indicates that one group of MI records the geochemical evolution of a volatile-saturated magma differentiating by polybaric fractional crystallization from \geq 200 MPa (\geq 7.5 km) to 30 MPa (\sim 1 km). Another group of MI records recharge of the magma chamber by a primitive basaltic magma that mixes with the preexisting primitive trachybasaltic magma before eruption. Extensive isobaric crystallization of the trachybasaltic magmas at \sim 7.5 km beneath CF may have generated trachytic-phonolitic magmas, such as those associated with the Neapolitan Yellow Tuff (NYT) that is characterized by a relatively high H₂O content. These volatile-saturated trachytic-phonolitic magmas likely trigger high-magnitude eruptions during their ascent to the surface.

Keywords: melt inclusion, volatiles, Phlegrean Fields, degassing path, rhyolite-MELTS

Introduction

Campi Flegrei (CF) and the Island of Procida (IP) are well known recently active volcanic complexes in the Campanian Plain of southern Italy that represent a volcanic hazard owing to their proximity to Naples and the towns surrounding Pozzuoli Bay (~1.5 million inhabitants). The area has been the site of volcanic activity for more than 60 ka (De Vivo et al., 2010; Orsi et al., 1999; Pappalardo et al., 1999). The most catastrophic eruption at CF is the Campanian Ignimbrite (e.g., Orsi et al., 1996), generating 300 km³ dense rock equivalent [DRE; (Fedele et al., 2007)], the source of which remains under debate (De Vivo et al., 2010; De Vivo et al., 2001; Rolandi et al., 2003). The later eruption of the Neapolitan Yellow Tuff (NYT) was extremely explosive and generated 40 km³ DRE of eruptive products (Orsi et al., 1992; Wohletz et al., 1995). The most recent eruption occurred in 1538 and formed the Monte Nuovo cinder cone volcano (Fig. 1).

The CF area has in recent decades attracted the interest of geoscientists owing to activity that consists of episodic slow ground uplift, followed by more rapid deflation (bradyseism). In recent years, the ground in the central part of the CF has been inflating, highlighting the critical need for understanding whether this activity is a precursor of an imminent eruption (e.g., Chiodini et al., 2015). Ground deformation and seismicity at CF are also associated with intense fumarolic and hydrothermal activity, concentrated mostly in the crater of Solfatara at Pozzuoli (Fig. 1). The relatively slow ground uplift may or may not represent a precursor of a volcanic eruption, depending on the cause of the inflation (Bodnar et al., 2007; Lima et al., 2009; Moretti et al., 2017). Though various models have been proposed to explain bradyseism at CF, it is now becoming clear that magmatic fluids released from deep and/or shallow magmas play an important role in ground movement, and the occurrence of ground movement does not require that a new batch of magma is intruding below CF (Lima et al., 2009; Lima et al., 2017).

The composition of exsolved magmatic fluids injected into the overlying hydrothermal system is controlled by the chemical evolution of volatiles during magma evolution (crystallization, mixing, and crustal assimilation). The compositions of MI hosted in olivine from CF and IP suggest that trachybasaltic parental magmas are the source of activity in both areas (Cannatelli et al., 2007; Mangiacapra et al., 2008; Mormone et al., 2011; Esposito et al., 2011). However, the isotopic compositions of

mafic bulk rocks suggest that the two areas experienced different magma evolution histories (e.g., Cannatelli, 2012; D'Antonio et al., 2007; Peccerillo, 2017 and references therein). While major and trace element trends in both localities are dominantly controlled by fractional crystallization, the variability of some elements such as potassium, the isotopic signature of the bulk rocks, and the composition and zoning of juvenile mineral phases combined suggest that other open-system magmatic processes also contributed to observed geochemical trends. The geochemical variability, evolution, and the importance of open-system processes associated with the generation and the differentiation of these magmas continue to be debated (Peccerillo, 2017 and references therein).

The pre-eruptive volatile contents of magmas associated with CF and IP have been studied by many workers by analyzing the glass of melt inclusions (MI) (Arienzo et al., 2016; Arienzo et al., 2010; Cannatelli et al., 2007; Cecchetti et al., 2001; Cecchetti et al., 2002-2003; Cipriani et al., 2008; Esposito et al., 2011; Fourmentraux et al., 2012; Mangiacapra et al., 2008; Mormone et al., 2011; Roach, 2005; Stock et al., 2016). MI provide information that is not easily obtained by studying bulk rocks or active fumaroles. MI often preserve pre-eruptive volatile contents because host phenocrysts act as an insulating capsule and MI are not affected by degassing of the surrounding magma that likely occurs during ascent and crystallization (Metrich and Wallace, 2008). However, interpretation of volatile data from MI, and thus the modeling of magma dynamics, is based on the assumption that MI record the composition of the melt from which the host minerals formed. However, MI may not preserve the original melt composition if (1) the composition of the glass phase does not represent the composition of the melt that was originally trapped owing to a variety of processes [e.g., post entrapment crystallization, diffusion of elements, formation of a vapor bubble, decrepitation (Cannatelli et al., 2016 and references therein)], (2) if boundary layer processes during trapping modified the composition of the melt adjacent to the growing crystal, such that the trapped melt does not represent the bulk (far-field) melt (e.g., Baker, 2008), or (3) the melt that was trapped was generated as a result of disequilibrium processes (e.g., Danyushevsky et al., 2004). It is important to note that while concentrations and ratios of elements that are compatible in the host will be modified by

post entrapment crystallization (PEC), PEC does not affect ratios of incompatible elements in the melt (now glass) (Danyushevsky et al., 2002a; Lima et al., 2003).

The most rigorous and dependable approach to confirm that the composition of a MI is representative of the melt from which the host crystal grew is to study groups of MI that were trapped at the same time, defined as a "melt inclusion assemblage" (MIA; Bodnar and Student, 2006). All MI within an MIA would have been trapped at the same temperature and pressure, and all would have trapped a melt of the same composition. As such all of the MI within the MIA should show consistent phase behavior and chemistry (Bodnar and Student, 2006). While studying MIAs can provide unarguable evidence that the MI have trapped and preserved the original melt from which the host crystal was growing, melt inclusion assemblages are uncommon in most samples, and workers have rarely reported melt inclusion assemblages in studies of MI from CF and IP owing to their scarcity (Esposito et al., 2014). Also, the few MIA identified by Esposito et al. (2014) are comprised of small MI (<20 μ m), and therefore challenging or impossible to analyze by secondary ion mass spectrometry (SIMS) and/or Fourier-transform infrared (FTIR) spectroscopy.

As an alternative to the MIA approach to test that compositions of MI represent the original melt that was present when the phenocryst was growing, the composition of MI may be compared to the bulk rock compositions of samples from the same magmatic system (Danyushevsky et al., 2000). This comparison can help identify MI compositions that are anomalous relative to general geochemical trends defined by bulk rocks. While both the MIA approach and comparison of MI compositions with bulk rock compositions can be applied to determine if the volatile contents of MI represent the volatile content of the original, pre-eruptive melt, we note that most previous studies of MI from CF and IP have not reported or discussed methods to test whether the major elements and volatile contents of MI record the original, unmodified composition. Here, we use the term "representativeness" to identify a MI that traps and preserves a sample of the melt that was in equilibrium with the host phenocryst at the time of trapping. In other words, MI represent a "snapshot" of the liquid (melt) composition during magmatic differentiation, representing melt that was in equilibrium with crystals \pm vapor. One of the main factors that limits our ability to determine whether volatile contents of MI from CF and IP

reported in the literature represent the original volatile content of the trapped melt is that contributions of the vapor bubble in the MI to the total volatile content of the MI are not discussed or considered, even though vapor bubbles are reported in the descriptions of MI petrography. Recent studies confirm that analyzing only the glass phase of a bubble-bearing MI and ignoring the CO₂ content of the bubble significantly underestimates the total CO₂ (and other volatiles) content of the trapped melt (e.g., Aster et al., 2016; Esposito et al., 2016; Moore et al., 2015). Because most of the CO₂ is contained in the vapor bubble of a bubble-bearing MI, a more realistic and accurate estimate of the CO₂ content of the trapped melt is obtained if only the bubble, rather than only the glass, is analyzed. Concentrations of other volatiles, including H₂O and S, will similarly be underestimated if the volatile content of the bubbles is not considered (Esposito et al., 2016).

Given these concerns, it is appropriate to re-evaluate MI data from CF and IP because published reports often do not specify whether or not the MI that were studied contain vapor bubbles. In addition, MI compositions are often not compared with bulk rock compositions and geochemical trends are often not described. Moreover, if MI compositions do not follow the main bulk rock trends, the significance of these anomalous MI compositions is not considered. It is important to note that all, or most, of the MI in the studies we cited (and in one case, conducted) may be representative of the bulk melt during differentiation, but the representativeness has not been rigorously evaluated. Thus, it remains unclear whether the variations in volatile contents observed in MI represent variations in the composition of melts in equilibrium with the growing crystal at the time of trapping, or instead are due to modifications after trapping.

In this study, we review published data for MI from the CF and IP volcanic areas (Arienzo et al., 2016; Arienzo et al., 2010; Cannatelli et al., 2007; Cecchetti et al., 2002-2003; Cipriani et al., 2008; Esposito et al., 2011; Fourmentraux et al., 2012; Mangiacapra et al., 2008; Mormone et al., 2011; Roach, 2005; Stock et al., 2016), and we present new geochemical data obtained from MI from the CF and IP volcanic fields. The new data are from representative samples from the Neapolitan Yellow Tuff (NYT), Solchiaro, Bacoli, Agnano-Monte Spina (AMS), Solfatara, and Fossa Lupara eruptions. These new data supplement the database of MI compositions from the literature. We selected MI from the

NYT. Bacoli, and Fossa Lupara eruptions because, to our knowledge, MI from these eruptions have not yet been studied. Moreover, the selected samples represent a significant range in time (~23.6 ka to 3.7 ka) and space within the CF and IP (Fig. 1). By conducting new analyses within a rigorous analytical protocol, our goal was to develop a better understanding of the reliability of MI as recorders of the pre-eruptive magma history at CF and IP. We compared compositions of MI from this study with those of bulk rocks and MI from the literature to better understand the correlation between MI and bulk rock compositions (Appendix Table D). The compiled literature data, combined with our new data, allow examination of possible correlations between the major element and volatile contents of MI and the compositions of host phenocrysts (mainly olivine, clinopyroxene, and sanidine). In addition, we compared compositions of experimentally reheated MI with data from naturally quenched MI. The selected MI data for CF and IP and mineral data were also compared with differentiation trends and mineral compositions predicted using rhyolite-MELTS simulations to better understand if crystallization occurred under volatile-saturated conditions (Ghiorso and Gualda, 2015). Finally, we describe in detail a protocol to test the representativeness of MI in the absence of melt inclusion assemblages. We demonstrate that re-evaluating MI data following the method employed here reduces uncertainty and instills confidence that the MI compositions are representative of the original pre-eruptive melt.

Geology and geochronology of Campi Flegrei and Procida

Island

Campi Flegrei (CF) and Procida Island (IP) are part of the Phlegrean Volcanic District (PVD; Orsi et al., 1996). The PVD, along with the Somma-Vesuvius volcanic district, is part of the Campanian Comagmatic Province, which in turn is part of the circum-Tyrrhenian magmatic event that began in the Plio-Quaternary (Peccerillo, 1999 and references therein). Campanian magmatism is associated with NW-SE and NE-SW trending normal faults that reflect the extensional/trans-tensional tectonic regime of the Campanian margin (Milia, 2010 and references therein). The magmas generated in the

 CF and IP share a common origin dating back at least 40 ka (De Astis et al., 2004). The oldest volcanic products in the entire Campanian Plain do not outcrop but, rather, were collected from drill cores and give ages of $2.0 \pm 0.4\,$ Ma (Barbieri et al., 1979), $\sim 1\,$ Ma (Ippolito et al., 1975) and $\sim 0.4\,$ Ma (Brocchini et al., 2001).

Campi Flegrei

The Campi Flegrei (CF) volcanic field is located NW of Naples and is characterized by the presence of several volcanic cones, rings, and caldera structures. The volcanic framework at CF is interpreted by some researchers as representing a nested and resurgent caldera that is partially submerged under the Bay of Pozzuoli (Orsi et al., 1995; Orsi et al., 1992; Orsi et al., 1996; Perrotta et al., 2006) (Fig. 1). In this model, the outer caldera rim was formed during eruption of the Campanian Ignimbrite (CI), the largest eruption in the entire Campanian Plain, that occurred at ~39 ka (De Vivo et al., 2001; Rolandi et al., 2003), and the inner caldera was formed later by the Neapolitan Yellow Tuff (NYT) eruption at ~15 ka (Deino et al., 2004). While most workers agree that a caldera at CF was formed during the NYT eruption, both the existence of an outer caldera formed by the CI and the source of the CI are subjects to debate (Scandone et al., 2006). Rosi and Sbrana (1987), Orsi et al. (1996), and Piochi et al. (2013) suggest that the CI was erupted from a vent located in the center of the CF. In contrast, Scandone et al. (1991) suggest that the CI originated from the Acerra depression northeast of Naples. Another interpretation is that the CI was produced as the result of multiple fissure eruptions that occurred along faults associated with the local extensional tectonic regime (De Vivo et al., 2010; De Vivo et al., 2001; Rolandi et al., 2003). As summarized by De Vivo et al. (2010), these eruptions fed by regional faults range in age from > 300 ka to 39 ka. Recent findings based on a new borehole at CF support this latter hypothesis that the CI originated through fissure vents from outside of the CF (De Natale et al., 2016). In particular, these researchers reported that the volume of the NYT is 2.5 larger than that of the CI, and that the volume of the CI deposits contrasts with the hypothesis that the CI formed a caldera structure larger than that associated with the NYT. In addition, we note that there is some debate concerning the location of both the CI and the NYT caldera rims (e.g., Orsi et al., 1996; Perrotta et al., 2006; Rosi and Sbrana, 1987; Vitale and Isaia, 2014). Regardless of the origin of the CI, we do not include data from MI from CI in this

 242 (Ma243 pos244 are

 assessment because (1) no basaltic or trachybasaltic MI are reported from this eruption (Marianelli et al., 2006; Signorelli et al., 1999; Webster et al., 2003) (2) it is generally not possible to determine from the published studies which MI are bubble-bearing and which are not, and (3) the origin of the CI and its possible genetic relationship to CF and PI are still under debate for the reasons mentioned above.

The oldest outcropping volcanic products in the CF volcanic field, dated at 58±3 ka, are found only in escarpments in the northern part of CF (Pappalardo et al., 1999). Activity occurring in the interval between these oldest recognized eruptions and the eruption of the CI (~39 ka; De Vivo et al., 2001; Rolandi et al., 2003) is referred to as pre-CI activity. Pre-CI activity includes the Punta di Marmolite and Cuma lava domes (Gillot et al., 1982), two of the few lava domes at CF. Other mostly alkali-trachytic explosive eruptions have been recognized during the pre-CI activity (Pappalardo et al., 1999). A lithic breccia associated with an ignimbrite deposit and dated at ~39 ka (De Vivo et al., 2001; Rolandi et al., 2003) formed after this period of relatively minor volcanic activity. This lithic breccia, known as the Breccia Museo-Piperno formation, outcrops at many localities around the CF and some authors suggest that it represents the proximal phase of the CI (Orsi et al., 1996; Pappalardo et al., 1999; Perrotta et al., 2006). Various estimates of the volume of material erupted during the CI range from 80 km³ (Thunell et al., 1979), to 150 km³ (Civetta et al., 1997), to 200 km³ (Rolandi et al., 2003), to 300 km³ (Fedele et al., 2007) DRE. The estimated volume is related to the ignimbrite dated at ~39 ka by De Vivo et al. (2001).

Following the CI eruption, volcanic activity is characterized by several eruptions referred to as "tufi biancastri" (whitish tuffs) that occur mainly in eastern CF (Di Girolamo et al., 1984). These eruptions span a period from <39 ka to 15 ka, at which time the NYT erupted. The age of the NYT is controversial because two different analytical methods give significantly different ages. The NYT has been dated at 12 ka using the ¹⁴C method (Alessio et al., 1971) and at ~15 ka using the ³⁹Ar/⁴⁰Ar method (Deino et al., 2004). As mentioned above, the NYT is interpreted to be the eruption that formed the CF caldera, and the NYT deposits cover an area of 1000 km² and consist of 40 km³ DRE (Orsi et al., 1992; Wohletz et al., 1995). Volcanic activity at CF that occurred after the NYT eruption is referred to as "recent activity" by Di Girolamo et al. (1984). Di Vito et

al. (1999) grouped post-NYT activity into three epochs of volcanic activity; epoch I between ~15 and 10.6 kg; epoch II between ~9.6 and 9.1 kg; and epoch III between ~5.5 and 3.5 ka, based on a recalculated age reported by Smith et al. (2011). Di Vito et al. (1999) recognized 64 volcanic units that were deposited after the eruption of the NYT. The common characteristic of this recent activity is that eruptions were mostly explosive. generated from monogenetic centers, and produced a small amount of material compared to the NYT eruption. The eruptions of the first two epochs are located mainly near the periphery of CF, while more recent eruptions occurred mostly in the interior of CF. Recently, Lirer et al. (2011) recognized a new volcanic unit that they named Torretta. ¹⁴C dating of samples from the Torretta unit revealed an age of 2.8 ka (Lirer et al., 2011). The Monte Nuovo eruption in 1538 AD represents the only historical eruption at CF, and a historical chronicle describes in detail the week-long eruption that formed a scoria cone (Da Toledo, 1539).

Procida

The Island of Procida (IP) represents the products of volcanic activity from five monogenetic volcanoes: Vivara, Terra Murata, Pozzo Vecchio, Fiumicello, and Solchiaro (De Astis et al., 2004; Di Girolamo et al., 1984; Di Girolamo and Stanzione, 1973; Pescatore and Rolandi, 1981; Rosi et al., 1988a; Rosi et al., 1988b). These volcanoes are aligned along a NE-SW trending volcanic belt that extends from the Island of Ischia southwest of IP to Monte di Procida to the northeast (Fig. 1). The importance of the NE-SW transverse faults that are associated with the Appennine (NW-SE) normal fault in the formation of the Procida Island volcanoes is noted in several studies (Acocella et al., 1999; De Astis et al., 2004; Orsi et al., 1996). The IP volcanism has likely been active over the last 80 ka, but no historical volcanic activity has been recorded (De Astis et al., 2004 and references therein). Volcanic deposits resulting from the activity of the five volcanoes are interlayered with deposits from higher magnitude eruptions sourced from Ischia Island and CF. The most recent eruptive materials on Procida are associated with the Solchiaro eruption. Paleosols at the base of the Solchiaro deposits have been dated at 17.3 ka and 19.6 ka, respectively by Lirer et al. (1991) and by Alessio et al. (1989). All of the paleosol ages were based on radiocarbon (¹⁴C) measurements. Also, Alessio et al. (1989) reported an age of 14.3 ka for a paleosol above the Solchiaro deposits. This

 suggests that the last volcanic activity at Procida occurred between 19.6 ka and 14.3 ka. More recently, Morabito et al. (2014) recalibrated the 19.6 ka age reported by Alessio et al. (1989) to obtain an age of 23.624 ± 0.33 cal ka BP, moving the age of the Solchiaro eruption to an earlier time.

Genesis and differentiation of magma at Campi Flegrei and Procida Island

The CF and IP magmatism is part of the Quaternary magmatism that is characterized by high K₂O contents in relatively primitive melts (Peccerillo, 2017). The trend is defined by the potassic series starting from least evolved trachybasalts, continuing through shoshinites and latites, and ending with trachytes and phonolites (Suppl. Fig. 1a). There is no correlation between the age and compositional evolution of rocks erupted in the Phlegrean area. The more primitive magmas of the last 23.6 ka erupted along regional normal faults oriented NE-SW, along the NYT caldera border and continuing through Procida and Ischia Islands (Acocella and Funiciello, 1999; De Astis et al., 2004; Orsi et al., 1996). The volume of trachyte is much larger than the combined volumes of trachybasalt, shoshonite and latite. In particular, the intermediate composition rocks represent the smallest volume of erupted products.

Bulk rock major element compositions show trends mostly consistent with simple fractional crystallization (D'Antonio, 2011 and references therein), in which olivine is the predominant mineral phase in the least evolved members. Clinopyroxene is present throughout the entire differentiation trend and predominates in the intermediate members, and sanidine is more abundant in the more evolved stages. Plagioclase also crystallized along the trend, with accessory phases chromite, Ti-magnetite, apatite and biotite observed. Melluso et al. (2012) calculated that ~90% of fractional crystallization (alkalifeldspar, plagioclase, clinopyroxene and olivine in order of abundance) is required to generate the trachyte-phonolites from the latitic bulk composition of CF. However, simple fractional crystallization models cannot explain either the variability of K for the least evolved rocks, nor the K-enrichment of some of the more evolved rocks. Other elements (e.g., Cl, Sb) show similar anomalous variability and enrichment (Villemant, 1988). The combination of isotopic and trace element data suggests that a mechanism of percolation of fluids from the wall rock into the magma reservoir caused selective

 enrichment of K-Sb-Cl during fractional crystallization (Civetta et al., 1991; Villemant, 1988).

In several studies, the large variation of CO₂ and H₂O concentrations of MI at CF and IP is interpreted as the combination of continued degassing of volatile-saturated magmas during ascent and multiple CO₂ fluxing events (Arienzo et al., 2016; Arienzo et al., 2010; Mangiacapra et al., 2008; Mormone et al., 2011). In addition, Moretti et al. (2013) studied major elements and volatiles in trachybasaltic and shoshonitic MI from Ischia Island (West/South-West from CF and IP) and discussed the importance of CO₂ fluxing for the geochemical evolution of magmas associated with Neapolitan volcanism. It is important to note that studies advocating the importance of CO₂ fluxing corroborate the hypothesis of selective enrichment of K, Sb, and Cl by percolation of fluids through magmas at CF (Civetta et al., 1991; Villemant, 1988). However, D'Antonio and Di Girolamo (1994) noted that the selective enrichment of K-Sb-Cl in mafic rocks from IP is accompanied by the enrichment of other trace elements that are not compatible with fluids (e.g., Nb). In addition, "shrinkage" bubbles in MI are reported in the MI from studies advocating CO₂ fluxing, raising concerns about the reliability of the volatile data recorded by MI (i.e., did the MI trap some CO₂ along with melt?). Alternatively, D'Antonio and Di Girolamo (1994) invoked mixing between magma batches showing different degrees of evolution (e.g., trachybasalt and latite) and having different Srisotopic signatures to explain the observed trends.

There is a general agreement regarding the depth at which extensive crystallization and possible CO₂ fluxing occurred (and is occurring) beneath the CF and PI volcanic fields. Seismic reflection data suggest a partial melting zone ~1 km thick at 7.5 km beneath CF. In agreement with geophysical data, data from MI suggest that extensive crystallization and CO₂ fluxing occurred at ~200 MPa (Arienzo et al., 2010; Mangiacapra et al., 2008; Moretti et al., 2013).

Several hypotheses have been proposed for magma generation in the Phlegrean area. Many researchers argue that magmatism originated from an intraplate-type mantle source that was subsequently metasomatized by slab-derived fluids (Peccerillo, 2017 and references therein). Trace element data for CF and IP mafic magmas are enriched in LILE and LREE relative to MORB, and the trace element patterns are similar to those of

intraplate basalts. In contrast, Ti, Y, and Yb are depleted relative to MORB and the HFSE show lower degrees of enrichment relative to LILE and LREE, characteristics of an arctype signature (De Astis et al., 2004; Peccerillo, 1999 and references therein).

 Volcanic rocks erupted from the CF volcanic field during the last 60 ka show highly variable isotopic compositions. In particular, the ⁸⁷Sr/⁸⁶Sr ratio varies from ~0.7065 to 0.7086. ¹⁴³Nd/¹⁴⁴Nd varies from ~0.5124 to 0.5128. ²⁰⁶Pb/²⁰⁴Pb from ~18.90 to 19.25, 207 Pb/ 204 Pb from ~15.65 to 15.77, and 208 Pb/ 204 Pb from ~38.95 to 39.38 (see Peccerillo 2017, Chapter 7 and references therein). The isotopic data document a general increase in ⁸⁷Sr/⁸⁶Sr and decrease in ¹⁴³Nd/¹⁴⁴Nd and ²⁰⁶Pb/²⁰⁴Pb from older to younger rocks. However, the same ⁸⁷Sr/⁸⁶Sr increase and ¹⁴³Nd/¹⁴⁴Nd and ²⁰⁶Pb/²⁰⁴Pb decrease is noted with increasing MgO content (Suppl. Fig. 1b). The isotopic variability indicates that simple fractional crystallization cannot be the only process responsible for the geochemical trends defined by rocks of the CF volcanic field. Pappalardo et al. (2002) interpret the correlation between 87Sr/86Sr and age to reflect crustal contamination. Thus, the younger erupted magmas would have resided in the crust for a longer time, underwent more extensive crustal contamination and, therefore, show higher ⁸⁷Sr/⁸⁶Sr. However, it is important to note that the age - isotopic signature correlation is not observed if only the NYT and post-NYT bulk rock data are examined (Di Renzo et al., 2011). It is also worth noting that the NYT shows homogeneous Sr-isotope ratios, and based on this Gebauer et al. (2014) suggest minimal wall rock contamination for NYT magmas. In contrast with the interpretation of Pappalardo et al. (2002), Peccerillo (2017) argues that the correlation between isotopic composition and MgO may suggest that hotter and less viscous mafic magmas experience more contamination relative to more evolved, cooler and more viscous magmas, as has been invoked for Alicudi volcano in the Aeolian arc (Peccerillo et al. 2017 and references therein). According to this latter interpretation, the isotopic variability is not necessarily controlled by residence time of magmas in the crust.

Although most of the major element trends at IP suggest simple fractional crystallization, variability of incompatible elements and variability of isotopic composition of bulk rocks suggest that open-system magma processes must have also been involved. The most mafic rocks in the Campanian Province are found in the IP, with few of the lithic lava clasts considered to be primitive (MgO up to ~11.5 wt% and Ni up

 to ~230 ppm; D'Antonio et al., 1999a). In addition, a juvenile sample from the Solchiaro I deposits at IP indicates that lower Sr-isotopic ratios in the CF and IP (\sim 0.7052) are not restricted to lithic lava clasts (De Astis et al., 2004). The 87Sr/86Sr (0.7051 to 0.7065) of IP bulk rocks is lower than that of CF rocks, and vice versa for ¹⁴³Nd/¹⁴⁴Nd. D'Antonio et al. (2007) recognize two trends based on ¹¹B and ²⁰⁶Pb/²⁰⁴Pb versus ⁸⁷Sr/⁸⁶Sr systematics of bulk rocks from CF, IP, and Ischia Island. They interpret one trend to represent contamination of the mantle source by slab-derived fluids or sediment-derived melts. In particular, the CF rocks are interpreted to have been generated by a transitional MORBtype asthenospheric mantle contaminated by sediment-derived melts, while the IP rocks were generated by the same mantle source contaminated by slab-derived fluid. The other trend records crustal contamination during crystallization of volcanic rocks younger than 39 ka. In addition, D'Antonio et al. (2007) suggest that some rocks younger than 39 ka were affected by mixing-mingling processes between chemically and isotopically distinct magmas, based on disequilibria among mineral and groundmass. Mazzeo et al. (2014) also studied lithic lava clasts from the Solchiaro deposits at IP and hypothesized that the mantle wedge from which primary magmas at IP were sourced was contaminated by 2-4% of slab-derived components represented by partial melts from shale and carbonates, and aqueous fluids from the slab. It is important to note that the mafic rocks from CF are not primitive. Consequently, Pappalardo et al. (2002) and Peccerillo (2017) emphasize that an interpretation whereby the difference in isotopic composition between CF and IP is related to different types of contamination of the source is speculative.

Sample description

Six new samples were collected to supplement existing data from the two volcanic areas. Five are from CF and one is from the IP. The CF samples are representative of five volcanic units erupted at different times in this volcanic field. The six eruptions sampled are, from oldest to youngest: Fossa Lupara (also named Senga in the literature), Solfatara, Agnano-Monte Spina, Bacoli, and Neapolitan Yellow Tuff for CF, and Solchiaro from the IP (Table 1 and Appendix Table A).

The Fossa Lupara sample (RESE17: Fig. 1) consists of black, sharp-edged scoriae < 20 mm. The Fossa Lupara eruption has been dated at 3.82 ka by Di Vito et al. (1999),

and Smith et al. (2011) recalculated the age to be 3.98-4.20 ka using a more recently developed and more precise method to interpret the isotopic data. The scoriae were selected from Fossa Lupara deposits ejected during the intermediate stages of the eruption (Lirer et al., 2011). The scoriae are porphyritic with abundant phenocrysts of clinopyroxene and subordinate sanidine and were sampled at the northeast sector of the crater associated with this eruption.

One sample representative of the upper deposits of the Solfatara eruption was collected close to the northwest crater rim of Solfatara (RESO8: Fig. 1), and consists of centimeter-scale fragments of rounded pumice contained in pyroclastic brownish ash layers. The pumices contain abundant sanidine and clinopyroxene. The age of the Solfatara eruption was recalculated from earlier data to be 4.15-4.35 ka by Smith et al. (2011) based on chronological data reported by Di Vito et al. (1999) and by Isaia et al. (2009).

The Agnano-Monte Spina sample (REMS12: Fig. 1) was collected ~ 200 m southwest from the top of Monte Spina. The sample consists of sharp-edged pinkish-grey pumices representing a 30-cm thick layer. The pumices are well sorted, characteristic of a fallout deposit. This layer of pumice also shows reverse grading suggesting that some changes occurred during the deposition such us (1) progressive increase in initial gas velocity, (2) change in vent morphology or, (3) increase in eruption column density (Self, 1976 and references therein). Abundant sanidine, clinopyroxene, rare biotite and olivine were observed.

The Bacoli sample (REBA1: Fig. 1) was collected close to the northern rim of the crater of the Bacoli volcanic formation in the western rim of CF caldera (12.8 ka, Di Renzo et al., 2011; 8.58 ka, Fedele et al., 2011; 11.51-14.15 ka, Smith et al., 2011). The sample consists of a yellow tuff containing abundant isolated euhedral sanidine and clinopyroxene phenocrysts.

The Neapolitan Yellow Tuff sample (14.9 ka; Deino et al., 2004) was collected from the eastern caldera rim (northwestern part of Naples urban area, Ponti Rossi; REPR11: Fig. 1). The sample consists of ash fall deposits with abundant sanidine and clinopyroxene phenocrysts representing the unlithified facies of the NYT (this deposit is referred to as Pozzolana, the material used for concrete production in Roman times). We

 selected only single phenocrysts showing euhedral habit and rim glass to avoid including xenocrysts in our sample suite.

The Solchiaro sample (RESC2: Fig. 1) was collected on the northeastern coast of IP and represents the distal unlithified facies of the Solchiaro deposits. The sample consists of grey ash, brown lapilli, and isolated olivine, clinopyroxene, and sanidine crystals [sample RESC2 in Esposito et al. (2011)].

Analytical methods

The samples selected for this study were gently crushed and individual phenocrysts were hand-picked from the crushed material under a binocular microscope. Each phenocryst was mounted on a 2.5 mm-diameter glass rod (Esposito et al., 2014; Thomas and Bodnar, 2002) using CrystalbondTM cement. Phenocrysts were polished on the top and bottom surfaces and those crystals containing rounded to regular-shaped MI were selected for study. After we selected 20-30 crystals (depending on size), the phenocrysts were pressed into a one-inch diameter indium mount. Indium was used as the mounting medium to prevent H-C contamination during secondary ion mass spectrometric (SIMS) analysis, as occurs when epoxy mounts are used.

MI in the Fossa Lupara sample and one MI hosted in sanidine from the Agnano Monte Spina sample were partially to completely crystallized as found. We performed heating experiments on the crystallized MI using a Vernadsky heating stage (Sobolev et al., 1980). The heating stage was calibrated according to the 1-atm melting temperatures of silver (962 °C) and gold (1064 °C). During the heating experiment, a continuous flow of He into the furnace of the heating stage prevented (or minimized) Fe-oxide formation on the surface of Fe-rich phenocrysts. MI were heated until the T of homogenization (MI containing only silicate melt) was reached. Following homogenization, the sample was quenched rapidly to room temperature. The T uncertainty is $\sim \pm 5^{\circ}$ C at 1064 °C. Heating rates were varied during the run, depending on phase behavior of the MI (Esposito et al., 2012).

The major element compositions of glasses and minerals were determined first using a JEOL JXA 8900 electron microprobe (EMP) at the USGS (Reston, VA, USA). The analyses were conducted using an accelerating voltage of 15 kV. The beam current

 was 10 nA and a defocused beam of 10 μ m diameter was used. For oxide concentrations > 1 wt%, 1-sigma errors are < 2% relative, while for oxide concentrations < 1 wt%, 1 sigma errors are generally < 10% relative. Additional information relative to EMP standards used for the analyses are included in Supplementary Table B.

Following EMP analyses, volatile elements (O, H, C, F, S, Cl) were measured by SIMS (Cameca IMS 1280) at the Woods Hole Oceanographic Institution (Woods Hole, MA, USA). We performed the analyses using ¹³³Cs⁺ as the ion source and the current varied between 1.0 and 1.6 nA. For each spot analyzed, the surface of the sample was pre-sputtered for 240 seconds to remove surface contamination. The size of the rastered area was 30 µm x 30 µm, and a 15 µm x 15 µm spot in the center of the rastered area was analyzed from 10 to 15 times in depth profile mode. We tuned the SIMS to count ions related to masses ¹⁶O, ¹H, ¹²C, ¹⁹F, ³²S, ³⁵Cl, and ³⁰Si. Ratios between ion counts per unit time of each mass measured and ion counts per unit time of ³⁰Si were used to quantify the volatile contents. Six basaltic to basaltic-andesitic glass standards were used for calibration of the SIMS, and additional information on the glass standards is reported by Helo et al. (2011). For the SIMS measurements, using glass standards with silicate compositions that differ from MI compositions may introduce a matrix effect. However, Hauri et al. (2002) showed that SIMS calibration curves for H₂O, CO₂, F, S, and Cl obtained using rhyolitic, and esitic, and basaltic glass standards do not show significant differences below certain absolute concentrations – specifically, for H₂O contents <2 wt% and CO₂ contents < 1000 ppm. Most of the volatile concentrations of the MI reported in this study are below these upper limits. We used the calibration curves of Esposito et al. (2011) to calculate volatile concentrations in MI. To avoid contamination from the C-coating used for earlier EMP analysis, we adopted a specific protocol (see also discussion by Esposito et al. 2014) to remove the C coating. In particular, ~5 μm of sample was removed by polishing following EMP and before SIMS analysis, and the SIMS analytical area was pre-sputtered for 290 s before data collection started. We selected only flat depth profiles whereby the C counts did not vary significantly with depth, and we continuously monitored the ion-count response image to confirm a homogeneous carbon signal across the rastered area during analysis. Relative precision

for CO₂, H₂O, F, Cl, and S by SIMS is <10% relative, based on repeated analysis of glass standards (see Esposito et al, 2014; their Figure 14).

Results

 Petrography of melt inclusions. Many (but not all) of the phenocrysts examined contain MI and other mineral inclusions. Fluid inclusions are rare in the phenocrysts studied. Various types of MI, based on phases present at room temperature, were observed in all five samples as described below.

Sanidine, clinopyroxene, and plagioclase from Bacoli, Solfatara, Solchiaro, and NYT samples contain MI filled with mostly glass. Most of these naturally glassy MI contain one bubble in addition to the glass phase, and some contain glass plus bubble(s) plus an associated mineral (most commonly apatite). In a few cases, naturally glassy MI contain only glass (bubble-free MI). MI containing more than one bubble are found mostly in sanidine phenocrysts. This is thought to represent bubble formation in the MI after the melt has become sufficiently viscous to prevent the multiple bubbles from coalescing into a single bubble. Bubble-bearing MI (glass plus one bubble) show similar volume fractions of vapor (i.e., volume_{bubble}/volume_{MI}) in single phenocrysts selected for our study, and the proportion of vapor never exceeds 5 volume %, suggesting that the vapor bubble nucleated after trapping of a homogeneous silicate liquid (Moore et al., 2015), i.e., vapor bubbles were not trapped along with the melt. It is important to note that NYT MI show a larger proportion of bubble-free MI relative to MI from the other CF and IP eruptions studied.

The phenocrysts selected from Agnano-Monte Spina and Fossa Lupara samples contain partially to totally crystallized MI, in addition to naturally glassy MI as described above. In particular, MI in sanidine from Agnano-Monte Spina are sometimes found partially or totally crystallized, while partially crystallized MI are rarely found in clinopyroxene. Most of the Fossa Lupara phenocrysts contain partially to totally crystallized MI, but sometimes sanidine phenocrysts contain naturally glassy MI. Some sanidine phenocrysts in the Fossa Lupara sample show decrepitation halos, suggesting that the MI developed high fluid pressures after trapping and have lost some of their volatiles via fracturing of the surrounding host (Cannatelli et al., 2016).

In general, MI in all samples are ovoid or negative-crystal shape, but sometimes slightly to highly irregular shapes were observed (Table 1). For this study, we selected regularly shaped MI because irregularly-shaped MI are more likely to have leaked or were in communication with the melt adjacent to the growing crystal for a prolonged period of time, (Humphreys et al., 2008a; Humphreys et al., 2008b; Welsch et al., 2013) or represent MI that have decrepitated (Maclennan, 2017). In addition, irregularly shaped MI hosted in plagioclase may be the result of dissolution reactions and record a chemical composition that is not representative of the melt in equilibrium with the host (Nakamura and Shimakita, 1998). Size ranges from a few microns to ~300 μm considering the longest dimension, and we selected only MI > 20 µm to assure that analytical spots for EMP and SIMS would be contained entirely within the MI, thus avoiding contributions from the surrounding host. Most of the MI are isolated in the cores of phenocrysts without any geometrical correlation with their host (i.e., the MI are not obviously aligned along crystal growth surfaces). Some phenocrysts contain more than one MI. Consistent with the results of Esposito et al. (2014), MIA are rarely observed; where they are, individual MI are $\leq 20 \mu m$, a size that is smaller than the optimal instrumental conditions for analyzing major elements and volatiles.

Microthermometry. As mentioned above, most of the Fossa Lupara MI were crystallized as found. For this reason, we performed heating experiments using a Vernadsky heating stage to produce a homogenous glass before analysis. All MI-bearing clinopyroxenes from Fossa Lupara show a homogeneous silicate melt phase upon heating to ~ 1200°C and all were quenched at this temperature. Most MI contain only glass after quenching from ~1200°C, but some MI developed a vapor bubble during quenching. MI in sanidine phenocrysts from Fossa Lupara were quenched from ~1070°C and most MI show only glass after quenching.

Major element compositions. Major element concentrations of MI are plotted on Harker diagrams versus SiO₂ (Fig. 2). The major element compositions of MI from this study (Table 2) overlap with published MI compositions (Arienzo et al., 2016; Arienzo et al., 2010; Cannatelli et al., 2007; Cecchetti et al., 2002-2003; Cipriani et al., 2008; Esposito et al., 2011; Fourmentraux et al., 2012; Mangiacapra et al., 2008; Mormone et al., 2011; Roach, 2005; Stock et al., 2016) and with bulk rock compositions from the

 literature (Albini et al., 1977; Beccaluva et al., 1991; Brocchini et al., 2001; Cannatelli et al., 2007; Capaldi et al., 1972; D'Antonio et al., 1999a; D'Antonio et al., 1999b; De Astis et al., 2004; de Vita et al., 1999; Di Girolamo et al., 1984; Di Vito et al., 2011; Ghiara et al., 1979; Mastrolorenzo and Pappalardo, 2006; Orsi et al., 1995; Orsi et al., 1992; Pappalardo et al., 2002; Piochi et al., 2005; Piochi et al., 2008; Scarpati et al., 1993; Tonarini et al., 2009; Tonarini et al., 2004; Turi et al., 1991; Villemant, 1988; Wohletz et al., 1995) (Fig. 2).

Compositions of MI studied here define differentiation trends with higher degrees of scatter relative to trends defined by bulk rock compositions – this is similar to trends defined by data for MI from the literature. In particular, at the same SiO₂ concentration, some major element concentrations (e.g., K₂O and Na₂O) span a wider range compared to that for the bulk rocks (Fig. 2). This behavior is commonly observed in MI studies (Kent, 2008, and references therein). In general, the major element concentrations of MI plotted as a function of SiO₂ show continuous differentiation trends (Fig. 2 a, b, d, and e). MI compositions from this study mostly agree with differentiation trends for bulk rocks, representing mainly fractional crystallization dominated by olivine plus clinopyroxene crystallization for less evolved magmas, clinopyroxene for intermediate magmas, and sanidine plus clinopyroxene for more evolved magmas.

Differentiation trends for TiO₂, FeO_{tot}, and P₂O₅ (Fig. 2), as well as for Al₂O₃, show poorer agreement compared to trends defined by bulk rock compositions from the literature. This behavior is consistent with MI data reported in the literature for other magmatic systems. For instance, TiO₂ contents of MI from this study show weak correlations with crystallization indicators relative to bulk rock data from the literature (Fig. 2d). For the least evolved MI compositions, TiO₂ concentrations span a wide range, while for more evolved compositions TiO₂ concentrations are more restricted.

For the MI studied here, FeO_{tot} behaves in a manner similar to TiO₂ (Fig. 2e). In particular, less evolved MI show more scatter relative to the more evolved MI. Some MI from the less evolved group (SiO₂ concentration ranging from ~47 to ~54 wt%) are FeO-depleted relative to the bulk rocks. The Fe-poor MI are all hosted in clinopyroxene from the Fossa Lupara sample. Some MI data from the literature for the Minopoli1 and Fondo Riccio eruptions (Cannatelli et al., 2007) and for the Solchiaro eruption (Mormone et al.,

2011) show the same behavior, and most of the MI are hosted in clinopyroxene (three MI are hosted in olivine). In addition, a group of MI hosted in olivine and clinopyroxene from the Minopoli2 and Fondo Riccio eruptions (Mangiacapra et al., 2008) show extremely low FeO_{tot} contents at intermediate SiO₂ contents. Also, some MI hosted in clinopyroxene from the Astroni1 eruption (Stock et al., 2016) show a depletion in FeOtot relative to the bulk rock trend. The depletion of FeO may reflect Fe loss from the MI to the Fe-Mg host via diffusion, as has been proposed and documented for other volcanic systems (Danyushevsky et al., 2000). It is important to note that most of the Fe-poor and less evolved MI from CF were heated experimentally. Some of the Fe-poor MI also show slight depletion in Al₂O₃, slightly higher CaO contents, lower Na₂O contents, and slightly higher K₂O (Fig. 2).

Several evolved MI from this study show a slight depletion of Na₂O relative to the bulk rock geochemical trends, with the exception of MI from the Solfatara and Astroni samples. Some of the bulk rock compositions show the same Na-depletion, and several MI compositions reported in the literature show the same behavior. Na₂O-poor MI are not preferentially hosted in sanidine or clinopyroxene phenocrysts, and they include both heated and naturally quenched MI. Na₂O-poor MI can indicate that Na has been lost from the MI by diffusion, and to test this hypothesis we calculated totals considering both EMP and SIMS concentrations. Some of the Na-poor MI show ~ 100 wt% totals (Table 2), suggesting that Na loss is minimal. Also, there is no correlation between Na₂O and H₂O concentrations. In addition, the group of MI showing depletion of Na₂O shows a slight enrichment in K₂O. Potassium should not increase as a result of Na loss by diffusion (Morgan and London, 2005). It is also important to note that Na-loss should not be significant at the conditions used to analyze major element concentrations (Hayward, 2012). The least evolved MI from this study, as well as those from the literature, show a wide range of K₂O concentrations. For instance, for MI with SiO₂ of ~50 wt%, K₂O varies by a factor of 6 (from ~ 1 to ~ 6 wt%) (Fig. 2b).

Among major and minor elements, P₂O₅ shows the poorest correlation with SiO₂ content. P₂O₅ concentrations of mafic and intermediate composition MI both from this study and from the literature show considerable scatter (from ~45 to ~57 wt% SiO₂, see

Fig. 2 f), while evolved MI (from ~57 to ~66 wt% SiO₂) show good correlations between P₂O₅ contents and crystallization indicators.

A group of MI hosted in plagioclase from the Bacoli eruption and one bulk rock composition from the literature do not overlap with the general trends defined by MI from the literature, or with bulk rock data for most of the major elements. The compositions of plagioclase-hosted MI are Qz normative, an observation that is rare for bulk rocks of CF and IP. These plagioclase-hosted MI show Na₂O and K₂O concentrations consistent with CF and IP bulk rock differentiation trends, while Al₂O₃ and SiO₂ concentrations are slightly higher than the bulk rock differentiation trends (Fig. 2). Concentrations of TiO₂, CaO, FeO, and P₂O₅ are lower than those shown by the bulk rock differentiation trends. The compositions of the MI hosted in plagioclase are not representative of CF and IP magmatism, suggesting that plagioclase selected for the study represent xenocrysts or that they formed under disequilibrium conditions.

Finally, we note that some of the individual bulk rock compositions project off the main bulk-rock trend (Fig. 2), and these tend to lie along mixing lines that point toward clinopyroxene or feldspar compositions. This suggests that some of the bulk rock compositions represent mixtures of melt plus entrained crystals. These "anomalous" bulk rock compositions represent a small fraction of the complete dataset.

Volatiles. Among all volatiles analyzed, Cl shows the best correlation with SiO₂ concentration, especially for less-evolved melts, while S shows a weak correlation, and H₂O, CO₂, and F show no correlation with SiO₂ (Fig. 3). Considering MI hosted in all phases, we observed two important features: (1) volatile concentrations of the MI studied here overlap with volatile concentrations of MI from CF and IP reported in the literature and (2) volatile concentrations of MI from this study are higher relative to CF and IP bulk rocks reported in the literature. This latter observation highlights the limitations of using bulk rocks to determine volatile compositions of magmas, because these samples have partially or totally degassed during ascent and eruption onto the surface. Conversely, MI are more likely to retain the original pre-eruptive volatile content during ascent and eruption.

Chlorine concentrations range from 913 to 7931 ppm. Chlorine behaves incompatibly through most of the magmatic differentiation showing a good correlation

with $SiO_2 < 60$ wt% (0.85 r²), but for $SiO_2 > 60$ wt% Cl shows a sub-vertical trend from 7710 to 1188 ppm (Fig. 3a). This vertical trend is observed for all MI hosted in sanidine.

Sulfur concentrations range from below detection limit (bdl) to 2884 ppm. Sulfur generally decreases from less evolved MI to more evolved MI. The S contents of MI are more scattered for less evolved MI, while S is more clustered for more evolved compositions (Fig. 3b).

Concentrations of H₂O in the MI studied here range from bdl to 2.54 wt%. In contrast to Cl and S, H₂O shows poor correlations with SiO₂, but for MI with >60 wt% SiO₂ a sub-vertical distribution is observed (Fig. 3d). It is important to recognize that the H₂O-SiO₂ trend for MI with <60 SiO₂ is defined by only five MI.

Fluorine concentrations range from 81 to 3860 ppm. Fluorine concentrations of MI show a behavior similar to Cl, but the correlation is weaker. For MI >60 SiO₂ the distribution is sub-vertical as observed for Cl and H₂O. Since there are only five MI showing SiO₂ <60 wt%, the apparent vertical trend may reflect the small sample size (Fig. 3e).

Carbon dioxide concentrations range from below detection limit to 258 ppm with one MI from the NYT sample showing 1046 ppm (Fig. 3c). Carbon dioxide does not correlate with SiO₂ even when a single eruption is considered (Fig. 3c), and H₂O-CO₂ systematics do not define a trend (Fig. 4a). In contrast, MI from individual eruptions are considered, the NYT MI show a positive trend (Fig. 4b). The correlation shown by NYT MI should be viewed with caution because only three analyses are available.

In general, volatile abundances of MI do not correlate with each other, with the exception of Cl vs F (Fig. 4c) which shows a strong positive correlation. This suggests that Cl and F are retained in the melt during the initial and intermediate stages of differentiation (trachybasalt-shoshonite-latite). During the last stages of crystallization, Cl likely partitions strongly into the fluid phase while F is retained in the melt.

Host mineral compositions. MI from this study are hosted in clinopyroxene (cpx), sanidine, and plagioclase. The ferrosilite component of cpx hosting MI ranges from 6 to 18 mol%, the wollastonite component from 46 to 49 mol%, and the enstatite component ranges from 34 to 48 mol% (Suppl. Fig. 2 c). The MI compositions and host phase compositions are both consistent with trapping of a melt that was in equilibrium with cpx

1293 701 1295 702 1296 703

during crystallization. For example, the SiO_2 concentration of MI correlates with the ferrosilite component. Note that MI data show some significant scatter, and we will discuss the reasons for this in the discussion section. MI and clinopyroxene host compositions are consistent with data reported in the literature.

The sanidines containing MI analyzed in this study possess 54 to 86 mol% orthoclase component, with most in the range 76-86 mol% (Suppl. Fig. 2 a and b). The Or-poor sanidines are restricted to the Solchiaro sample and show up to 42 mol% albite component. No correlation is observed between host composition and SiO₂ concentration of MI (Suppl. Fig. 2 a). One possible explanation is that sanidine began to crystallize over a restricted interval of SiO₂ concentrations (see discussion section for more details). However, a good correlation is observed if the orthoclase component of the host is plotted versus SiO₂/CaO ratio of the MI (Suppl. Fig. 2 b). The SiO₂/CaO ratio is likely a better crystallization indicator at this differentiation stage, and, also, this ratio is not affected by PEC or host dissolution (see the discussion section for more details). The orthoclase component decreases and the albite component increases as crystallization progresses. This behavior was reported and documented by Melluso et al. (2012) who showed that the NaO content of the alkali feldspar increases in the more evolved bulk rocks.

Only six MI from this study and from the literature combined are hosted in plagioclase. The anorthite component ranges from 75 to 81 mol%, and the anorthite component of the host correlates with the SiO₂ concentration of the MI. This observation, based on only six MI, should be taken with caution.

Post entrapment crystallization or dissolution. In this study we did not attempt to correct for changes in MI composition associated with post entrapment crystallization (PEC) owing to the lack of a reliable model to implement the correction. We note that Kress and Ghiorso (2004) report that an algorithm incorporated into the MELTS platform could be used to estimate PEC based on the composition of the MI and the host for various phenocrysts, including pyroxene and feldspar. We attempted to apply this method to correct the MI of this study but the results indicated that ~ 90% PEC had to occur for many MI. This value is not realistic and is not supported by petrographic examination of the MI. As such, we consider bubble-free MI having compositions that overlap with bulk

rock compositions to have experienced only minimal PEC, and have assumed that the compositions of the MI reasonably approximate the original melt composition.

Discussion

 Our interpretation of geochemical trends in MI from CF and IP is based on new data from this study as well as published data for CF and IP. First, we focus on major element concentrations of MI that do not follow the general trends defined by bulk rock compositions. We test if the MI compositions are representative of the silicate melt in equilibrium with the host mineral, based on major element compositions. We discuss the significance of anomalous MI, and we exclude the non-representative anomalous MI from the interpretation of volatile evolution at CF and IP. Second, we focus on volatile and major element concentrations of normal MI that have trapped and preserved a representative sample of the melt at the time of trapping. We discuss the significance of volatile concentrations of all MI, and we select only the bubble-free MI to investigate crystallization trends using the rhyolite-MELTS code (Ghiorso and Gualda, 2015).

Significance of Anomalous MI

Anomalous melt inclusions are those whose compositions cannot be reasonably inferred to represent compositions of melts along a fractionation trend. Below we discuss the anomalous MI that were identified and possible processes that may have produced the anomalous compositions.

Al₂O₃ and P₂O₅ anomalies of MI

Several processes can lead to anomalous Al₂O₃ and P₂O₅ concentrations in MI. These anomalous compositions can represent the trapping of a boundary layer associated with rapid crystal growth rates (e.g., Baker, 2008), or could represent trapping of melt produced as a result of dissolution-reaction-mixing (DRM) processes in the mush zone (Danyushevsky et al., 2004). Alternatively, these anomalies can be artifacts generated as a result of overheating during laboratory heating experiments. In this section, we discuss which processes are likely responsible for the anomalous MI observed at CF and IP.

As reported above, several MI are enriched in Al₂O₃ relative to bulk rocks in differentiation plots. Including MI from the literature, we observed that Al₂O₃ is one of the major components that shows large deviations from bulk rock geochemical trends. MI hosted in clinopyroxene show the largest variations for Al₂O₃ (Fig. 5a). At intermediate CaO concentrations (between 5 and 8 wt%), some MI hosted in clinopyroxene show Al₂O₃ contents that are elevated relative to bulk rocks. At high CaO concentrations, other MI hosted in clinopyroxene shows anomalously low Al₂O₃ concentrations relative to the bulk rocks. It is worth noting that a few MI hosted in olivine show a slight enrichment in Al₂O₃ content. Experimental studies suggest that host-incompatible element concentrations of MI could be affected by boundary layer process. In particular, Faure and Schiano (2005) reported that MI trapped in fast growing olivine show a significant enrichment in Al concentration. However, boundary layer effects alone cannot explain the CaO vs. Al₂O₃ deviations of MI from the bulk rock trends. Interestingly, the Al₂O₃poor MI were all reheated in the laboratory, while the most of the Al₂O₃-rich MI are naturally quenched (Fig. 5b). These Al₂O₃-rich MI show low TiO₂, FeO_{tot}, and MgO, and this observation is consistent with high degrees of PEC or with a plagioclase component added to the "normal" CF melt composition. However, it is important to note that most of the Al₂O₃-rich MI also show elevated P₂O₅ and some show high Cl concentrations, consistent either with trapping of apatite along with the melt or that some MI hosted in clinopyroxene trapped a boundary layer melt that was enriched in P (Baker, 2008).

For most of the Al-rich MI, the P_2O_5 enrichment cannot be attributed to PEC. If we consider the Al-rich MI showing the highest P_2O_5 concentration [1.38 wt%, "FRC2-P7-M1" from Cannatelli et al. (2007), see database Appendix Table D] and the BR showing the highest P_2O_5 concentration (0.6 wt%, "s 97110PNA-S"), ~ 57% PEC would be required to bring the MI composition into coincidence with the BR trend. With this amount of PEC other phases in addition to the host would also be crystallizing in the MI. Also, the Al-rich MI under consideration was reheated in the lab, and was quenched when the MI homogenized, indicating only minor PEC if the quenching occurred from a temperature that was lower than the trapping temperature. Also, at 57% PEC the Al_2O_3 concentration should have been ~11 wt%, a value that is much lower than the BR with similar extent of differentiation. To explain the P_2O_5 enrichment of FRC2-P7-M1 only

requires \sim 2% apatite component, while the enrichment of Al₂O₃ would require a \sim 23% plagioclase component.

 It is generally assumed that boundary layer processes would affect compositions of smaller inclusions to a greater extent compared to larger inclusions being trapped at the same crystal-melt interface. Esposito et al. (2011) found no correlation between the MI size and the P_2O_5 and K_2O concentration, suggesting that boundary layer processes alone cannot explain the Al_2O_3 - P_2O_5 MI trends. Furthermore, an inverse correlation between the size of MI and the concentration of slow diffusing elements should be expected only if there is evidence that all the MI being considered trapped the same melt. In other words, we cannot compare data for a group of MI if there is no evidence that each MI was originally trapped from the same bulk melt. This fact underscores the importance of studying MIA (Bodnar and Student, 2006) to test for correlations (if any) between MI composition and size. With the assumption that all MI comprising the MIA trapped the same melt, the correlation between size and concentration of slow diffusing elements can be used to test whether boundary layer processes significantly affected the composition of those MI, and corrections to determine the original trapped melt composition can be proposed.

In this study, all MI hosted in sanidine show similar compositions and show no correlation between size of the MI and the K₂O concentration (Suppl. Fig. 4), suggesting that boundary layer processes did not affect the composition of sanidine-hosted MI. The selective enrichment of major and trace elements can be interpreted as the result of dissolution-reaction-mixing (DRM) in a mush zone at the interface between a magma body and wall rock (Danyushevsky et al., 2004; Esposito et al., 2011). Thus, the enrichment of Al₂O₃ can be explained by DRM between plagioclase and melts at various stages of evolution. Combined enrichment of Al₂O₃ and P₂O₅ can represent DRM between less evolved melt and mush zone material of more evolved magmas rich in plagioclase and apatite beneath CF and IP. The DRM interpretation implies micro-scale heterogeneity that results when a less evolved melt ascends and interacts with a preexisting mush zone. In particular, the DRM interpretation corroborates the hypothesis that basaltic and trachybasaltic magmas interacted with a mush zone consisting of

cogenetic evolved latitic and trachytic-phonolitic magmas at CF and IP, as reported in other studies (D'Antonio, 2011 and references therein).

As reported above, some of the heated and less evolved MI hosted in clinopyroxene show enrichment in CaO and MgO, and depletion in Al_2O_3 , TiO_2 , and Na_2O . These anomalies indicate that MI have likely been over-heated in the laboratory and the resulting composition of MI shows dilution of clinopyroxene-incompatible elements and enrichment in clinopyroxene-compatible elements (Fig 5b). We attempted to correct compositions of reheated MI hosted in clinopyroxene by adjusting the CaO and Al_2O_3 to the regression line of the bulk rock data or to the bulk rock data "cloud" in the CaO vs. Al_2O_3 plot (Suppl. Fig. 3a). This correction suggests that 30 to 33% of host dissolution would have occurred during heating. However, after this correction, FeO, K_2O and P_2O_5 still show anomalous concentrations (Suppl. Fig. 3 b, c, and d). In fact, a "correction" for 30-33% host dissolution tends to drive both K_2O and P_2O_5 towards more anomalous compositions. This suggests that a simple host dissolution correction cannot be used to restore the original MI composition.

Heated and more evolved MI hosted in sanidine show higher K₂O concentrations relative to unheated and more evolved MI (Suppl. Fig. 4), similar to MI hosted in cpx. MI showing anomalous compositions for some major elements may also show volatile concentrations that are not representative of the silicate melt that was in equilibrium with the host at the time of trapping. For instance, if the anomalous composition of a MI is the result of DRM, the MI volatile budget could be modified, and the concentrations of individual volatile components could be differentially affected. If the wallrocks involved are dominantly composed of anhydrous phases, concentrations of all volatiles would be lowered by simple dilution (Danyushevsky et al., 2004; Esposito et al., 2011). Alternatively, if the wallrocks contain carbonates, as has been inferred for Vesuvius (Gilg et al., 2001) and Merapi (Deegan et al., 2010), the concentration of CO₂ in the magma could be increased by DRM processes. The eruptive products at CF lack carbonatebearing xenoliths or skarn materials (D'Antonio, 2011). This suggests that DRM at CF should lower the volatile contents of the melts, and this is consistent with observations by Esposito et al. (2011) who reported very low S, CO₂ and Cl concentrations of some anomalous MI and compositions plot towards the origin on S-CO₂-Cl vs Zr binary

 diagrams. The low concentration of volatiles is expected for overheated MI. Even though the lowering of the volatile concentration caused by dissolving excess host during the heating experiment is likely insignificant, two additional issues are associated with overheated MI. If MI are heated to a temperature above the "true" trapping temperature, the total amount of time that the MI would have been exposed to "high" temperatures will be longer, compared to heating to a lower temperature at the same rate. This, in turn, translates into a greater likelihood to lose H⁺ by diffusion (Bucholz et al., 2013; Mironov and Portnyagin, 2011). Hydrogen can also be lost from the MI in nature (before eruption), leading to an increase in the homogenization temperature of the MI and requiring heating to higher temperatures to achieve homogenization during re-heating experiments in the lab.

Fe exchange

Numerous studies have documented Fe loss from MI based on the negative correlation between FeOtot of the MI and the composition (Fo mol%) of the host, as well as the lower FeOtot in the MI relative to bulk rocks and matrix glasses of the same magmatic system at comparable degrees of differentiation (Danyushevsky et al., 2000; Danyushevsky et al., 2002b; Esposito et al., 2011; Norman et al., 2002; Sobolev and Danyushevsky, 1994; Yaxley et al., 2004). Six MI from this study show anomalously low Fe concentrations relative to the main differentiation trend defined by bulk rocks (Fig. 2) e). Three MI are hosted in plagioclase from the Bacoli eruption, and the other three MI are hosted in clinopyroxene from the Fossa Lupara eruption, and these were heated in the laboratory to obtain a homogeneous glass. The Fe-poor MI hosted in plagioclase from Bacoli are discussed in a later section because, in addition to anomalous FeOtot concentrations, these MI show anomalous compositions for most of the other major elements. The lower FeO concentrations (from 4.1 to 6.2 wt%) of Fossa Lupara MI are consistent with overheating during experiments owing to the low FeO concentrations of clinopyroxenes hosting these MI (3.7 to 4.5 wt%). These MI show elevated concentrations of CaO and MgO and a general depletion of the other major elements (Fig. 5 c and d). The effect of overheating can be observed in most of the MI hosted in clinopyroxene from this study and in MI from the literature. In fact, most of the reheated

MI (red triangles in Fig 5 d) that fall outside of the field defined by bulk rocks and can be distinguished from the unheated MI (blue triangles in Fig. 5 d) based on their generally lower FeO_{tot} concentrations and slightly elevated CaO contents.

Roedder (1979) reported that homogenization temperatures obtained from MI might be higher than the temperature of trapping owing mainly to three factors: (1) inadequate time for re-equilibration (heating rates during experiment are too fast), (2) loss of hydrogen or water from hydrous MI (which increases the liquidus temperature relative to more H₂O-rich compositions), and (3) thermal gradients in the stage. In addition to these factors, heating beyond the original trapping temperature would be required to homogenize the MI if it did not originally trap a single homogeneous silicate melt phase (Klébesz et al., 2015; Student and Bodnar, 2004). Anomalously high homogenization temperatures can also result if the MI original trapped a silicate melt plus a mineral inclusion (see Figure 1-15 in Bodnar and Student, 2006). Small minerals trapped along with melt might be easily misidentified as daughter crystals, although this interpretation can be ruled out by comparing the final quenched glass compositions because MI containing trapped solid(s) will be enriched in components that are major constituents of the trapped mineral phase(s) (e.g., P₂O₅ enrichment if the co-trapped mineral inclusion is apatite). Finally, homogenization temperatures in excess of trapping temperatures will result during re-heating if an MI has been affected by leakage after trapping (see Figure 1-3, D and E in Bodnar and Student, 2006). This last possibility can often be ruled out with careful petrographic analysis of the studied MI. Even though it is important to understand which factors could have affected the MI analyzed here to produce elevated homogenization temperatures, the overheating observation highlights the importance of performing heating runs through kinetic experiments if the correct (or approximate) temperature of trapping is required (Danyushevsky et al., 2002a). An additional consideration is that heating stage experiments are performed at atmospheric pressure. Because the phenocryst host precipitated at pressures higher than ambient (1 atm) pressure, the pressure in the MI at ambient laboratory pressure would necessarily be lower than that at trapping owing to the lower confining pressure, thus requiring heating to temperatures higher than the formation temperature to produce a single homogeneous melt phase.

In addition to overheating, post-entrapment loss of FeO from the MI could have contributed to the observed depletion in FeO_{tot}. In particular, a few MI, which were not heated in the laboratory, show low FeO_{tot} concentrations relative to the differentiation trend defined by bulk rocks, suggesting diffusive Fe loss. MI data from the literature also suggest that diffusive Fe loss has affected some MI from CF and IP. Esposito et al. (2011) studied samples representative of the Solchiaro eruption and reported a negative correlation between FeO_{tot} concentrations of MI and the Fo content of the olivine host. For this reason, Esposito et al. (2011) corrected MI compositions for diffusive Fe loss, and here we use the corrected compositions. Similarly, Mangiacapra et al. (2008) studied representative samples of Fondo Riccio and Minopoli2 eruptions and reported a group of MI showing FeO_{tot} < 1 wt%, which suggests some MI were affected by Fe loss. It is important to note that the Fe-poor MI reported by Mangiacapra et al. (2008) do not show anomalous concentrations for the other major elements. In addition, MI data from the literature show a wide range of FeO_{tot} concentrations for SiO₂ <55 wt%, and more evolved MI show FeOtot concentrations that are consistent with the bulk rock FeOtot versus SiO₂ trend, indicating that more evolved MI are less affected by Fe loss/gain. Because MI examined here show evidence that the original MI composition has been modified either by diffusive Fe loss or overheating, we question whether volatile contents obtained from the MI are representative of CF and IP pre-eruptive melts. The three overheated MI from the Fossa Lupara eruption studied here show the lowest volatile contents among all the MI considered (including the MI data from the literature), supporting the interpretation that Fe-poor MI and MI that were overheated in the laboratory should be avoided when studying volatile evolution in magmatic systems.

Considering data from this study and from the literature, not only do MI from CF and IP show evidence for Fe loss, but also some MI show evidence that the Fe concentration has increased. For instance, a group of MI hosted in olivine from the Solchiaro eruption (Mormone et al., 2011) shows higher FeO_{tot} concentrations relative to the trend defined by bulk rock compositions (Fig. 5 b). These MI were not reheated in the laboratory. It is important to note that the Fe-rich MI reported by Mormone et al. (2011) are also depleted in MgO. In particular, the MgO concentrations of the MI reported by Mormone et al. (2011) range from 4.2 to 6.5 wt%, with three MI showing MgO from 0.5

 to 1.7 wt% (see Table 1 by Mormone et al., 2011), values that are much lower than the respective bulk rock compositions (8.58 wt%; sample Pro7/11 by De Astis et al., 2004). Mormone et al. (2011) interpreted the MI based on EMP data, arguing that the correction for PEC was not necessary. Moreover, Fe-rich and Mg-poor MI described by Mormone et al. (2011) are difficult to reconcile based on PEC because, when olivine crystallizes on the MI wall, both the MgO and the FeO_{tot} contents of an MI should decrease because the FeO content of the olivine host that crystallizes on the wall is generally higher than the FeO_{tot} content of the initially trapped melt.

Different processes can be proposed to explain the enrichment in FeO_{tot} of a MI. First, the Fe-rich MI can result from Fe diffusing into the MI from the olivine host during re-equilibration due to natural overheating and melting of some olivine from the MI wall. In fact, as more olivine component is added to the MI, the melt must decrease its Mg# to be in equilibrium with its host (Danyushevsky and Plechov, 2011 and references therein). For the same reason, Fe gain will be accompanied by Mg loss. Second, natural overheating can cause dissolution of a pre-existing Fe-oxide. In their study of rehomogenized MI hosted in olivine from scoria and basaltic lavas, Rowe et al. (2006) reported that several MI show higher FeO_{tot} contents relative to bulk rocks and suggested two explanations (1) dissolution of olivine host and (2) dissolution of co-trapped mineral inclusions such as chromite, sulfide, and magnetite. In the case of the Fe-rich MI from CF and IP, the Fe gain can be explained by natural overheating of MI originally containing co-trapped chromite. This natural overheating could be due to less evolved/hotter magma mixing with the olivine-bearing magma or to olivine sinking to hotter levels of the magma reservoir. These processes are consistent with reverse zoning of olivine as reported in several studies (e.g., D'Antonio and Di Girolamo, 1994) and the presence of chromite inclusions in olivine from Solchiaro (Esposito et al., 2011). The Fe-rich MI from CF and IP show significantly lower SiO₂ compared to other MI from these locations, and the SiO₂ vs Al₂O₃ trend points towards chromite composition, supporting an interpretation that melting of a co-trapped chromite is responsible for the elevated Fe contents. It is also important to note that some of the Fe-rich MI were defined by Mormone et al. (2011) as exhibiting "high" or "low" degrees of crystallization. An

enrichment of FeO_{tot} can result from measuring a heterogeneous ("high" or "low" crystallized MI) material containing Fe-oxides.

TiO₂ variability of less evolved MI

In this study, MI show TiO_2 contents spanning a wide range, particularly for less evolved MI that vary from ~0.5 to ~1.7 wt% TiO_2 . This behavior is consistent with the wide range in TiO_2 concentrations of MI reported in other studies (Cannatelli et al., 2007; Esposito et al., 2011; Mormone et al., 2011). In particular, Esposito et al. (2011) reported TiO_2 -rich MI containing up to ~2.4 wt% TiO_2 and TiO_2 -poor MI with concentrations as low as 0.4 wt%, and interpreted these anomalies to be the result of diffusion-mixing reaction in the mush zone. In contrast to MI, TiO_2 concentrations of less evolved bulk rocks at CF show less variation for the same degree of differentiation (Fig. 2 d). It is worth noting that TiO_2 and SiO_2 show positive trends for less evolved IP bulk rocks, while the bulk rocks of CF show a quasi-horizontal TiO_2 vs. SiO_2 trend (see Fig. 2 d). One interpretation is that this difference indicates that crystallization of Ti-magnetite started earlier in the evolution of CF magmas compared to magmas associated with IP.

1821 990

Anomalous plagioclase-hosted MI from the Bacoli eruption.

As reported in the results section, three MI hosted in plagioclase from the Bacoli eruption do not adhere to most of the differentiation trends defined by bulk rock compositions (Fig. 2 a to e). The MI are Qz-normative, which is rare for melts of CF and IP. The origin of these MI may be interpreted in three ways: (1) the melt may have been locally affected by dissolution-reaction-mixing (DRM) (Danyushevsky et al., 2004 and references therein), (2) the plagioclase containing these MI may be xenocrystic and formed in a different (temporal and/or spatial) part of the overall magmatic system, and (3) the melt in plagioclase may be representative of the magma chamber/country rock interface. It is important to note that these three MI show lower major oxide totals relative to the other MI of this study (from 89.6 to 94.4 wt%). Unfortunately, we cannot assess the origin of these anomalous MI at this time.

1842 1003

Summary of the major element anomalies observed in MI data

In summary, the comparison between MI data and whole rock data indicates that some MI show anomalous compositions that do not follow the bulk rock trend, and these compositions cannot be explained by the main differentiation trend. The anomalous MI compositions cannot be corrected by simply adding aliquots of mineral host back into the melt (PEC correction) or by subtracting the host mineral composition from the melt composition (host dissolution correction). MI showing anomalous compositions either trapped a melt that was not in equilibrium with the host (DRM or boundary layer processes), or the composition was modified by processes other than simple PEC or host dissolution after trapping. For these reasons, we conclude that anomalous MI likely record volatile contents that are not representative of the melt that was in equilibrium with the growing phenocryst host. Moreover, most of the processes invoked to produce anomalous MI can also affect the volatile concentrations of melt (glass) owing to the dependence of volatile solubility on the major element composition of melts (Papale et al., 2006; Shishkina et al., 2010). In addition, trapping of apatite inclusions within the MI as a component of DRM can affect the Cl, F, and H₂O concentration of the melt. We recommend that MI showing anomalous major element concentrations should not be selected for volatile analysis because the volatile concentrations of these MI are likely not representative of the magmatic system. If the major element composition of the MI is not known, one cannot know that the MI composition is anomalous, and, thus whether the volatile content of that MI is representative. Therefore, it is fundamental that each MI is analyzed to determine major element composition before it is analyzed for volatiles. Even though this study is focused on CF and IP volcanic fields, anomalous MI are reported in many other volcanic systems (Danyushevsky et al., 2004 and references therein), and these same conclusions and recommendations apply to all such anomalous MI.

In the following sections, we interpret and discuss the volatile budgets of MI from this study and from the literature. We do not consider MI showing anomalous major element compositions in this assessment. Similarly, we exclude any MI from the literature for which major element compositions are not reported. Additionally, MI hosted in plagioclase were not included because the three MI hosted in plagioclase that we analyzed all showed anomalous compositions relative to the bulk rocks. It is important of note that our data filtering does not eliminate MI affected by PEC but only

 MI that could not be corrected by simply adding or subtracting the mineral host to the anomalous MI. In the following discussion we use ratios of elements that are incompatible with the host because these ratios should not be affected by PEC (e.g., Lima et al., 2003). Also, as noted above, while it is possible to apply relatively robust PEC corrections for MI hosted in olivine (Danyushevsky and Plechov, 2011), reliable models are not available to correct for PEC for MI hosted in clinopyroxene and feldspar.

Evolution of volatile concentrations of MI

Several studies reported bubble-bearing MI in samples from CF and IP, but fewer studies have identified which MI (bubble-bearing or bubble-free) correspond to a specific volatile analysis. One exception is the work of Esposito et al. (2011), who identified each MI as either bubble-bearing or bubble-free before exposing the MI at the surface of the host for analysis. Based on recent studies (e.g., Aster et al., 2016; Moore et al., 2015), it is not possible to determine if the reported volatile content of an MI represents the actual volatile content of the trapped melt or represents only a portion of the total volatile budget in the original melt if the type of MI (bubble-bearing versus bubble-free) is not reported. Thus, the following discussion relies only on data from bubble-free MI that do not show anomalous major element compositions.

By including only bubble-free MI data in this interpretation, it is not necessary to account for any volatiles that might have been lost to the bubble after trapping of a single homogeneous silicate melt phase. Even though bubble-free MI may have been affected by H loss, we argue that extensive diffusive H loss would lead to the formation of a vapor bubble (Steele-MacInnis et al., 2017). Thus, the lack of a bubble supports the interpretation that H loss was not significant for the bubble-free MI considered here. Moreover, we do not observe any correlation between CO₂ and H₂O as would be expected if all MI started with the same volatile contents, and each MI experienced different degrees of H loss (Bucholz et al., 2013). Also, If diffusive H loss is only controlled by redox reactions of the MI-host system (Danyushevsky et al., 2002a), then it is unlikely that a significant amount of H₂O was lost from the MI because magnetite that would be produced by this process it is not observed in the studied MI.

Finally, it is important to note that filtering the MI data based on the presence or absence of a bubble may mask the complete variability represented by all the MI. In fact, it is more likely that a volatile-rich MI will form a bubble after trapping, compared to an MI that is relatively volatile-poor. Considering only bubble-free MI may unintentionally exclude some MI that trapped melts with higher volatile contents. We suggest that the best practice would be to analyze the volatile contents of the MI bubble and correct the original volatile content using methods described in the literature (e.g., Esposito et al., 2011; Mironov et al., 2015; Moore et al., 2015). In the next section, we interpret the H₂O-CO₂ data of MI from CF and IP volcanic fields considering only bubble-free MI.

H₂O and CO₂ degassing, crystallization and mixing of basaltic-trachybasaltic magmas

The volatile content of the glass phase in MI can be used as a geobarometer because CO₂ and H₂O solubilities in silicate melts are highly pressure dependent (Blundy and Cashman, 2008). A large range in CO₂ contents of MI, combined with a narrow range of H₂O concentrations, is often interpreted to reflect MI trapping along a degassing (ascent) path because CO₂ is lost from the melt early and before significant H₂O loss occurs. In this scenario, MI are trapped during crystallization of phenocrysts at different depths (pressures) as the magma ascends through the crust. Alternatively, different phenocrysts might trap MI from essentially the same silicate melt at various depths within a stagnant plumbing system. Thus, H₂O-CO₂ systematics within a single eruptive event can support or dismiss the hypothesis that crystallization in the plumbing system occurred under volatile-saturated conditions, and if the crystallization occurs over a large or narrow range of pressure (depths.)

For CF and IP, MI data from individual eruptions are often interpreted to represent trapping during ascent as the magma degasses (Arienzo et al., 2016; Arienzo et al., 2010; Cecchetti et al., 2001; Cipriani et al., 2008; Esposito et al., 2011; Esposito et al., 2014; Mangiacapra et al., 2008; Moretti et al., 2013; Mormone et al., 2011) and that crystallization occurred under volatile-saturated conditions, and over a large range of pressures. As reported above, earlier studies interpreted the variability in H₂O vs. CO₂ systematics observed in MI as a combination of trapping at various depths along a

degassing path, combined with episodic CO₂ fluxing events (Arienzo et al., 2016; Arienzo et al., 2010; Mangiacapra et al., 2008; Moretti et al., 2013; Mormone et al., 2011). However, we emphasize that "shrinkage" bubbles are often reported in MI from studies advocating for CO₂ fluxing, and most workers do not distinguish between bubble-free and bubble-bearing MI, nor do they account for volatiles contained in the bubble. Because these studies do not discuss these issues, their interpretations concerning degassing and CO₂ fluxing cannot be tested because the true, pre-eruptive volatile contents of the melt are unknown. In fact, Esposito et al. (2011), Hartley et al. (2014), Moore et al. (2015) and Esposito et al. (2016) all demonstrated that the bubble may contain as much as 99% of the originally trapped CO₂. For this reason, the discussion that follows is based on data from bubble-free MI only.

When we consider bubble-free MI of basaltic and trachybasaltic composition, the distribution of H₂O-CO₂ data shows less variability relative to data from all types of MI (bubble-free and bubble-bearing). The maximum CO₂ content of bubble-free MI (1248 ppm) is lower than that of bubble-bearing MI (1706 ppm). Also, the H₂O content of bubble-free MI shows less variability relative to the bubble-bearing group. Thus, the large variability in CO₂ contents combined with the narrow range of H₂O contents of bubble-free MI is more pronounced relative to bubble-bearing MI, suggesting that the magma was volatile-saturated and that olivine crystallized at various depths. For this discussion, we consider bubble-free MI as well as one bubble-bearing MI for which the original CO₂ content was corrected based on Raman analysis of the vapor bubble (MI RESC2-O26-MI3; Esposito et al., 2011).

In order to test the hypothesis that trapping of MI occurs during fractional crystallization under volatile-saturated conditions at various sub-volcanic depths, we computed fractional crystallization paths using the rhyolite-MELTS code (Ghiorso and Gualda, 2015). We considered MgO-rich bulk rocks from the IP and noted that the Al_2O_3/K_2O ratios of these rocks span a wide range (Figs. 6 and 7). We performed fractional crystallization calculations using rhyolite-MELTS to test if the general trend in Al_2O_3/K_2O vs. MgO systematics of bulk rocks is consistent with trends predicted during fractional crystallization. The first question we addressed was whether the previously reported MgO-rich bulk rock compositions can be assumed to represent liquid

compositions. D'Antonio and Di Girolamo (1994) and D'Antonio et al. (1999a) noted that, for some of the bulk rocks, oliving phenocrysts may represent cumulus material and would thus be considered xenocrysts. In the studies by D'Antonio and Di Girolamo (1994) and D'Antonio et al. (1999a), the olivine showing the highest forsterite content was compared to the olivine composition predicted using various partition coefficients, KD_{Fe-Mg}, following the method of Rhodes (1981). These calculations indicated that olivine compositions in some of the bulk rocks were sometimes significantly different from the predicted olivine compositions, but the forsterite content of olivine never exceeded the calculated values (Table 3). Using the same bulk rock data from the literature, we compared the olivine composition calculated at the liquidus using rhyolite-MELTS with the observed data, as reported in Table 3. We noted that the olivine compositions of the bulk rocks are comparable to the olivine composition predicted by rhyolite-MELTS, assuming 200 MPa, NNO, and H₂O-CO₂ saturation (see discussion below). In particular, bulk rock sample Apr22 shows Fo_{max} of 86.6. The rhyolite-MELTS predictions showed that a liquid composition equivalent to Apr22 is in equilibrium with Fo_{87.3} at its liquidus (Table 3). D'Antonio and Di Girolamo (1994) reported that bulk rock Apr22 contains 11 vol% phenocrysts (olivine plus clinopyroxene). In other samples olivine ranges from 2.2 to 12.8 vol\%, and clinopyroxene ranges from 2.5 to 7.6 vol\%. We used the rhyolite-MELTS predictions as a starting composition to evaluate the consistency of predicted volume proportions of olivine and clinopyroxene and compared these values to values reported in the literature. According to these calculations, the magma should contain 12 vol% phenocrysts (olivine plus clinopyroxene) and 88 vol% liquid after ~115°C cooling. At this stage, the magma contains ~4 vol% olivine and ~8 vol% clinopyroxene. The liquid would initially be in equilibrium with an Fo₈₇ olivine and the final olivine to crystallize would be Fo_{84} . These results are consistent with the information reported in the literature and support the interpretation that trapping of MI occurs during fractional crystallization.

We selected five starting compositions for rhyolite-MELTS calculations: three bulk rock compositions, and two MI compositions that were corrected for PEC. Sample Apr18 (D'Antonio and Di Girolamo, 1994) was selected because this bulk rock composition shows both the highest MgO content and highest Al₂O₃/K₂O ratio. We also

selected Apr22 (D'Antonio and Di Girolamo, 1994) because this rock showed the best match between the maximum forsterite content of olivine and the composition of olivine calculated to be in equilibrium with the rock composition on its liquidus (Table 3). In addition, we selected an initial composition that was based on the MI exhibiting the highest Al₂O₃/K₂O ratio [RESC5-O5-MA; Esposito et al. (2011)]. It is important to note that while bulk rock compositions can be affected by secondary processes (such as post depositional water-rock interactions) or entrainment of xenocrysts, the compositions of MI should not be affected by entrainment of xenocrysts into the surrounding liquid. As described by Fowler et al. (2007), we started with the uncorrected composition of MI RESC5-O5-MA (Esposito et al., 2011) and added aliquots of olivine host until the MI composition was in equilibrium with the host olivine measured adjacent to the MI. This allowed us to correct the MI composition for the effects of PEC. The fourth composition selected was bulk-rock sample Ps3 reported by Di Girolamo et al. (1984) because this composition shows relatively high MgO and relatively low Al₂O₃/K₂O. Finally, we selected the uncorrected composition of MI RESC3-O9-MA described by Esposito et al. (2011). This MI showed relatively low Al₂O₃/K₂O and the host olivine had a high forsterite content. We applied the same correction for PEC that was applied to MI RESC5-O5-MA.

Using these five initial compositions, we ran the models using specific starting conditions. For the bulk rocks (Apr18, Apr22 and Ps3), we calculated the liquid line of descent using rhyolite-MELTS, assuming H₂O (1.25 wt%) and CO₂ (1400 ppm) contents based on the H₂O-CO₂ systematics of bubble-free MI hosted in olivine. We assumed 200 MPa as the initial pressure, consistent with solubility experiments under volatile-saturated conditions for a trachybasaltic melt at the H₂O-CO₂ concentrations of our models (Fanara et al., 2015). As shown in Fig. 8, isobaric crystallization in the absence of volatile saturation produces trends that are inconsistent with the mafic MI data. Specifically, during crystallization at volatile-undersaturated conditions, both H₂O and CO₂ concentrations increase simultaneously. Conversely, the calculated trends based on bubble-free, basaltic-trachybasaltic MI data are consistent with polybaric crystallization under volatile-saturated conditions. For the model using the MI composition as the starting composition (PEC-corrected MIs RESC5-O5-MA and RESC3-O9-MA), we

normalized the measured volatile contents to 100%, resulting in 1.21 wt% H₂O and 954 ppm CO₂ for RESC5-O5-MA, and 1.13 wt% H₂O and 479 ppm CO₂ for RESC3-O9-MA, respectively. The pressure at volatile saturation (thus, the initial pressure in the models) was 160 MPa for RESC5-O5-MA and 90 MPa for RESC3-O9-MA.

Effect of starting composition. The first step was to test if the three high-Al₂O₃/K₂O starting compositions (Apr18, Apr22, and RESC5-O5-MA) could reproduce the geochemical trends defined by bulk rocks, the phases that crystallized, and the compositions of the phases. For this test, we assumed isobaric crystallization and a fixed oxidation state. The results are shown in Figs. 6, 9-11. The three starting compositions do not reproduce consistent geochemical trends for MgO and SiO₂/CaO vs. Al₂O₃/K₂O (Fig. 6a and d). The range of olivine compositions is consistent with the range from previous studies (Fig. 12). However, the calculated trend in Fo mol\% vs. Al₂O₃/K₂O space does not agree with data from the bubble-free MI (Fig. 12). The clinopyroxene compositions predicted by rhyolite-MELTS show a good match with measured compositions (Fig. 9a), but the calculated feldspar compositions do not reproduce the observed alkali-feldspar composition (Fig. 10a). On the TAS diagram, only data from sample Apr22 produces a trend that is consistent with the "normal" MI compositions from the literature and from this study, but all three starting compositions reproduce the trachybasalt-shoshonitelatite-phonolite/trachyte bulk rock trend (Fig. 11a). It is important to note that the MI data plotted in the TAS diagram can be used to track the stage in the differentiation sequence that the host phase for each MI crystallized, and we compared the relative timing of olivine, clinopyroxene and sanidine formation predicted by rhyolite-MELTS with results based on MI. For the Apr22 experiment, sanidine crystallization was predicted only during the last stages of crystallization, which does not match with compositions of MI hosted in sanidine. In addition, rhyolite-MELTS predicts that clinopyroxene crystallization ended earlier than sanidine crystallization, and that these two phases did not crystallize in equilibrium, in disagreement with petrographic analysis of more evolved rocks (e.g., Di Girolamo et al. 1984). Trends predicted by rhyolite-MELTS for MI and Apr18 starting compositions do not reproduce the observed crystallization trend of alkali-feldspar.

We also examined if the low-Al₂O₃/K₂O bulk rock composition and/or MI compositions would produce a better match between rhyolite-MELTS predictions and data from natural samples. For MgO and SiO₂/CaO vs. Al₂O₃/K₂O, the predicted fractional crystallization trends are consistent for the general bulk rock data for $Al_2O_3/K_2O < 7$ (Fig. 13). As shown in Figs. 7a and d and 13a, the match applies not only to bulk rock data, but also to MI data. What is even more striking is the match between rhyolite-MELTS predictions and "normal" MI in the TAS diagram. Experiments assuming Ps3 and RESC3-O9-MA as the starting composition better predicted the occurrence of sanidine crystallization, relative to calculations based on Apr22 and Apr18 and RESC5-O5-MA reported above. In addition, RESC3-O9-MA experiments predicted clinopyroxene crystallization throughout the fractionation trend and that clinopyroxene coexisted with sanidine. The only mismatch for this run is that olivine crystallization ended later in the differentiation sequence than is observed in the samples. However, as shown in the supplementary material (Appendix Table C), the mass fraction of olivine crystallizing as the path moves through the shoshonite field continuously decreases. Thus, predictions based on Ps3 and RESC3-O9-MA starting compositions are in better agreement with observations, compared to Apr22, Apr18, and RESC5-O5-MA for both the TAS trend and mineral phase appearance (Fig. 11d). The same conclusion can be drawn for the feldspar compositions (Fig. 10d). The plagioclase compositions predicted by Ps3 and RESC3-O9-MA starting compositions are more representative of plagioclase compositions reported in the literature. In addition, the trends extend toward a higher sanidine component and show better agreement with sanidine compositions from the literature. The trend predicted for Fo mol% vs. Al₂O₃/K₂O, assuming Ps3 and RESC3-O9-MA starting compositions, is consistent with several of the MI compositions (Fig. 12).

Effect of pressure (depth) evolution during crystallization. In order to better understand if crystallization occurred while the magma was ponded in the subsurface (at a constant pressure) or occurred in the plumbing system as the magma ascended through the crust, we ran rhyolite-MELTS experiments assuming both isobaric and polybaric trends. We first selected sample Apr18 and assumed isobaric crystallization under volatile-saturated conditions at 200 MPa. In addition, we ran the same model under

polybaric conditions with crystallization occurring as the pressure dropped from 200 to 14 MPa. The oxidation state was fixed by the NNO buffer in both examples. We note that the polybaric model improves the fit for alkali feldspar compositions (Fig. 10b). However, the TAS trend does not improve, and sanidine crystallization is predicted to occur later than is suggested by MI hosted in sanidine (Fig. 11b). In addition, the predicted SiO₂ concentration extends toward rhyolitic liquid. It is worth noting that for polybaric conditions, rhyolite-MELTS does not predict the formation of Ca-Ti-rich clinopyroxene.

We also considered Ps3 as the starting composition and compared the isobaric trend at 200 MPa with two polybaric trends. The polybaric model conditions were defined based on H₂O vs. CO₂ systematics (Fig. 8). The first polybaric trend assumed a 0.5 °C/MPa path from 200 MPa to 5 MPa, at which point the CO₂ content of the melt was 2 ppm. After the pressure reached 5 MPa, continued fractional crystallization was assumed to be isobaric. The second polybaric model assumed a 0.1 °C/MPa path from 200 MPa to 11 MPa, or until the CO₂ concentration in the melt was 9 ppm. Continued crystallization was assumed to be isobaric at 11 MPa. As can be seen in the SiO₂/CaO vs. Al₂O₃/K₂O trends, the polybaric models provide a better fit to the bulk rock and MI data (Fig. 7b and e). The difference between isobaric and polybaric conditions is not significant for the TAS trends. However, differences are observed during the final differentiation steps, and sanidine appearance occurs at the limit of the field defined by MI hosted in sanidine. The polybaric model shows a better fit to the sanidine compositions from the literature (Fig. 10e). Importantly, Ca-Ti-rich clinopyroxene is not predicted in two of the polybaric crystallization models (Fig. 9e).

Effect of oxidation state on predicted trends. The final test using rhyolite-MELTS examined potential effects of oxidation state on the differentiation trends by varying oxygen fugacity over the range from QFM-2 and QFM+2. We assumed isobaric crystallization and Apr22 as the starting composition. We recognize that oxidation state is expected to vary during extended periods of crystal fractionation (e.g., Moussallam et al., 2014), but we have not conducted experiments that allow the oxygen fugacity to vary during a crystallization sequence.

Our results for Apr22 suggest that oxidation state does not significantly affect the various geochemical trends predicted by rhyolite-MELTS that were tested here. Trends for MgO and SiO₂/CaO vs. Al₂O₃/K₂O show similar patterns that do not match the bulk rock trends (Fig. 6c and f). The various oxidation states tested did not reproduce TAS trends during crystallization of clinopyroxene for the most evolved compositions (Fig. 11c and f), and feldspar compositions predicted by the models do not improve the match with the real data (Fig. 10c).

We also selected sample Ps3 (low Al₂O₃/K₂O ratio) as the starting composition with a range of oxidation states from QFM-2 and QFM+2. The different oxidation states have little effect on the liquid trend during the initial differentiation step (Fig. 7c and f). The match between predicted feldspar compositions and feldspar compositions from the literature does not improve (Fig. 10f). Varying the oxidation state did affect the trajectory of the liquid on the TAS diagram and the trends for different oxidation states delimit a field consistent with the MI data (Fig. 11f), an observation that is consistent with an evolving oxidation state during fractional crystallization.

Summary of rhyolite-MELTS modeling results. Selecting initial compositions based on bulk rocks and MI with high MgO concentrations and Al₂O₃/K₂O ratios does not yield trends consistent with the analytical data. In contrast, it is reasonable to infer that samples Ps3 (bulk rock) and RESC3-O9-MA (MI) represent mafic liquids that could produce geochemical trends toward trachytic and phonolitic melts during fractional crystallization. The consistency between bulk rock data, data from bubble-free MI, and rhyolite-MELTS predictions supports this hypothesis. In addition, the phases predicted to form during crystallization, and their compositions, are consistent with the literature data. Furthermore, the TAS trends based on "normal" MI and the correlation between MI composition and host mineral match with rhyolite-MELTS predictions. In particular, the predicted order of appearance of mineral phases is in good agreement with the phase fields defined by the MI compositions and the compositions of the MI hosts. The best agreement between the model results and the analytical data is obtained when the crystallization path is polybaric, especially for sanidine compositions and the predicted absence of Ca-Ti-rich clinopyroxene. The oxidation state does not appear to significantly influence the results.

To compare bubble-free MI data with rhyolite-MELTS trends and bulk rock data, we compared ratios of olivine-incompatible elements (e.g., SiO₂/CaO and Al₂O₃/K₂O) rather than using absolute concentrations of elements in MI (Fig. 13a and b). Comparing olivine-incompatible element ratios minimizes the effect of PEC (Lima et al., 2003) and these ratios are independent of methods used to correct the MI compositions (e.g., Danyushevsky et al., 2002a). As shown by the SiO₂/CaO vs. Al₂O₃/K₂O trends in Fig. 13, the major element ratios suggest that bubble-free MI cannot be explained solely by a single fractional crystallization trend starting from a single primitive melt. As for bulk rocks, a group of MI (hereafter referred to as Mixed-MI) forms a trend consistent with a mixing model (Fig. 14), and another group of bubble-free MI (hereafter referred to as Melt-1 MI) is consistent with simple fractional crystallization from Melt-1. These groups of bubble-free MI overlap with the same two groups of bulk rocks that can be identified based on geochemistry (Fig. 13a). It is important to note that the overlap in bulk rock composition and compositions of several MI indicates that the examined bulk rocks can be assumed to be representative liquids of magmas associated with volcanism at CF and PI. Consequentially, SiO₂/CaO or MgO vs. Al₂O₃/K₂O trends of bulk rocks cannot be the result of plagioclase crystal assimilation. Some of the trace element ratios of bubble-free MI show the same behavior as ratios of major elements, showing two distinct trends that cannot be produced by simple crystallization from a single starting composition represented by either Melt-1 or Mixed-MI and bulk rocks showing high-Al₂O₃/K₂O. For instance, Rb, Pb, Ba, U, Th, Nb, Ce, La, Pr, and Ta show the same trend as K₂O in the SiO₂/CaO vs. Al₂O₃/K₂O diagram. The Mixed-MI form a different trend relative to Melt-1 MI (Fig. 14a). The same behavior is observed when trace element ratios are plotted against each other (e.g., Ba/Sr vs. Yb/Rb and Eu/Rb Fig. 14 b and c). We used a simple binary mixing model based on Albarède (1996) assuming MI compositions RESC5-O5-MA (for Mixed-MI) and RESC3-O9-MA (for Melt-1) as end members. Spider diagrams also highlight the difference between Mixed-MI and Melt-1 MI

Spider diagrams also highlight the difference between Mixed-MI and Melt-1 MI (Fig. 15). For instance, the Primitive Mantle-normalized spider diagram (Sun, 1980) shows that the normalized LILE are generally lower for Mixed-MI, but that the same Mixed-MI show generally higher normalized HFSE (Fig. 15 c). Comparing the less evolved Melt-1 MI (RESC3-O9-MA) with the mixed MI that shows the strongest

evidence of mixing (RESC5-O5-MA) highlights the difference in trace element contents, such as for Rb, P, Eu, and Yb (Fig. 15c). These two MI are hosted in olivine with similar forsterite content and, therefore, crystal fractionation cannot be invoked to explain the difference in the trace element patterns. Similar observations are suggested from the REE spider diagrams (Sun and McDonough, 1989), whereby Mixed-MI show lower normalized LREE but generally higher normalized HREE, relative to Melt-1 MI (Fig. 15b). It is important to note that for intermediate REE, the two groups of MI overlap, with more erratic behavior shown by Mixed-MI. These observations indicate that the difference between these two groups cannot be explained by simple fractional crystallization but, rather, are explained by mixing of two different primitive melts. This is in agreement with D'Antonio et al. (2007), who suggested that primitive magmas of differing composition can be generated by contamination of the mantle source by various proportions of slab-derived fluids or by sediment-derived melts.

The systematics of Cl and S are also consistent with the mixing model proposed in this study. Here again, the Mixed-MI form well-defined trends and diverge from the general trend determined by Melt-1 MI (Fig. 16). This behavior can be observed in the Cl/Yb vs. Al₂O₃/K₂O plots, where the Mixed-MI show lower Cl/Yb and higher Al₂O₃/K₂O compared to Melt 1 MI (Fig. 16a). This suggests that, not only is Mixed-MI different from Melt-1 in terms of major and trace element trends, but also differs in terms of volatile contents.

To further test the hypothesis that mafic magmas beneath IP crystallize under volatile-saturated conditions and over a range of pressures, we first compared the volatile ratios (e.g., H_2O/CO_2) of bubble-free MI with the composition of the olivine hosts (Fig. 17a). It is important to note that the composition of the host was measured ~40 µm away from the MI/host interface (Esposito et al., 2011). No correlation is observed between H_2O/CO_2 ratio and the mol% Fo of the host.

The H₂O/CO₂ versus mol% Fo systematics could be explained by assuming different pressure-temperature evolution paths (Fig. 17a). A possible explanation of the different pressure-temperature paths is that feeding conduits of different geometries (e.g., thickness) could transport magmas of different temperatures to the same depth (Spera, 1980). Thus, cogenetic magmas of slightly different temperatures may occur at the same

depth below a volcano. This scenario is consistent with the "mush column" model proposed by Marsh (1996). As summarized by Putirka (2017; see his Fig.1a and c) and by Cashman et al. (2017), the plumbing system beneath a volcano represents a mosaic of scattered bodies which may or may not be connected to each other. The most likely result is that co-genetic magma pools in a plumbing system may follow different pressure-temperature paths, consistent with the variability of volatiles found in MI hosted in olivine that show the same forsterite contents (Fig. 17a). This scenario is also consistent with the presence of anomalous MI in olivine as discussed by Danyushevsky et al. (2004).

Volatile ratios were plotted versus Al₂O₃/K₂O to test for consistency between volatile content of MI and major element compositions of MI. The distribution of bubble-free MI data in the H₂O/CO₂ versus Al₂O₃/K₂O diagram is plotted along the same polybaric crystallization trends. As was observed for major, trace and other volatile element ratios, H₂O/CO₂ ratios of Melt-1 MI are consistent with polybaric crystallization trends of Melt-1 and Mixed-MI, which define a mixing trend (Fig. 17b).

We further investigated the chronology of the magmatic processes to assess whether crystal fractionation starting from Melt-1 occurred before or after mixing by examining textural and petrographic relationships of olivine and MI. First, we note that reverse zoning of olivine phenocrysts that were erupted in the IP is reported by many researchers (e.g., D'Antonio and Di Girolamo, 1994). Secondly, we re-evaluated data reported by Esposito et al. (2011) to search for correlations between type of zonation of the host olivine crystals of the bubble-free MI reported in their Table 3 and the type of MI defined here. Also, we investigated the correlation between the position of the bubble-free MI within the host and the type of MI (Mixed-MI and Melt-1 MI) as defined here. This effort showed that 73% of the Mixed-MI are hosted in zoned olivine crystals and half of the Melt-1 MI are hosted in unzoned olivine phenocrysts. No Mixed-MI are hosted in the cores of olivine phenocrysts while the majority of Melt-1 MI are, indeed, hosted in olivine cores (Table 4). This textural and petrographic information suggests that fractional crystallization of Melt-1 began in the various magma pools below the volcano before the mixing event associated with the later Solchiaro eruption.

In conclusion, taken together, the volatile, major and trace element compositions of bubble-free MI, host-mineral compositions, bulk rocks, and trends predicted by rhyolite-MELTS models all suggest that crystallization of melt beneath Solchiaro first occurred by simple fractional crystallization under volatile-saturated conditions at depths between ~1 and 5 km (Fig. 18a). This interpretation is consistent with other MI studies that suggest that differentiation of magmas at shallow depths beneath CF and IP, as well as in the nearby Ischia Islands, is characterized by H₂O-CO₂ volatile saturation (Arienzo et al., 2016; Arienzo et al., 2010; Cannatelli et al., 2007; Cecchetti et al., 2002-2003; Cipriani et al., 2008; Esposito et al., 2011; Fourmentraux et al., 2012; Mangiacapra et al., 2008; Mormone et al., 2011; Roach, 2005). Crystallization continued under polybaric conditions during magma ascent to shallower crustal levels. Well-constrained MI indicate that magmas in shallower reservoirs were slightly more evolved than those in deeper reservoirs, as predicted by Cashman et al. (2017). After this first stage dominated by magma ascent and crystallization, recharging by a second high-Al₂O₃/K₂O basaltic melt occurred at depths between ~1 to ~6 km (Fig. 18b). During this pre-eruptive stage, Melt-1 that had undergone varying degrees of crystallization mixed with various proportions of high-Al₂O₃/K₂O basaltic melt. Although mixing has been suggested previously based on the isotopic composition of bulk rocks from different localities and different degrees of differentiation (e.g., D'Antonio et al., 2007; D'Antonio and Di Girolamo 1994), our interpretation of mixing is based on MI and is representative of a single eruption (single location), with mixing between two near-primitive magmas showing similar degrees of differentiation. Most importantly, well-constrained bubble-free MI that record evidence of crystallization and mixing provide a chronological sequence of the magmatic processes occurring beneath Solchiaro. The recharging magma did not undergo extensive crystallization. In addition, well-constrained MI show no evidence for CO₂ fluxing as reported in other MI studies (e.g., Moretti et al., 2013). In fact, normal and bubble-free basaltic and trachybasaltic MI show that the H₂O contents remained essentially constant (within analytical error). In other words, well-constrained mafic MI show no evidence that H₂O/CO₂ decreases systematically with crystallization indicators (Fig. 17). Our results cannot disprove the CO₂ fluxing interpretation, but neither do the MI data support such an interpretation.

H₂O and CO₂ degassing during crystallization of trachytic magmas

After considering bubble-free MI from basaltic and trachybasaltic magmas, we investigated the bubble-free MI of more evolved magmas that likely originated from the differentiation of the same trachybasaltic melt. Ten bubble-free MI were analyzed in this study, nine of them are representative of the NYT magma and the other is from the Solfatara eruption. Seven bubble-free MI are hosted in sanidine and the three are hosted in clinopyroxene. The low number of bubble-free MI analyzed is because bubble-free MI large enough for SIMS analysis are rare in the studied phenocrysts. The bubble-free MI from the NYT and Solfatara samples were likely trapped during isobaric crystallization at a relatively high pressure, ca. 200 MPa, followed by polybaric crystallization during ascent (Fig. 17c). This interpretation is consistent with the trend predicted by rhyolite-MELTS, starting from Melt-1 composition as reported above. Isobaric crystallization of a trachybasaltic magma at ~200 MPa under volatile-saturated conditions assumed here is consistent with results of other studies (e.g., Arienzo et al., 2010). A melt zone at ~200 MPa is also suggested by geophysical data (e.g., Zollo et al. (2008), not only for CF and IP but for all of the Neapolitan volcanic area (see Moretti et al., 2013 and references therein). While our interpretation is based on only a few well-constrained MI, we demonstrated that melts with high H₂O contents can be generated during fractional crystallization, starting from trachybasaltic melts. The elevated H₂O contents have obvious and important implications for generating high-magnitude (explosive) eruptions.

The composition of the trachytic bubble-free MI can be obtained after $\sim\!66\%$ to 85% of isobaric crystallization under volatile-saturated conditions (Fig. 13b) (see also Appendix Table C). The mineral assemblage predicted by rhyolite-MELTS is consistent with the mineral assemblage of selected rock samples that are mainly composed of clinopyroxene and feldspar \pm biotite and Ti-magnetite (see Appendix Table C). We discriminated between trachytic bubble-free MI by host using ratios of elements incompatible or slightly compatible with the host (Fig. 13c and d). For instance, bubble-free MI hosted in sanidine show good agreement with rhyolite-MELTS predictions and bulk rock trends for SiO₂/CaO vs. MgO/TiO₂ (Fig. 13c). Consistently, bubble-free MI hosted in clinopyroxene show agreement with rhyolite-MELTS predictions and bulk rock

trends for SiO₂/TiO₂ vs. Al₂O₃/K₂O (Fig. 13d). It is important to note that trachytic bubble-free MI show good agreement even when ratios such as SiO₂/CaO (CaO highly compatible with clinopyroxene) and Al₂O₃/K₂O (K₂O and Al₂O₃ compatible with sanidine) are considered (Fig. 13b). These trends suggest that PEC or other modifications after trapping and before eruption were not extensive and did not significantly affect the composition of the trapped melt. The inferred low degree of PEC is also consistent with agreement between compositions of MI and the bulk rocks, and with the occurrence of bubble-free MI (Steele-MacInnis et al., 2011). CO₂ and H₂O contents are available for two bubble-free, trachytic MI from the NYT eruption. One bubble-free MI is hosted in clinopyroxene and the other in sanidine. The isobaric crystallization model is consistent with the volatile contents of bubble-free MI hosted in clinopyroxene, but not with the bubble-free MI hosted in sanidine (Fig. 16c). In order to evolve a melt with the volatile content recorded by the bubble-free MI hosted in sanidine, the system must crystallize at a lower pressure (shallower depth). Thus, our interpretation is that the last stage of crystallization for the NYT eruption occurs at shallower levels, compared to the earlier stages of crystallization. Under volatile-saturated conditions, the H₂O content of the melt can only increase if the magma evolves from trachybasalt to trachyte isobarically. With this scenario, the CO₂ content of the melt decreases and the melt becomes enriched in H₂O and the fluid exsolving from the melt becomes progressively enriched in H₂O (red dashed line in Fig. 8). The higher the pressure of isobaric crystallization, the higher the H₂O content of the evolved melts, as suggested by H₂O-CO₂-silicate melt solubility models. The higher the H₂O content of more evolved melts the greater the likelihood of a highly explosive eruption (e.g., NYT eruption), especially if crystallization occurs at relatively shallow depths where the difference between the partial molar volume of H₂O dissolved in the melt and the molar volume of H₂O-rich magmatic fluid is large (Bodnar et al., 2007). In conclusion, some of the trachybasaltic magmas must undergo extensive isobaric crystallization (from 66% to 85%) to produce the relatively H₂O-rich NYT-like magmas. These magmas can migrate to a shallower level, triggering further exsolution of fluids and crystallization of sanidine. In agreement with our data and modeling, the NYT is the most explosive eruption (VEI 6) to occur in this area in the last 23.6 ka. This interpretation is consistent with Mastrolorenzo and Pappalardo (2006), who showed that

 explosivity of eruptions at CF is mostly controlled by initial conditions in the magma chamber, including the volatile content, temperature and pressure. If the magnitude of the eruption is mainly driven by the pre-eruptive H₂O content of melts (Edmonds and Wallace, 2017; Webster et al., 2001), then extensive crystallization of a trachybasaltic magma occurring at relatively high pressure (relatively great depth) sets the stage for a later possible highly explosive eruption, because it will generate a more evolved, H₂O-rich melt.

Concluding remarks

Major element compositions of MI trapped in the most abundant crystal phases (olivine, clinopyroxene, sanidine and plagioclase) precipitating from CF and IP magmas younger than 23.6 ka, both from this study and from the literature, show compositional trends that to a large extent overlap with bulk rock compositions. Some MI show anomalous compositions, especially for Al₂O₃, P₂O₅, FeO, MgO, CaO and TiO₂. These anomalous MI can be explained through various processes, including grain scale dissolution—reaction—mixing (Danyushevsky et al., 2004), Fe loss and/or gain, and boundary layer processes. Anomalous MI exhibit volatile concentrations that likely deviate significantly from actual melt compositions. For these reasons, we suggest that all MI analyzed for volatile concentrations must also be analyzed for major elements to test for the representativeness of the trapped melt. In this study, all anomalous MI data were filtered from the dataset before interpreting volatile concentrations recorded by MI.

Another potential concern associated with determining the pre-eruptive volatile content of the original trapped melt based on MI analysis is the presence of a vapor bubble. Only a portion of the total volatile budget in the original trapped melt will be accounted for if the volatile content of the bubble is not considered (Esposito et al., 2016 and references therein), and interpretation of volatile contents based only on analysis of the glass phase of bubble-bearing MI may lead to erroneous conclusions. Thus, volatile concentrations of "normal" and bubble-free MI are shown to be more reliable monitors of volatile evolution during differentiation from trachybasaltic to trachyte magmas younger than 23.6 ka associated with the CF and IP eruptions. Major and trace element systematics, volatile contents, and petrological modeling based on "normal" and bubble-

free MI suggest that trachybasaltic magmas ascended through the crust from depths of at least ~7.5 km (~200 MPa). This depth is consistent with geophysical data reported by Zollo et al. (2008), who suggest a 1-2 km thick layer of partially molten rocks at a depth of 8 km. At \geq 7.5 km depth, trachybasalts can ascend through the crust to shallower levels while undergoing minimal crystallization under volatile saturation and pond to feed eruptions associated with relatively less-differentiated magmas, as in the case of the Solchiaro eruption (23.6 ka ago). At 7.5 km depth, the same poorly differentiated magmas undergo extensive isobaric crystallization to form trachytic-phonolitic magmas feeding eruptions such as the NYT (15 ka ago; Deino et al., 2004). During extensive isobaric crystallization, the magma could also assimilate 1%-2% crustal material (D'Antonio et al., 2007). Isobaric crystallization at ~7 km depth of the parental melt of the Fondo Riccio eruption at CF was also suggested by Cannatelli (2012) based on MI data and MELTS simulations. Extensive crystallization under volatile-saturated conditions increases the H₂O content of the magma and, in turn, increases the likelihood of generating a high magnitude (explosive) eruption, as occurred for the NYT eruption (40 km³ DRE). In another case, the trachybasaltic magmas may evolve to trachyticphonolitic magmas at shallower levels and H₂O enrichment of the magma during isobaric crystallization would be limited.

Bubble-free MI representative of magmas associated with the Solchiaro eruption suggest that mixing between trachybasaltic magmas and basaltic magmas occurred beneath the IP. One group of bubble-free MI is associated with simple polybaric crystallization from a trachybasaltic primitive melt, while another group of MI define a trend consistent with mixing between the trachybasaltic primitive magma and another basaltic primitive magma. The primitive basaltic magma shows a more moderate enrichment of elements compatible with a slab-derived fluid. The mixing occurred at depths of at least ~6 km after simple crystallization of the trachybasaltic magma and likely did not affect the shallowest levels of the plumbing system.

Finally, even though interpretations based on volatile concentrations from MI may be sometimes problematic, they provide the only direct means to investigate magmatic processes such as degassing during magma ascent and crystallization. In this

study, we show that MI provide more reliable information concerning the pre-eruptive volatile contents of magmas if the following steps are taken:

- 1- MI showing anomalous major element compositions relative to the bulk rock trends are omitted from the interpretation.
- 2- A detailed petrographic description of MI (e.g., size, shape, distance from the host edge, presence of the bubble, presence of magnetite dust etc.) should be performed to rule out processes affecting the reliability of MI such as boundary layer effects, and diffusive loss or gain of volatiles after trapping.
- 3- Bubbles of bubble-bearing MI should be analyzed to check for the presence of volatiles. Recent studies show that up to 90% of the total original CO₂ content of an MI could be stored in the vapor bubble (Aster et al., 2016; Hartley et al., 2014; Moore et al., 2015). For certain conditions, significant amounts of H₂O and S could also be lost into the bubble of MI (Esposito et al., 2016).
- 4- Temporal relationships between MI studied and host phase should be assessed to test various interpretations defined by volatile trends. When available, groups of MI trapped at the same time (Melt Inclusion Assemblages) should be examined to test the reliability of the data recorded by MI.

 Cathodoluminescence mapping of quartz phenocrysts (Peppard et al., 2001) or phosphorous maps in olivine (Esposito et al., 2015) can be used to assess relative time of MI formation. Time constraints on MI formation can be used to support or rule out interpretations on volatile trends recorded by MI.

Acknowledgments

We would like to thank H.E. Belkin for his help and kind assistance with EMP measurements, and N. Shimizu for assistance with SIMS analyses. In addition, we would like to thank G. Rolandi and A. Paone for their assistance during the sampling campaign. Part of this project was funded by the PON-BIOENERGCHEM. CEM and RE acknowledge support from the Deep Carbon Observatory and National Science Foundation Grant EAR 1732256. Support for RJB during the course of this investigation was provided by NSF grant EAR-1624589. Review comments by three anonymous

0040		
2913 2914		
2914		
2916	1587	reviewers and A. Gómez-Tuena helped to identify some inconsistencies in earlier
2917	1588	versions and led to a much improved manuscript.
2918	1589	•
2919 2920	1307	
2921	1590	
2922		
2923		
2924		
2925		
2926		
2927 2928		
2929		
2930		
2931		
2932		
2933		
2934		
2935		
2936 2937		
2938		
2939		
2940		
2941		
2942		
2943		
2944 2945		
2946		
2947		
2948		
2949		
2950		
2951 2952		
2952 2953		
2954		
2955		
2956		
2957		
2050		

References

- Acocella, V. and Funiciello, R., 1999. The interaction between regional and local tectonics during resurgent doming: the case of the island of Ischia, Italy. Journal of Volcanology and Geothermal Research, 88(1): 109-123.
- Acocella, V., Salvini, F., Funiciello, R. and Faccenna, C., 1999. The role of transfer structures on volcanic activity at Campi Flegrei (Southern Italy). Journal of Volcanology and Geothermal Research, 91(2): 123-139.
- Albarède, F., 1996. Introduction to geochemical modeling. Cambridge University Press.
- Albini, A., Cristofolini, R., Di Girolamo, P., Nardi, G., Rolandi, G. and Stanzione, D., 1977. Rare earth element and thorium distribution in volcanic rocks of the potassic kindred from Procida Island and the Phlegraen Fields, southern Italy. Atti Accademia Nazionale dei Lincei, Classe di Scienze Fisiche Matematiche e Naturali, Rendiconti, 63(5): 416-429.
- Alessio, M., Allegri, L., Azzi, C., Calderoni, G., Cortesi, C., Improta, S. and Petrone, V., 1989. ¹⁴C tephrochronology with different fractions of Paleosol humic matter at Procida Island, Italy. Radiocarbon, 31: 664-671.
- Alessio, M., Bella, F., Improta, S., Belluomini, G., Cortesi, C. and Turi, B., 1971. University of Rome carbon-14 dates IX. Radiocarbon, 13(2): 395-411.
- Arienzo, I., Mazzeo, F., Moretti, R., Cavallo, A. and D'Antonio, M., 2016. Open-system magma evolution and fluid transfer at Campi Flegrei caldera (Southern Italy) during the past 5ka as revealed by geochemical and isotopic data: The example of the Nisida eruption. Chemical Geology, 427: 109-124.
- Arienzo, I., Moretti, R., Civetta, L., Orsi, G. and Papale, P., 2010. The feeding system of Agnano–Monte Spina eruption (Campi Flegrei, Italy): Dragging the past into present activity and future scenarios. Chemical Geology, 270(1–4): 135-147.
- Aster, E.M., Wallace, P.J., Moore, L.R., Watkins, J., Gazel, E. and Bodnar, R.J., 2016. Reconstructing CO 2 concentrations in basaltic melt inclusions using Raman analysis of vapor bubbles. Journal of Volcanology and Geothermal Research, 323: 148-162.
- Baker, D., 2008. The fidelity of melt inclusions as records of melt composition. Contributions to Mineralogy and Petrology, 156(3): 377-395.
- Barbieri, M., Di Girolamo, P., Locardi, E., Lombardi, G. and Stanzione, D., 1979. Petrology of the calcalkaline volcanics of the Parete 2 well (Campania, Italy). Periodico di Mineralogia, 48: 53-74.
- Beccaluva, L., Di Girolamo, P. and Serri, G., 1991. Petrogenesis and tectonic setting of the Roman Volcanic Province, Italy. Lithos, 26: 191-221.
- Blundy, J. and Cashman, K., 2008. Petrologic reconstruction of magmatic system variables and processes. Reviews in Mineralogy and Geochemistry, 69(1): 179-239.
- Bodnar, R.J., Cannatelli, C., De Vivo, B., Lima, A., Belkin, H.E. and Milia, A., 2007. Quantitative model for magma degassing and ground deformation (bradyseism) at Campi Flegrei, Italy; implications for future eruptions. Geology, 35(9): 791-794.
- Bodnar, R.J. and Student, J.J., 2006. Melt inclusions in plutonic rocks: Petrography and microthermometry. In: J.D. Webster (Editor), Melt Inclusions in Plutonic Rocks. Mineralogical Association of Canada, Montreal, Quebec, Canada, pp. 1-25.
- Brocchini, D., Principe, C., Castradori, D., Laurenzi, M.A. and Gorla, L., 2001. Quaternary evolution of the southern sector of the Campanian Plain and early Somma-Vesuvius activity: insights from the Trecase 1 well. Mineralogy and Petrology, 73(1-3): 67-91.
- Bucholz, C.E., Gaetani, G.A., Behn, M.D. and Shimizu, N., 2013. Post-entrapment modification of volatiles and oxygen fugacity in olivine-hosted melt inclusions. Earth and Planetary Science Letters, 374(0): 145-155.
- Cannatelli, C., 2012. Understanding magma evolution at Campi Flegrei (Campania, Italy) volcanic complex using melt inclusions and phase equilibria. Mineralogy and Petrology, 104(1-2): 29-42.
- Cannatelli, C., Doherty, A., Esposito, R., Lima, A. and De Vivo, B., 2016. Understanding a volcano through a droplet: A melt inclusion approach. Journal of Geochemical Exploration, 171: 4-19.

3046 1664 3047 1665 3048 1666 3049 1667

- Cannatelli, C., Lima, A., Bodnar, R.J., De Vivo, B., Webster, J.D. and Fedele, L., 2007. Geochemistry of melt inclusions from the Fondo Riccio and Minopoli 1 eruptions at Campi Flegrei (Italy). Chemical Geology, 237: 418-432. Capaldi, G., Gasparini, P., Moauro, A., Salvia, E. and Travaglione, O., 1972. Rare Earth abundances in th
 - Capaldi, G., Gasparini, P., Moauro, A., Salvia, E. and Travaglione, O., 1972. Rare Earth abundances in the alkaline volcanic rocks from Campania, South Italy. Earth and Planetary Science Letters, 17: 247-257.
 - Cashman, K.V., Sparks, R.S.J. and Blundy, J.D., 2017. Vertically extensive and unstable magmatic systems: A unified view of igneous processes. Science, 355(6331): eaag3055.
 - Cecchetti, A., Fulignati, P., Marianelli, P., Proto, N. and Sbrana, A., 2001. The feeding system of Campi Flegrei. Insights from melt and fluid inclusions on Ignimbrite Campana, Solchiaro and Minopoli eruptions, GNV-INGV Meeting, Rome, Italy, pp. 190–191.
 - Cecchetti, A., Marianelli, P. and Sbrana, A., 2002-2003. L'eruzione di Astroni (caldera dei Campi Flegrei): dati preliminari dallo studio di inclusioni silicatiche. Atti Soc. tosc. Sci. nat., Mem., 108: 59-63.
 - Chiodini, G., Vandemeulebrouck, J., Caliro, S., D'Auria, L., De Martino, P., Mangiacapra, A. and Petrillo, Z., 2015. Evidence of thermal-driven processes triggering the 2005–2014 unrest at Campi Flegrei caldera. Earth and Planetary Science Letters, 414: 58-67.
 - Cipriani, F., Marianelli, P. and Sbrana, A., 2008. Study of a pyroclastic sequence of Solfatara volcano (Phlegrean Fields). Insights on volcanological and feeding system processes. Atti della Societa Toscana di Scienze Naturali, Memorie Serie A, 113: 39-48.
 - Civetta, L., Carluccio, E., Innocenti, F., Sbrana, A. and Taddeucci, G., 1991. Magma chamber evolution under the Phlegraean Fields during the last 10 ka; trace element and isotope data. European Journal of Mineralogy, 3(2): 415-428.
 - Civetta, L., Orsi, G., Pappalardo, L., Fisher, R.V., Heiken, G. and Ort, M., 1997. Geochemical zoning, mingling, eruptive dynamics and depositional processes The Campanian Ignimbrite, Campi Flegrei caldera, Italy. Journal of Volcanology and Geothermal Research, 75(3-4): 183-219.
 - D'Antonio, M., 2011. Lithology of the basement underlying the Campi Flegrei caldera: Volcanological and petrological constraints. Journal of Volcanology and Geothermal Research, 200(1–2): 91-98.
 - D'Antonio, M., Civetta, L. and Di Girolamo, P., 1999a. Mantle source heterogeneity in the Campanian Region (South Italy) as inferred from geochemical and isotopic features of mafic volcanic rocks with shoshonitic affinity. Mineralogy and Petrology 67: 163–192.
 - D'Antonio, M., Civetta, L., Orsi, G., Pappalardo, L., Piochi, M., Carandente, A., De Vita, S., Di Vito, M.A. and Isaia, R., 1999b. The present state of the magmatic system of the Campi Flegrei caldera based on a reconstruction of its behavior in the past 12 ka. Journal of Volcanology and Geothermal Research, 91(2-4): 247-268.
 - D'Antonio, M. and Di Girolamo, P., 1994. Petrological and geochemical study of mafic shoshonitic volcanics from Procida-Vivara and Ventotene Islands (Campanian Region, South Italy). Acta Vulcanol, 5: 69-80.
 - D'Antonio, M., Tonarini, S., Arienzo, I., Civetta, L. and Di Renzo, V., 2007. Components and processes in the magma genesis of the Phlegrean Volcanic District, southern Italy. Geological Society of America Special Papers, 418: 203-220.
 - Da Toledo, P., Giacomo, 1539. Ragionamento del terremoto, del Nvovo monte, del aprimento di terra in Pozvolo nel anno 1538 : e dela significatione d'essi. Giouanni Sulztbah alemano, Napoli.
 - Danyushevsky, L.V., Della-Pasqua, F.N. and Sokolov, S., 2000. Re-equilibration of melt inclusions trapped by magnesian olivine phenocrysts from subduction-related magmas: petrological implications. Contributions to Mineralogy and Petrology, 138(1): 68-83.
 - Danyushevsky, L.V., Leslie, R.A.J., Crawford, A.J. and Durance, P., 2004. Melt inclusions in primitive olivine phenocrysts; the role of localized reaction processes in the origin of anomalous compositions. Journal of Petrology, 45(12): 2531-2553.
 - Danyushevsky, L.V., McNeill, A.W. and Sobolev, A.V., 2002a. Experimental and petrological studies of melt inclusions in phenocrysts from mantle-derived magmas: an overview of techniques, advantages and complications. Chemical Geology, 183(1–4): 5-24.
 - Danyushevsky, L.V. and Plechov, P., 2011. Petrolog3: Integrated software for modeling crystallization processes. Geochemistry, Geophysics, Geosystems, 12(7): Q07021.
 - Danyushevsky, L.V., Sokolov, S. and Falloon, T.J., 2002b. Melt inclusions in olivine phenocrysts; using diffusive re-equilibration to determine the cooling history of a crystal, with implications for the origin of olivine-phyric volcanic rocks. Journal of Petrology, 43(9): 1651-1671.

3083 3084

3084 3085 3086

3086 1702 3087 1703 3088 1704 3089 1705

1699

1700

1701

1715

1716

1717

1723

1724

1725

1726

1727

1728

1729

1730

1731

1732

1733

1734

1735

1736

1742

1743

1744

3089 1703 3090 1706 3091 1707 3092 1709

3093 1710 3094 1711 3095 1712 3096 1713 2007 1714

3100 1718 3101 1719 3102 1720 3103 1721 3104 1722

3104 3105 3106

3107 3108 3109

3114 3115 3116

3117 1737 3118 1738 3119 1739 3120 1740 2424 1741

3122 3123 3124

3121

3124 1745 3125 1746 3126 1747 3127 1748

3127 1748 3128 1749 3129 1750 3130 1753

3129 3130 3131 3131 3132 3132 3133 3133

3134

- De Astis, G., Pappalardo, L. and Piochi, M., 2004. Procida Volcanic History: new insights in the evolution of the Phlegraean Volcanic District (Campania, Italy). Bulletin of Volcanology, 66: 622-641.
- De Natale, G., Troise, C., Mark, D., Mormone, A., Piochi, M., Di Vito, M.A., Isaia, R., Carlino, S., Barra, D. and Somma, R., 2016. The Campi Flegrei Deep Drilling Project (CFDDP): New insight on caldera structure, evolution and hazard implications for the Naples area (Southern Italy). Geochemistry, Geophysics, Geosystems, 17(12): 4836-4847.
- de Vita, S., Orsi, G., Civetta, L., Carandente, A., D'Antonio, M., Deino, A., di Cesare, T., Di Vito, M.A., Fisher, R.V., Isaia, R., Marotta, E., Necco, A., Ort, M., Pappalardo, L., Piochi, M. and Southon, J., 1999. The Agnano–Monte Spina eruption (4100 years BP) in the restless Campi Flegrei caldera (Italy). Journal of Volcanology and Geothermal Research, 91: 269-301.
- De Vivo, B., Petrosino, P., Lima, A., Rolandi, G. and Belkin, H., 2010. Research progress in volcanology in the Neapolitan area, southern Italy: a review and some alternative views. Mineralogy and Petrology, 99(1): 1-28.
- De Vivo, B., Rolandi, G., Gans, P.B., Calvert, A., Bohrson, W.A., Spera, F.J. and Belkin, H.E., 2001. New constraints on the pyroclastic eruptive history of the Campanian volcanic plain (Italy). Mineralogy and Petrology, 73(1-3): 47-65.
- Deegan, F., Troll, V., Freda, C., Misiti, V., Chadwick, J.P., McLeod, C. and Davidson, J.P., 2010. Magmacarbonate interaction processes and associated CO2 release at Merapi Volcano, Indonesia: insights from experimental petrology. Journal of Petrology, 51(5): 1027-1051.
- Deino, A.L., Orsi, G., De Vita, S. and Piochi, M., 2004. The age of the Neapolitan Yellow Tuff calderaforming eruption (Campi Flegrei Caldera, Italy) assessed by 40 Ar/39 Ar dating method. Journal of Volcanology and Geothermal Research, 133: 157-170.
- Di Girolamo, P., Ghiara, M.R., Lirer, Munno, R., Rolandi, G. and Stanzione, D., 1984. Vulcanologia e petrologia dei Campi Flegreei. Volcanology and petrology of Phlegraean Fields. Bollettino della Società Geologica Italiana 103: 349-413.
- Di Girolamo, P. and Stanzione, D., 1973. Lineamenti geologici e petrologici dell'isola di Procida. Rendiconti della Societa Italiana di Mineralogia e Petrologia, 29: 81-125.
- Di Renzo, V., Arienzo, I., Civetta, L., D'Antonio, M., Tonarini, S., Di Vito, M.A. and Orsi, G., 2011. The magmatic feeding system of the Campi Flegrei caldera: Architecture and temporal evolution. Chemical Geology, 281(3-4): 227-241.
- Di Vito, M., Lirer, L., Mastrolorenzo, G., Rolandi, G. and Scandone, R., 1985. Volcanological map of Campi Flegrei, Ministero Protezione Civile e Università di Napoli.
- Di Vito, M.A., Arienzo, I., Braia, G., Civetta, L., D'Antonio, M., Di Renzo, V. and Orsi, G., 2011. The Averno 2 fissure eruption: a recent small-size explosive event at the Campi Flegrei Caldera (Italy). Bulletin of Volcanology, 73: 295-320.
- Di Vito, M.A., Isaia, R., Orsi, G., Southon, J., De Vita, S., D'Antonio, M., Pappalardo, L. and Piochi, M., 1999. Volcanism and deformation since 12,000 years at the Campi Flegrei caldera (Italy). Journal of Volcanology and Geothermal Research, 91(2-4): 221-246.
- Edmonds, M. and Wallace, P.J., 2017. Volatiles and exsolved vapor in volcanic systems. Elements, 13(1): 29-34.
- Esposito, R., Badescu, K., Boyce, J.W. and Manning, C.E., 2015. Assessing the Origin of Olivines Based on Relative Age of Melt Inclusions. American Geophysical Union, Fall Meeting 2015, abstract volume: #V51D-3068.
- Esposito, R., Bodnar, R.J., Danyushevsky, L., De Vivo, B., Fedele, L., Hunter, J., Lima, A. and Shimizu, N., 2011. Volatile Evolution of Magma Associated with the Solchiaro Eruption in the Phlegrean Volcanic District (Italy). Journal of Petrology, 52(12): 2431-2460.
- Esposito, R., Hunter, J., Schiffbauer, J., Shimizu, N. and Bodnar, R.J., 2014. An assessment of the reliability of melt inclusions as recorders of the pre-eruptive volatile content of magmas. American Mineralogist, 99(5-6): 976-998.
- Esposito, R., Klebesz, R., Bartoli, O., Klyukin, Y.I., Moncada, D., Doherty, A.L. and Bodnar, R.J., 2012. Application of the Linkam TS1400XY heating stage to melt inclusion studies. Central European Journal of Geosciences, 4(2): 208-218.
- Esposito, R., Lamadrid, H.M., Redi, D., Steele-MacInnis, M., Bodnar, R.J., Manning, C.E., De Vivo, B., Cannatelli, C. and Lima, A., 2016. Detection of liquid H₂O in vapor bubbles in reheated melt inclusions: Implications for magmatic fluid composition and volatile budgets of magmas? American Mineralogist, 101(7): 1691-1695.

- Fanara, S., Botcharnikov, R.E., Palladino, D.M., Adams, F., Buddensieck, J., Mulch, A. and Behrens, H., 2015. Volatiles in magmas related to the Campanian Ignimbrite eruption: Experiments vs. natural findings. American Mineralogist, 100(10): 2284-2297.
- Faure, F. and Schiano, P., 2005. Experimental investigation of equilibration conditions during forsterite growth and melt inclusion formation. Earth and Planetary Science Letters, 236(3-4): 882-898.
- Fedele, F.G., Giaccio, B., Isaia, R., Orsi, G., Carroll, M. and Scaillet, B., 2007. The Campanian Ignimbrite factor: towards a reappraisal of the Middle to Upper Palaeolithic 'transition'. In: J. Grattan and R. Torrence (Editors), Living under the shadow: cultural impacts of volcanic eruptions. One World Archeology. Left Coast Press, Walnut Creek (CA), pp. 19-41.
- Fedele, L., Insinga, D., Calvert, A., Morra, V., Perrotta, A. and Scarpati, C., 2011. 40Ar/39Ar dating of tuff vents in the Campi Flegrei caldera (southern Italy): toward a new chronostratigraphic reconstruction of the Holocene volcanic activity. Bulletin of Volcanology, 73(9): 1323-1336.
- Fourmentraux, C., Metrich, N., Bertagnini, A. and Rosi, M., 2012. Crystal fractionation, magma step ascent, and syn-eruptive mingling; the Averno 2 eruption (Phlegraean Fields, Italy), Contributions to Mineralogy and Petrology, 163(6): 1121-1137.
- Fowler, S.J., Spera, F.J., Bohrson, W.A., Belkin, H.E. and De Vivo, B., 2007. Phase equilibria constraints on the chemical and physical evolution of the Campanian Ignimbrite. Journal of Petrology, 48(3): 459-493.
- Gebauer, S.K., Schmitt, A.K., Pappalardo, L., Stockli, D.F. and Lovera, O.M., 2014. Crystallization and eruption ages of Breccia Museo (Campi Flegrei caldera, Italy) plutonic clasts and their relation to the Campanian ignimbrite. Contributions to Mineralogy and Petrology, 167(1): 953.
- Ghiara, M.R., Lirer, L. and Munno, R., 1979. Mineralogy and geochemistry of the "Low-Potassium Series" of the Campania Volcanics (South Italy). Chemical Geology, 26: 29-49.
- Ghiorso, M.S. and Gualda, G.A., 2015. An H₂O–CO₂ mixed fluid saturation model compatible with rhyolite-MELTS. Contributions to Mineralogy and Petrology, 169(6): 1-30.
- Gilg, H., Lima, A., Somma, R., Belkin, H., De Vivo, B. and Ayuso, R., 2001. Isotope geochemistry and fluid inclusion study of skarns from Vesuvius. Mineralogy and Petrology, 73(1-3): 145-176.
- Gillot, P.Y., Chiesa, S., Pasquare, G. and Vezzoli, L., 1982. <33,000-yr K-Ar dating of the volcano-tectonic horst of the Isle of Ischia, Gulf of Naples. Nature, 299(5880): 242-245.
- Hartley, M.E., Maclennan, J., Edmonds, M. and Thordarson, T., 2014. Reconstructing the deep CO₂ degassing behaviour of large basaltic fissure eruptions. Earth and Planetary Science Letters, 393(0): 120-131.
- Hauri, E., Wang, J., Dixon, J.E., King, P.L., Mandeville, C. and Newman, S., 2002. SIMS analysis of volatiles in silicate glasses: 1. Calibration, matrix effects and comparisons with FTIR. Chemical Geology, 183(1): 99-114.
- Hayward, C., 2012. High spatial resolution electron probe microanalysis of tephras and melt inclusions without beam-induced chemical modification. The Holocene, 22(1): 119-125.
- Helo, C., Longpre, M.A., Shimizu, N., Clague, D.A. and Stix, J., 2011. Explosive eruptions at mid-ocean ridges driven by CO₂-rich magmas. Nature Geoscience, 4(4): 260-263.
- Humphreys, M.C.S., Blundy, J.D. and Sparks, R.S.J., 2008a. Shallow-level decompression crystallisation and deep magma supply at Shiveluch Volcano. Contributions to Mineralogy and Petrology, 155(1): 45-61.
- Humphreys, M.C.S., Menand, T., Blundy, J.D. and Klimm, K., 2008b. Magma ascent rates in explosive eruptions: Constraints from H2O diffusion in melt inclusions. Earth and Planetary Science Letters, 270(1-2): 25-40.
- Ippolito, F., D'Argenio, B., Pescatore, T. and Scandone, P., 1975. Structural-stratigraphic units and tectonic framework of the Southern Apennines. In: C.H. Squyres (Editor), Geology of Italy. Earth Sci. Soc. Libyan Arab Rep., Tripoli Libya, pp. 1-11.
- Isaia, R., Marianelli, P. and Sbrana, A., 2009. Caldera unrest prior to intense volcanism in Campi Flegrei (Italy) at 4.0 ka BP: Implications for caldera dynamics and future eruptive scenarios. Geophysical Research Letters, 36(21).
- Kent, A.J.R., 2008. Melt inclusions in basaltic and related volcanic rocks. In: K.D. Putirka and F.J. Tepley, III (Editors), MInerals, Inclusions and Volcanic Processes. The Mineralogical Society of America, pp. 273-331.
- Klébesz, R., Esposito, R., De Vivo, B. and Bodnar, R.J., 2015. Constraints on the origin of sub-effusive nodules from the Sarno (Pomici di Base) eruption of Mt. Somma-Vesuvius (Italy) based on

```
3193
3194
3195
3196
3197
3198
3199
3200
3201
```

- 1811 compositions of silicate-melt inclusions and clinopyroxene. American Mineralogist, 100(4): 760-1812 773.
 - Kress, V.C. and Ghiorso, M.S., 2004. Thermodynamic modeling of post-entrapment crystallization in igneous phases. Journal of Volcanology and Geothermal Research, 137(4): 247-260.
 - Lima, A., Danyushevsky, L.V., De Vivo, B. and Fedele, L., 2003. A model for the evolution of the Mt. Somma-Vesuvius magmatic system based on fluid and melt inclusion investigations. Developments in Volcanology, 5: 227-249.
 - Lima, A., De Vivo, B., Spera, F.J., Bodnar, R.J., Milia, A., Nunziata, C., Belkin, H.E. and Cannatelli, C., 2009. Thermodynamic model for uplift and deflation episodes (bradyseism) associated with magmatic-hydrothermal activity at the Campi Flegrei (Italy). Earth-Science Reviews, 97(1-4): 44-58.
 - Lima, A., Esposito, R. and De Vivo, B., 2017. Fluid and melt inclusions from subvolcanic to surface environment in the Campi Flegrei (Napoli, Italy) active volcanic system. Journal of the Geological Society of India, 90(5): 515-523.
 - Lirer, L., Petrosino, P., Alberico, I. and Armiero, V., 2011. Cartografia. In: L. Lirer (Editor), I Campi Flegrei, storia di un campo vulcanico. Quaderni dell'accademia pontiniana, Napoli, pp. 7-77.
 - Lirer, L., Rolandi, G. and Rubin, M., 1991. ¹⁴C age of the "Museum Breccia" (Campi Flegrei) and its relevance for the origin of the Campanian Ignimbrite. Journal of Volcanology and Geothermal Research, 48(1-2): 223-227.
 - Maclennan, J., 2017. Bubble formation and decrepitation control the CO2 content of olivine-hosted melt inclusions. Geochemistry, Geophysics, Geosystems, 18(2): 597-616.
 - Mangiacapra, A., Moretti, R., Rutherford, M., Civetta, L., Orsi, G. and Papale, P., 2008. The deep magmatic system of the Campi Flegrei caldera (Italy). Geophysical Research Letter, 35(21): L21304.
 - Marianelli, P., Sbrana, A. and Proto, M., 2006. Magma chamber of the Campi Flegrei supervolcano at the time of eruption of the Campanian Ignimbrite. Geology, 34(11): 937-940.
 - Marsh, B.D., 1996. Solidification fronts and magmatic evolution. Mineralogical Magazine, 60(1): 5-40. Mastrolorenzo, G. and Pappalardo, L., 2006. Magma degassing and crystallization processes during eruptions of high-risk Neapolitan-volcanoes: Evidence of common equilibrium rising processes in alkaline magmas. Earth and Planetary Science Letters, 250: 164-181.
 - Mazzeo, F., D'Antonio, M., Arienzo, I., Aulinas, M., Di Renzo, V. and Gimeno, D., 2014. Subduction-related enrichment of the Neapolitan Volcanoes (Southern Italy) mantle source: New constraints on the characteristics of the slab-derived components. Chemical Geology, 386: 165-183.
 - Melluso, L., De'Gennaro, R., Fedele, L., Franciosi, L. and Morra, V., 2012. Evidence of crystallization in residual, Cl–F-rich, agpaitic, trachyphonolitic magmas and primitive Mg-rich basalt—trachyphonolite interaction in the lava domes of the Phlegrean Fields (Italy). Geological Magazine, 149(3): 532.
 - Metrich, N. and Wallace, P.J., 2008. Volatile abundances in basaltic magmas and their degassing paths tracked by melt inclusions. Reviews in Mineralogy and Geochemistry, 69(1): 363-402.
 - Milia, A., 2010. The stratigraphic signature of volcanism off Campi Flegrei (Bay of Naples, Italy). In: G. Groppelli and L. Viereck-Goette (Editors), Stratigraphy and geology of volcanic areas. The Geological Society of America, Buolder, Colorado, pp. 155-170.
 - Mironov, N., Portnyagin, M., Botcharnikov, R., Gurenko, A., Hoernle, K. and Holtz, F., 2015. Quantification of the CO₂ budget and H₂O–CO₂ systematics in subduction-zone magmas through the experimental hydration of melt inclusions in olivine at high H₂O pressure. Earth and Planetary Science Letters, 425: 1-11.
 - Mironov, N. and Portnyagin, M.V., 2011. H₂O and CO₂ in parental magmas of Kliuchevskoi volcano inferred from study of melt and fluid inclusions in olivine. Russian Geology and Geophysics, 52(11): 1353-1367.
 - Moore, L.R., Gazel, E., Tuohy, R., Lloyd, A.S., Esposito, R., Steele-MacInnis, M., Hauri, E.H., Wallace, P.J., Plank, T. and Bodnar, R.J., 2015. Bubbles matter: An assessment of the contribution of vapor bubbles to melt inclusion volatile budgets. American Mineralogist, 100(4): 806-823.
 - Morabito, S., Petrosino, P., Milia, A., Sprovieri, M. and Tamburrino, S., 2014. A multidisciplinary approach for reconstructing the stratigraphic framework of the last 40ka in a bathyal area of the eastern Tyrrhenian Sea. Global and Planetary Change, 123: 121-138.

- Moretti, R., Arienzo, I., Orsi, G., Civetta, L. and D'Antonio, M., 2013. The Deep Plumbing System of Ischia: a Physico-chemical Window on the Fluid-saturated and CO₂-sustained Neapolitan Volcanism (Southern Italy). Journal of Petrology, 54(5): 951-984.
- Moretti, R., De Natale, G. and Troise, C., 2017. A geochemical and geophysical reappraisal to the significance of the recent unrest at Campi Flegrei caldera (Southern Italy), Geochemistry, Geophysics, Geosystems, 18(3): 1244-1269.
- Morgan, G.B. and London, D., 2005. Effect of current density on the electron microprobe analysis of alkali aluminosilicate glasses. American Mineralogist, 90(7): 1131-1138.
- Mormone, A., Piochi, M., Bellatreccia, F., De Astis, G., Moretti, R., Della Ventura, G., Cavallo, A. and Mangiacapra, A., 2011. A CO₂-rich magma source beneath the Phlegraean Volcanic District (Southern Italy): Evidence from a melt inclusion study. Chemical Geology, 287(1-2): 66-80.
- Moussallam, Y., Oppenheimer, C., Scaillet, B., Gaillard, F., Kyle, P., Peters, N., Hartley, M., Berlo, K. and Donovan, A., 2014. Tracking the changing oxidation state of Erebus magmas, from mantle to surface, driven by magma ascent and degassing. Earth and Planetary Science Letters, 393: 200-
- Nakamura, M. and Shimakita, S., 1998. Dissolution origin and syn-entrapment compositional change of melt inclusion in plagioclase. Earth and Planetary Science Letters, 161(1): 119-133.
- Norman, M.D., Garcia, M.O., Kamenetsky, V.S. and Nielsen, R.L., 2002. Olivine-hosted melt inclusions in Hawaiian picrites: equilibration, melting, and plume source characteristics. Chemical Geology, 183(1-4): 143-168.
- Orsi, G., Civetta, L., Dantonio, M., Digirolamo, P. and Piochi, M., 1995. Step-filling and development of a 3-layer magma chamber - the Neapolitan-Yellow-Tuff case-history. Journal of volcanology and geothermal research, 67(4): 291-312.
- Orsi, G., Civetta, L., Del Gaudio, C., De Vita, S., Di Vito, M.A., Isaia, R., Petrazzuoli, S.M., Ricciardi, G.P. and Ricco, C., 1999. Short-term ground deformations and seismicity in the resurgent Campi Flegrei Caldera (Italy); an example of active block-resurgence in a densely populated area. Journal of volcanology and geothermal research, 91(2-4): 415-451.
- Orsi, G., D'Antonio, M., de Vita, S. and Gallo, G., 1992. The Neapolitan Yellow Tuff, a large-magnitude trachytic phreatoplinian eruption; eruptive dynamics, magma withdrawal and caldera collapse. Journal of volcanology and geothermal research, 53(1-4): 275-287.
- Orsi, G., de Vita, S. and di Vito, M., 1996. The restless, resurgent Campi Flegrei nested caldera (Italy); constraints on its evolution and configuration. Journal of volcanology and geothermal research, 74(3-4): 179-214.
- Papale, P., Moretti, R. and Barbato, D., 2006. The compositional dependence of the saturation surface of H₂O + CO₂ fluids in silicate melts. Chemical Geology, 229(1-3): 78-95.
- Pappalardo, L., Civetta, L., D'Antonio, M., Deino, A., Di Vito, M.A., Orsi, G., Carandente, A., De Vita, S., Isaia, R. and Piochi, M., 1999. Chemical and Sr-isotopical evolution of the Phlegraean magmatic system before the Campanian Ignimbrite and the Neapolitan Yellow Tuff eruptions. Journal of volcanology and geothermal research, 91(2-4): 141-166.
- Pappalardo, L., Piochi, M., D'Antonio, M., Civetta, L. and Petrini, R., 2002. Evidence for Multi-stage Magmatic Evolution during the past 60kyr at Campi Flegrei (Italy) Dduced from Sr, Nd and Pb Isotope Data. Journal of Petrology, 43(8): 1415-1434.
- Peccerillo, A., 1999. Multiple mantle metasomatism in central-southern Italy; geochemical effects, timing and geodynamic implications. Geology, 27(4): 315-318.
- Peccerillo, A., 2017. The Campania Province, Cenozoic Volcanism in the Tyrrhenian Sea Region. Advances in Volcanology, Springer International Publishing AG, Cham, Switzerland, pp. 159-
- Peppard, B.T., Steele, I.M., Davis, A.M., Wallace, P.J. and Anderson, A.T., 2001. Zoned quartz phenocrysts from the rhyolitic Bishop Tuff. American Mineralogist, 86(9): 1034-1052.
- Perrotta, A., Scarpati, C., Luongo, G. and Morra, V., 2006. The Campi Flegrei caldera boundary in the city of Naples. In: B. De Vivo (Editor), Developments in Volcanology. Elsevier, pp. 85-96.
- Pescatore, T. and Rolandi, G., 1981. Osservazioni preliminari sulla stratigrafia dei depositi vulcanoclastici nel settore SW dei Campi Flegrei. Preliminary observations of the stratigraphy of volcaniclastic deposits of the south-west sector of Phlagrean Fields. Bollettino della Società Geologica Italiana, 100(2): 233-254.

```
3305
3306
```

- Piochi, M., Kilburn, C.R.J., Vito, M.A., Mormone, A., Tramelli, A., Troise, C. and Natale, G., 2013. The volcanic and geothermally active Campi Flegrei caldera: an integrated multidisciplinary image of its buried structure. International Journal of Earth Sciences: 1-21.
- Piochi, M., Mastrolorenzo, G. and Pappalardo, L., 2005. Magma ascent and eruptive processes from textural and compositional features of Monte Nuovo pyroclastic products. Campi Flegrei, Italy. Bulletin of Volcanology, 67(7): 663-678.
- Piochi, M., Polacci, M., De Astis, G., Zanetti, A., Mangiacapra, A., Vannucci, R. and Giordano, D., 2008. Texture and composition of pumices and scoriae from the Campi Flegrei caldera (Italy): Implications on the dynamics of explosive eruptions. Geochem. Geophys. Geosyst., 9(3): Q03013.
- Putirka, K.D., 2017. Down the Crater: Where Magmas are Stored and Why They Erupt. Elements, 13(1): 11-16.
- Rhodes, J., 1981. Characteristics of primary basaltic magmas. Basaltic Volcanism Study Project: Basaltic volcanism on the terrestrial planets. Pergamon Press, New York: 409-432.
- Roach, A.L., 2005. The evolution of silicic magmatism in the post-caldera volcanism of the Phlegrean Fields, Italy. Doctoral Thesis, Brown University, Providence.
- Roedder, E., 1979, Origin and significance of magmatic inclusions. Bulletin de Mineralogie, 102(5-6, Mineraux et Minerais): 487-510.
- Rolandi, G., Bellucci, F., Heizler, M.T., Belkin, H.E. and De Vivo, B., 2003. Tectonic controls on the genesis of ignimbrites from the Campanian Volcanic Zone, southern Italy. Mineralogy and Petrology, 79(1): 3-31.
- Rosi, M. and Sbrana, A., 1987. Campi flegrei. Quaderni de "La Ricerca Scientifica", 9: 175.
- Rosi, M., Sbrana, A. and Vezzoli, L., 1988a. Correlazioni tefrostratigraphiche di alcuni livelli di Ischia, Procida e Campi Flegrei. Memorie della Societa Geologica Italiana, 41: 1015-1027.
- Rosi, M., Sbrana, A. and Vezzoli, L., 1988b. Stratigraphy of Procida and Vivara islands. Bollettino Nazionale Geofisica e Vulcanologia, 4: 500-525.
- Rowe, M.C., Nielsen, R.L. and Kent, A.J.R., 2006. Anomalously high Fe contents in rehomogenized olivine-hosted melt inclusions from oxidized magmas. American Mineralogist, 91(1): 82-91.
- Scandone, R., 1997. Campi Flegrei, http://vulcan.fis.uniroma3.it/campi flegrei/Campi flegrei.html, pp. Geologic map of Campi Flegrei modified after Di Vito et al. (1985).
- Scandone, R., Bellucci, F., Lirer, L. and Rolandi, G., 1991. The structure of the Campanian Plain and the activity of the Neapolitan volcanoes (Italy). Journal of Volcanology and Geothermal Research, 48(1-2): 1-31.
- Scandone, R., Giacomelli, L. and Fattori Speranza, F., 2006. The volcanological history of the volcanoes of Naples: a review. In: B. De Vivo (Editor), Volcanism in the Campanian Plain Elsevier Sciences, pp. 1-26.
- Scarpati, C., Cole, P. and Perrotta, A., 1993. The Neapolitan Yellow Tuff A large volume multiphase eruption from Campi Flegrei, Southern Italy. Bulletin of Volcanology, 55: 343-356.
- Self, S., 1976. The recent volcanology of Terceira, Azores. Journal of the Geological Society, 132(6): 645-
- Shishkina, T., Botcharnikov, R., Holtz, F., Almeev, R. and Portnyagin, M.V., 2010. Solubility of H₂O- and CO₂-bearing fluids in tholeitic basalts at pressures up to 500 MPa. Chemical Geology, 277(1): 115-125.
- Signorelli, S., Vaggelli, G., Francalanci, L. and Rosi, M., 1999. Origin of magmas feeding the Plinian phase of the Campanian Ignimbrite eruption, Phlegrean Fields (Italy); constraints based on matrixglass and glass-inclusion compositions. Journal of Volcanology and Geothermal Research, 91(2-4): 199-220.
- Smith, V., Isaia, R. and Pearce, N., 2011. Tephrostratigraphy and glass compositions of post-15 kyr Campi Flegrei eruptions: implications for eruption history and chronostratigraphic markers. Quaternary Science Reviews, 30(25): 3638-3660.
- Sobolev, A.V. and Danyushevsky, L.V., 1994. Petrology and Geochemistry of Boninites from the North Termination of the Tonga Trench: Constraints on the Generation Conditions of Primary High-Ca Boninite Magmas. Journal of Petrology, 35(5): 1183-1211.
- Sobolev, A.V., Dmitriev, L.V., Barsukov, V.L., Nevsorov, V.N. and Slutsky, A.B., 1980. The formation conditions of the high magnesium olivines from the monomineralic fraction of Luna 24 regolith. Proceedings of the Lunar and Planetary Science Conference, 11: 105-116.
- Spera, F., 1980. Thermal evolution of plutons: a parameterized approach. Science, 207(4428): 299-301.

```
3361
3362
3363
        1977
3364
         1978
3365
        1979
        1980
3366
         1981
3367
         1982
3368
         1983
3369
         1984
3370
         1985
3371
         1986
3372
         1987
3373
         1988
        1989
3374
        1990
3375
         1991
3376
         1992
3377
         1993
3378
         1994
3379
         1995
3380
         1996
3381
         1997
        1998
3382
        1999
3383
        2000
3384
        2001
3385
        2002
3386
        2003
3387
        2004
3388
        2005
3389
        2006
        2007
3390
        2008
3391
        2009
3392
        2010
3393
        2011
3394
        2012
3395
        2013
3396
        2014
3397
        2015
        2016
3398
        2017
3399
        2018
3400
        2019
3401
        2020
3402
        2021
3403
        2022
3404
        2023
        2024
3405
        2025
3406
        2026
3407
```

- Steele-MacInnis, M., Esposito, R., Moore, L.R. and Hartley, M.E., 2017. Heterogeneously entrapped, vapor-rich melt inclusions record pre-eruptive magmatic volatile contents. Contributions to Mineralogy and Petrology, 172(4): 18.
- Steele-MacInnis, M.J., Esposito, R. and Bodnar, R.J., 2011. Thermodynamic model for the effect of post-entrapment crystallization on the H₂O-CO₂ systematics of volatile saturated silicate melt inclusions. Journal of Petrology, 52(12): 2461-2482.
- Stock, M.J., Humphreys, M.C., Smith, V.C., Isaia, R. and Pyle, D.M., 2016. Late-stage volatile saturation as a potential trigger for explosive volcanic eruptions. Nature Geoscience, 9(3): 249-254.
- Student, J.J. and Bodnar, R.J., 2004. Silicate melt inclusions in porphyry copper deposits; identification and homogenization behavior. In: D.J. Kontak, A.J. Anderson and D.D. Marshall (Editors), The Canadian Mineralogist, vol.42, Part 5. Mineralogical Association of Canada, Ottawa, pp. 1583-1599.
- Sun, S.S., 1980. Lead Isotopic Study of Young Volcanic-Rocks from Mid-Ocean Ridges, Ocean Islands and Island Arcs. Philosophical Transactions of the Royal Society of London Series a-Mathematical Physical and Engineering Sciences, 297(1431): 409-445.
- Sun, S.S. and McDonough, W.F., 1989. Chemical and isotopic systematics of oceanic basalts; implications for mantle composition and processes. Geological Society Special Publications, 42: 313-345.
- Thomas, J.B. and Bodnar, R.J., 2002. A technique for mounting and polishing melt inclusions in small (>1 mm) crystals. American Mineralogist, 87(10): 1505-1508.
- Thunell, R., Federman, A., Sparks, S. and Williams, D., 1979. Age, Origin, and Volcanological Significance of the Y-5 Ash Layer in the Mediterranean. Quaternary Research, 12(2): 241-253.
- Tonarini, S., D'Antonio, M., Di Vito, M.A., Orsi, G. and Carandente, A., 2009. Geochemical and B–Sr–Nd isotopic evidence for mingling and mixing processes in the magmatic system that fed the Astroni volcano (4.1–3.8 ka) within the Campi Flegrei caldera (southern Italy). Lithos, 107(3–4): 135-151.
- Tonarini, S., Leeman, W.P., Civetta, L., D'Antonio, M., Ferrara, G. and Necco, A., 2004. B/Nb and delta ¹¹B systematics in the Phlegrean volcanic district, Italy. Journal of volcanology and geothermal research, 133: 123-139.
- Turi, B., Taylor, H.P., Jr. and Ferrara, G., 1991. Comparisons of ¹⁸O ¹⁶O and ⁸⁷Sr/ ⁸⁶Sr in volcanic rocks from the Pontine Islands, M. Ernici, and Campania with other areas in Italy. Special Publication Geochemical Society, 3: 307-324.
- Villemant, B., 1988. Trace element evolution in the Phlegrean Fields (Central Italy): fractional crystallization and selective enrichment. Contributions to Mineralogy and Petrology, 98: 169-183.
- Vitale, S. and Isaia, R., 2014. Fractures and faults in volcanic rocks (Campi Flegrei, southern Italy): Insight into volcano-tectonic processes. International Journal of Earth Sciences, 103(3): 801-819.
- Webster, J.D., Raia, F., De Vivo, B. and Rolandi, G., 2001. The behavior of chlorine and sulfur during differentiation of the Mt. Somma-Vesuvius magmatic system. Mineralogy and Petrology, 73(1-3): 177-200.
- Webster, J.D., Raia, F., Tappen, C. and De Vivo, B., 2003. Pre-eruptive geochemistry of the ignimbrite-forming magmas of the Campanian Volcanic Zone, Southern Italy, determined from silicate melt inclusions. Mineralogy and Petrology, 79(1): 99-125.
- Welsch, B., Faure, F., Famin, V., Baronnet, A. and Bachèlery, P., 2013. Dendritic Crystallization: A Single Process for all the Textures of Olivine in Basalts? Journal of Petrology, 54(3): 539-574.
- Wohletz, K., Orsi, G. and Devita, S., 1995. Eruptive Mechanisms of the Neapolitan-Yellow-Tuff Interpreted from Stratigraphic, Chemical, and Granulometric Data. Journal of volcanology and geothermal research, 67(4): 263-290.
- Yaxley, G., Kamenetsky, V., Kamenetsky, M., Norman, M. and Francis, D., 2004. Origins of compositional heterogeneity in olivine-hosted melt inclusions from the Baffin Island picrites. Contributions to Mineralogy and Petrology, 148(4): 426-442.
- Zollo, A., Maercklin, N., Vassallo, M., Dello Iacono, D., Virieux, J. and Gasparini, P., 2008. Seismic reflections reveal a massive melt layer feeding Campi Flegrei Caldera. Geophysical Research Letters, 35: L12306.

3417 3418		
3419 3420 3421 3422 3423 3424 3425 3426 3427 3428 3429 3430 3431 3432 3433 3434 3435 3436 3437	2030	Tables
	2031	
	2032	Table 1. Sample details and petrographic description of MI from this study.
	2032	Table 1. Sample details and petrograpme description of Wil from this study.
	2034	Table 2. Major element and volatile compositions of MI from this study.
	2035	
	2036	Table 3. Calculated Fo _{max} predicted by rhyolite-MELTS compared with the Fo _{max}
	2037	reported by D'Antonio and Di Girolamo (1994).
	2038	
	2039	Table 4. MI and olivine host descriptions based on Melt-1 and Mixed groupping.
	2040	
	2041	Appendix Table A. GPS coordinates of samples collected for this study
3438 3439	2042	
3440 3441 3442 3443 3444 3445 3446 3447 3448	2043	Appendix Table B. Standards used for EMPA.
	2044	
	2045	Appendix Table C. Results of Rhyolite-Melts calculations
	2046	
	2047	Appendix Table D. Database of MI and bulk rock compositions of CF and IP eruptive
	2048	units.
3449 3450	2049	
3451 3452		
3453		
3454		
3455 3456		
3457		
3458 3459		
3460		
3461		
3462 3463		
3464		
3465		

Figure captions Figure 1. Simplified geological map of Campi Flegrei and Procida, modified after Di Vito et al. (1985) by Scandone (1997). Locations of the caldera rims are based on Vitale and Isaia (2014), though we attribute the source of the CI to outside CF (De Vivo et al, 2001; Rolandi et al., 2003; De Natale et al., 2016). White circles with red outlines are locations of samples analyzed in this study (sample names indicated). NYT = Neapolitan Yellow Tuff; AMS = Agnano-Monte Spina; CI = Campanian Ignimbrite Figure 2. Major-element compositions of MI. The six panels represent plots of SiO₂ concentration versus (a) CaO, (b) K₂O, (c) Na₂O, (d) TiO₂, (e) FeO_{tot} and (f) P₂O₅. Large symbols represent MI analyzed in this study (triangles = MI hosted in clinopyroxene; squares = MI hosted in sanidine; asterisks = MI hosted in plagioclase). Small symbols represent data from the literature (triangles = MI hosted in clinopyroxene; squares = MI hosted in sanidine; diamonds = MI hosted in olivine; circles = MI hosted in biotite). Bulk rock data from the literature are shown as stars (red stars = CF; black stars = IP) and xenoliths of CF are shown as x's. The red-dashed line encircles the range in compositions of MI from CF, and the black-dashed line encircles the range in compositions of MI from IP. Estimated uncertainties for the data from the present study are shown as error bars in the lower-right of each panel. See text for sources for the bulk rock and MI data from the literature. Figure 3. Volatile concentrations of MI versus SiO₂ concentration for (a) Cl, (b) S, (c) CO₂, (d) H₂O and (e) F. Symbols and fields are the same as in Figure 2, with the addition that bubble-free MI are differentiated using dark-blue symbols. Note that bulk rock data show only low contents of Cl, S and F, whereas bulk rock data for H₂O are absent. Estimated uncertainties for the data from the present study are shown as error bars in each panel. Figure 4. Volatile concentrations of MI. a) H₂O versus CO₂ showing full range of reported CO₂ concentrations; b) H₂O versus CO₂ showing MI with up to 1200 ppm CO₂

(red field encircles MI from the Neapolitan Yellow Tuff); c) F versus Cl. Note the positive correlation suggesting that F and Cl have similar behavior during the differentiation of magmas associated with CF and IP. Symbols and fields are the same as in Figures 2 and 3. Estimated uncertainties for the data from the present study are shown as error bars in each panel.

Figure 5. Major-element compositions of MI from this study and from the literature compared to bulk rock compositions. a) CaO vs. Al₂O₃ of MI discriminated by host phase (symbols the same as in Figure 2); arrows point to plagioclase and clinopyroxene compositions of PVD. Note some less evolved MI showing high CaO and low Al₂O₃ contents. MI plotting off of the main bulk rock trend are hosted in clinopyroxene. b) CaO vs. FeO_{tot} of MI discriminated based on host phase (symbols same as in Figure 2); note that several MI hosted in clinopyroxene and olivine plot outside the trend defined by the bulk rock data. The red star represents the composition of clinopyroxene host associated with the overheated MI (RESE17-AD12-M2, from this study). The white filled circle represents the hypothetical original trapped composition. Dashed lines represent trends associated with host dissolution, PEC, or Fe-loss by diffusion. c) CaO vs. Al₂O₃ of MI discriminated as either naturally glassy (unheated) MI or MI reheated in the lab. It is important to note that the Ca-rich and Al-poor inclusions were all reheated in the lab. d) CaO vs. FeO_{tot} of MI hosted in clinopyroxene, discriminated as either naturally glassy (unheated) MI or MI reheated in the lab. It is important to note that heated MI are generally distributed to the right (higher CaO) side of the bulk rock trend.

 Figure 6. Major element compositions of mafic bulk rocks from Procida and crystallization trends predicted by Rhyolite-MELTS using starting compositions based on bulk rocks or MI showing high Al₂O₃/K₂O. a), b) and c): MgO vs. Al₂O₃/K₂O; d), e) and f): SiO₂/CaO vs. Al₂O₃/K₂O. Symbols are for bulk rock compositions from Procida from the literature: red-filled stars = Solchiaro eruption (De Astis et al., 2004; Di Girolamo et al., 1984); red-open stars = Vivara or Solchiaro eruptions (D'Antonio et al., 1999a); yellow crosses = Fiumicello eruption; purple cross = Pozzo Vecchio eruption (Di Girolamo et al., 1984). Trends were calculated using rhyolite-MELTS (Gualda and

Ghiorso, 2015) with three initial compositions: Apr22, Apr18 (bulk rocks; D'Antonio et al., 1999), or RESC5-O5-MA (MI; Esposito et al., 2011). Panels a) and d) show results obtained using the three initial compositions at constant pressure of 200 MPa and at NNO oxidation state. Panels b) and e) show results obtained using Apr18 as the starting composition, the NNO redox buffer, and comparing isobaric versus polybaric crystallization paths (see text for details). Panels c) and f) show results obtained using Apr22 as the initial composition, constant pressure of 200 MPa, and assuming oxidation states of NNO, QFM+2 and QFM-2. The trends were calculated assuming the melt is saturated with respect to H₂O-CO₂. The calculated trends show a poor fit to the bulk rock data, suggesting that initial melts equivalent to the high Al₂O₃/K₂O bulk rocks and MI cannot generate the observed geochemical trends by crystal fractionation alone. Figure 7. Major element compositions of mafic bulk rocks from Procida and calculated crystallization trends using bulk rocks and MI showing low Al₂O₃/K₂O. a), b) and c): MgO vs. Al₂O₃/K₂O. d), e) and f): SiO₂/CaO vs. Al₂O₃/K₂O. Symbols are the same as in Figure 6. Trends were calculated using rhyolite-MELTS (Gualda and Ghiorso, 2015) with two initial compositions: Ps3 (bulk rock; Di Girolamo et al., 1984) and RESC3-O9-MA (MI; Esposito et al., 2011). Panels a) and d) show results obtained using the two initial compositions, a constant pressure of 200 MPa and at oxidation state equal to NNO. Panels b) and e) show results obtained using Ps3 as the starting composition, the NNO buffer, and compare isobaric versus polybaric crystallization paths (see text for details). Panels c) and f) show results obtained using Ps3 as the initial composition, constant pressure of 200 MPa, and oxidation states of NNO, QFM+2 and QFM-2. The trends were calculated assuming that the melt is saturated with respect to H₂O-CO₂. Note that trends show a good fit with the bulk rock data at low Al_2O_3/K_2O ratios, suggesting that the low Al₂O₃/K₂O rocks and MI are compatible with trends predicted based on crystal fractionation. **Figure 8.** H₂O-CO₂ systematics of bubble-free MI, with calculated crystallization trends predicted by rhyolite-MELTS (Gualda and Ghiorso, 2015). Note that the bubble-free MI

shown exclude any MI deemed anomalous based on major-element compositions (see

text for details). Symbols are the same as those in Figure 3, and uncertainties on each data point are the same as in Figure 4. Fractional crystallization trends are labelled as H₂O-CO₂ saturated isobaric versus polybaric, as well as H₂O-CO₂ undersaturated. Note that the H₂O-CO₂ systematics of MI hosted in olivine are consistent with polybaric crystallization under H₂O-CO₂ saturated conditions. **Figure 9.** Compositions of clinopyroxene hosting MI from this study and clinopyroxene compositions predicted by rhyolite-MELTS (Gualda and Ghiorso, 2015). Panels a), b) and c) compare measured clinopyroxene compositions with those predicted by the models using high-Al₂O₃/K₂O bulk rocks and MI (Apr22, Apr18 and RESC5-05-MA; as in Figure 6). Crosses are clinopyroxene analyses, and line styles are the same as in Figure 6. Panels d), e) and f) compare measured clinopyroxene compositions with those predicted by the models using low-Al₂O₃/K₂O bulk rocks and MI (Ps3 and RESC3-09-MA; as in Figure 7). Line styles are the same as in Figure 7. Note that trends calculated using Ps3 as starting composition and polybaric fractional crystallization (panel e) show the best fit. **Figure 10.** Compositions of feldspars hosting MI analyzed in this study (cross symbols) and from the literature (encircled fields), compared to feldspar compositions predicted by rhyolite-MELTS (trend lines; Gualda and Ghiorso, 2015). Panels a), b) and c) compare measured feldspar compositions and those predicted by the models using high-Al₂O₃/K₂O bulk rocks and MI (Apr22, Apr18 and RESC5-05-MA; as in Figure 6). Trend line styles are the same as in Figure 6. Panels d), e) and f) compare measured feldspar compositions and those predicted by the models using low-Al₂O₃/K₂O bulk rocks and MI (Ps3 and RESC3-09-MA; as in Figure 7). Line styles are the same as in Figure 7. Note that the best fit is calculated using Ps3 as starting composition (see panels d), e) and f)). Figure 11. TAS diagram comparing MI from CF and IP and liquid compositions predicted by Rhyolite-MELTS. Panels a), b) and c) compare MI compositions and liquid compositions predicted by the models using high-Al₂O₃/K₂O bulk rocks and MI (Apr22, Apr18 and RESC5-05-MA; as in Figure 6). Trend line styles are the same as in Figure 6.

Panels d), e) and f) compare MI compositions and liquid composition predicted by the models using low-Al₂O₃/K₂O bulk rocks and MI (Ps3 and RESC3-09-MA; as in Figure 7). Line styles are the same as in Figure 7. In all panels, the appearance and disappearance of olivine, clinopyroxene, and sanidine predicted by rhyolite-MELTS are highlighted. Note the good fit between the phase field defined by the MI and their hosts and rhyolite-MELTS predictions, relative to the appearance and disappearance of oliving, clinopyroxene, and sanidine, especially for panels d), e) and f). Data references for MI are as in the main text. Figure 12. Fo mol\% of host olivine versus the respective Al₂O₃/K₂O ratios of olivine-hosted MI, compared with rhyolite-MELTS calculations assuming 200 MPa isobaric conditions. Symbols are as in Figure 3, while trend line styles are as in Figures 6 and 7. Note that for all calculations Al₂O₃/K₂O of liquids does not change significantly during crystallization, whereas the bubble-free MI show a large variation Figure 13. Ratios of oxide concentrations (wt%), comparing bubble-free MI, bulk rock compositions and rhyolite-MELTS modeling results. The MI data exclude MI deemed anomalous based on major-element concentrations (see text for details). Symbols are the same as in Figures 2 and 3, and trend line styles are the same as in Figures 6 and 7. a) SiO₂/CaO vs. Al₂O₃/K₂O of basaltic and trachybasaltic bubble-free MI hosted in olivine. b) SiO₂/CaO vs. Al₂O₃/K₂O including trachytic bubble-free MI (symbols indicate host mineral). c) SiO₂/CaO vs. MgO/TiO₂ of bubble-free MI hosted in sanidine. d) SiO₂/TiO₂ vs. Al₂O₃/K₂O of bubble-free MI hosted in clinopyroxene. **Figure 14.** Trace element compositions of bubble-free MI hosted in olivine. Symbols are the same as in Figures 2 and 3. a) SiO₂/CaO vs. Al₂O₃/ Rb, b) Ba/Sr vs. Yb/Rb, and c) Ba/Sr vs. Eu/Rb. Note that for trace elements, fewer bulk rock data are available compared to major element data. The green arrow on each panel indicates the expected trend for polybaric crystallization. The red line on each panel represents a calculated mixing trend based on the same MI end members for all three panels. Mixing calculations were based on a simple binary mixing (Albarède, 1996)

Figure 15. Spider diagrams of the MI and bulk rocks. Symbols in a) and b) are the same as in Figures 2 and 3. a) Incompatible trace element spider diagram with normalization to primitive mantle as in (Sun, 1980), and b) Rare Earth elements spider diagram with normalization to chondrite as in Sun and McDonough (1989). c) Incompatible trace element spider diagram of two MI: RESC3-O9-MA and RESC5-05-MA. These two MI are hosted in olivine showing similar Fo-rich compositions, but these MI show very different Al₂O₃/K₂O ratios. Note that RESC3-O9-MA was selected as the low-Al₂O₃/K₂O starting composition for rhyolite melts simulations, whereas RESC5-05-MA was selected as the high-Al₂O₃/K₂O starting composition for these simulations, shown in Figures 6 to 13. **Figure 16.** Ratios of volatile, trace and major element compositions for bubble-free MI. Symbols the same as in Figure 3. a) Cl/Yb vs. Al₂O₃/K₂O; b) TiO₂/S vs. Al₂O₃/Rb. Note that including Cl and S in these element ratio diagrams still differentiates the trends formed by the two different groups of MI as seen in Figure 14. The arrows indicate trends predicted for polybaric fractional crystallization versus mixing. **Figure 17.** Volatile compositions of bubble-free MI compared to a) host compositions. and b) and c) major element compositions of the MI. Symbols the same as in Figure 3, whereas trend line styles are the same as in Figures 6 and 7. a) mol% Fo vs. H₂O/CO₂; b) Al₂O₃/K₂O vs. H₂O/CO₂ for mafic bubble-free MI; c) Al₂O₃/K₂O vs. H₂O/CO₂ trachytic and mafic bubble-free MI. **Figure 18.** Simplified temporal evolution model for the Solchiaro eruption based on bubble-free MI hosted in olivine. The results are based on the column-mush model of Marsh (1996), in which the plumbing system is represented by numerous sill-like pools of magma variably connected by dikes. The different thicknesses of these sills and dikes can result in different P-T histories for the same type of melt. This is consistent with MI data that show no correlation between Fo mol% of the host and the extrapolated depths of formation. Calculated pressures of formation of MI and interpreted depths were reported

by Esposito et al. (2011) based on the solubility model of Papale et al. (2006). (t₁) the magma evolves mainly by fractional crystallization of magmas in separate pools. (t₂) recharge of new magma that mixes with the pre-existing magmas leading to the Solchiaro eruption.

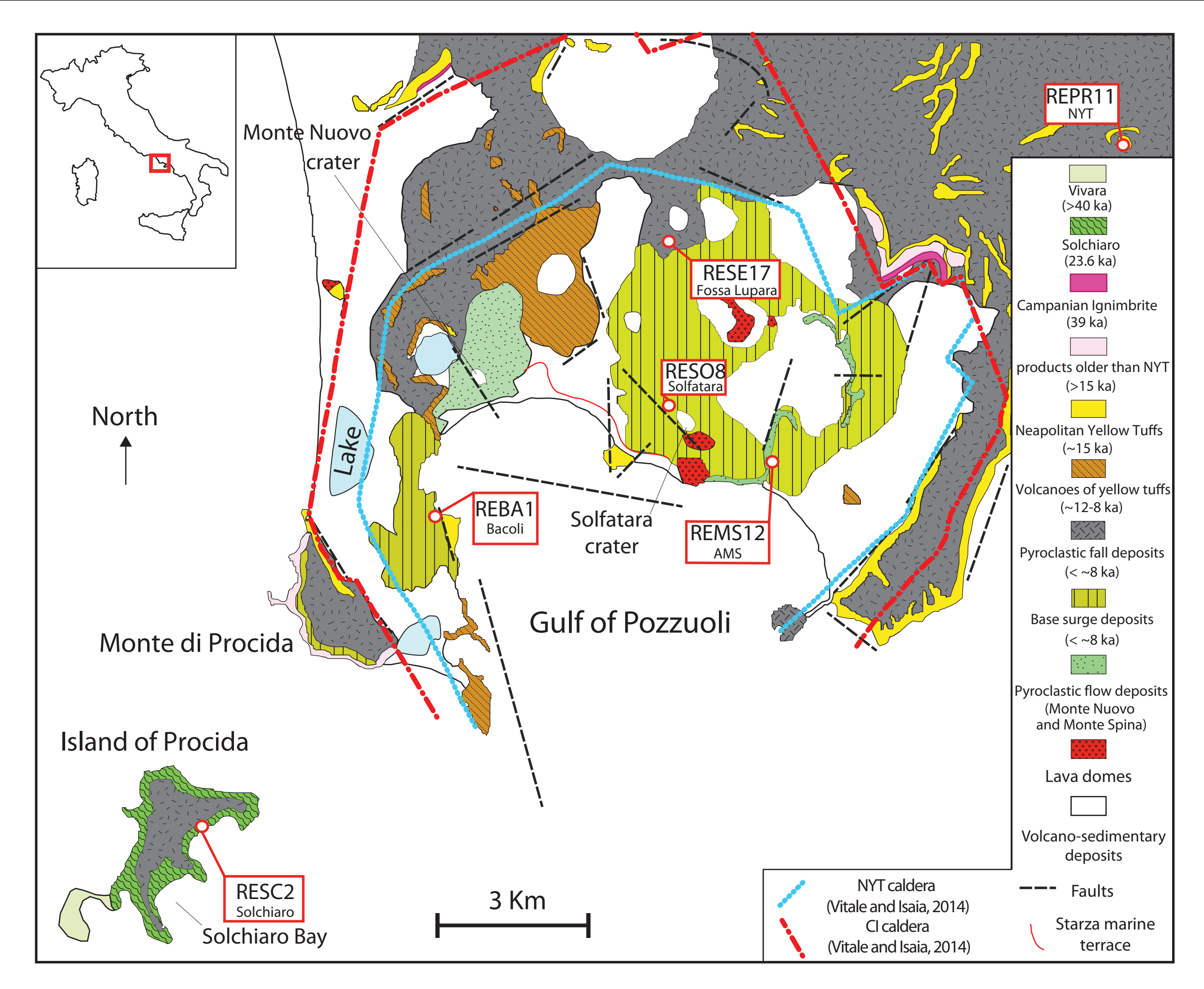


Fig. 1

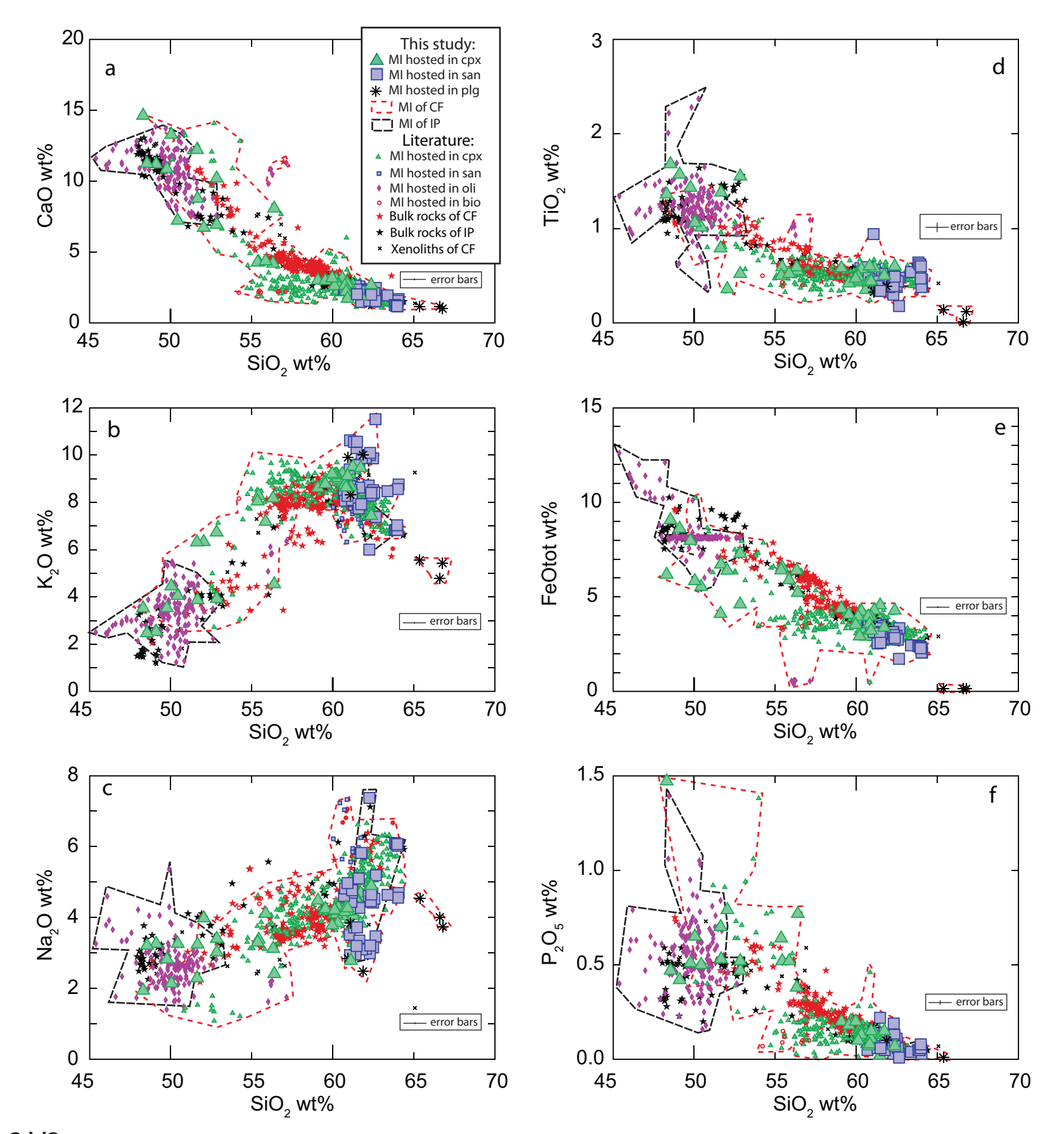


Fig.2 V2

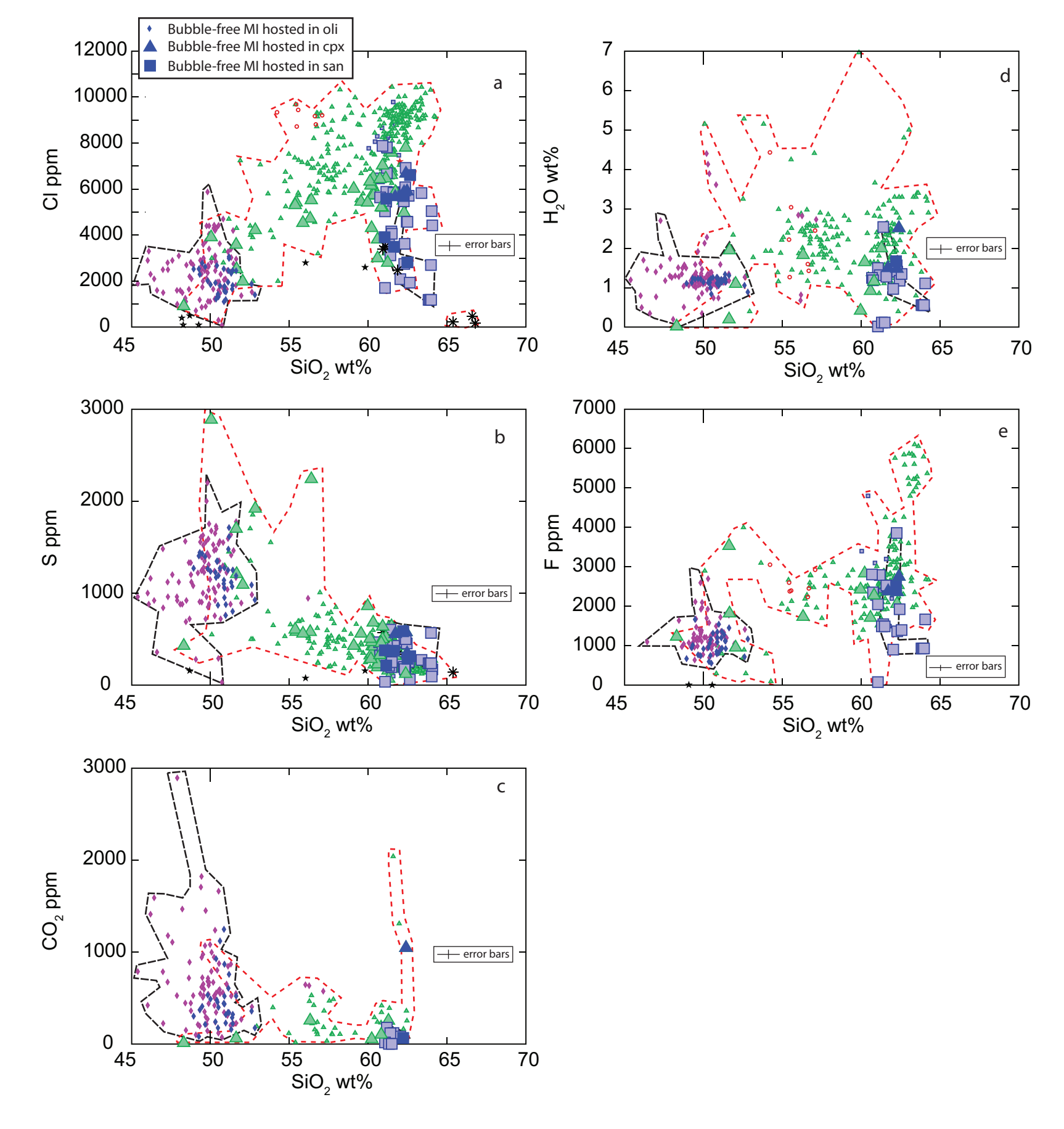


Fig. 3 Rev2

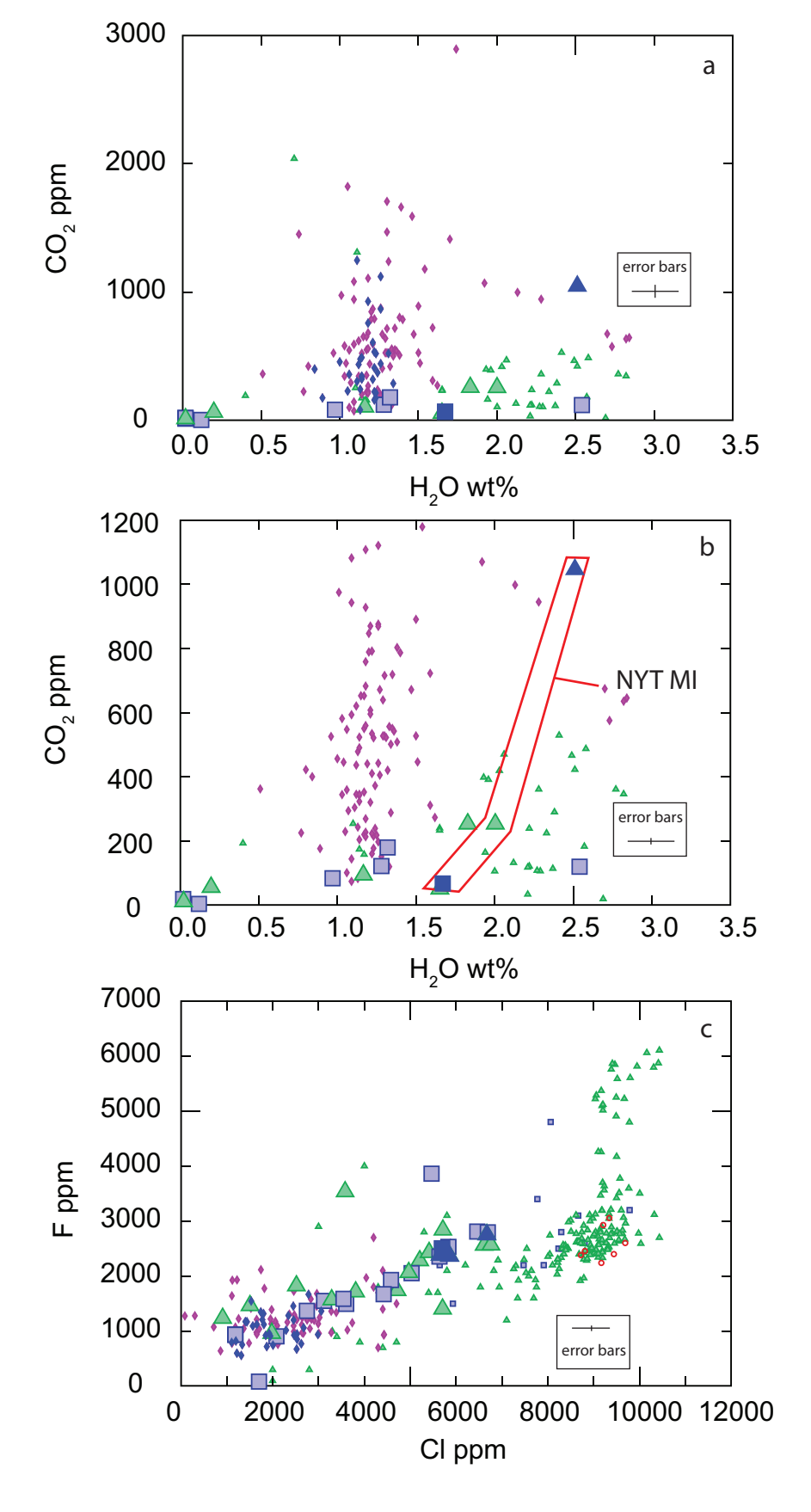


Fig. 2 Rev2

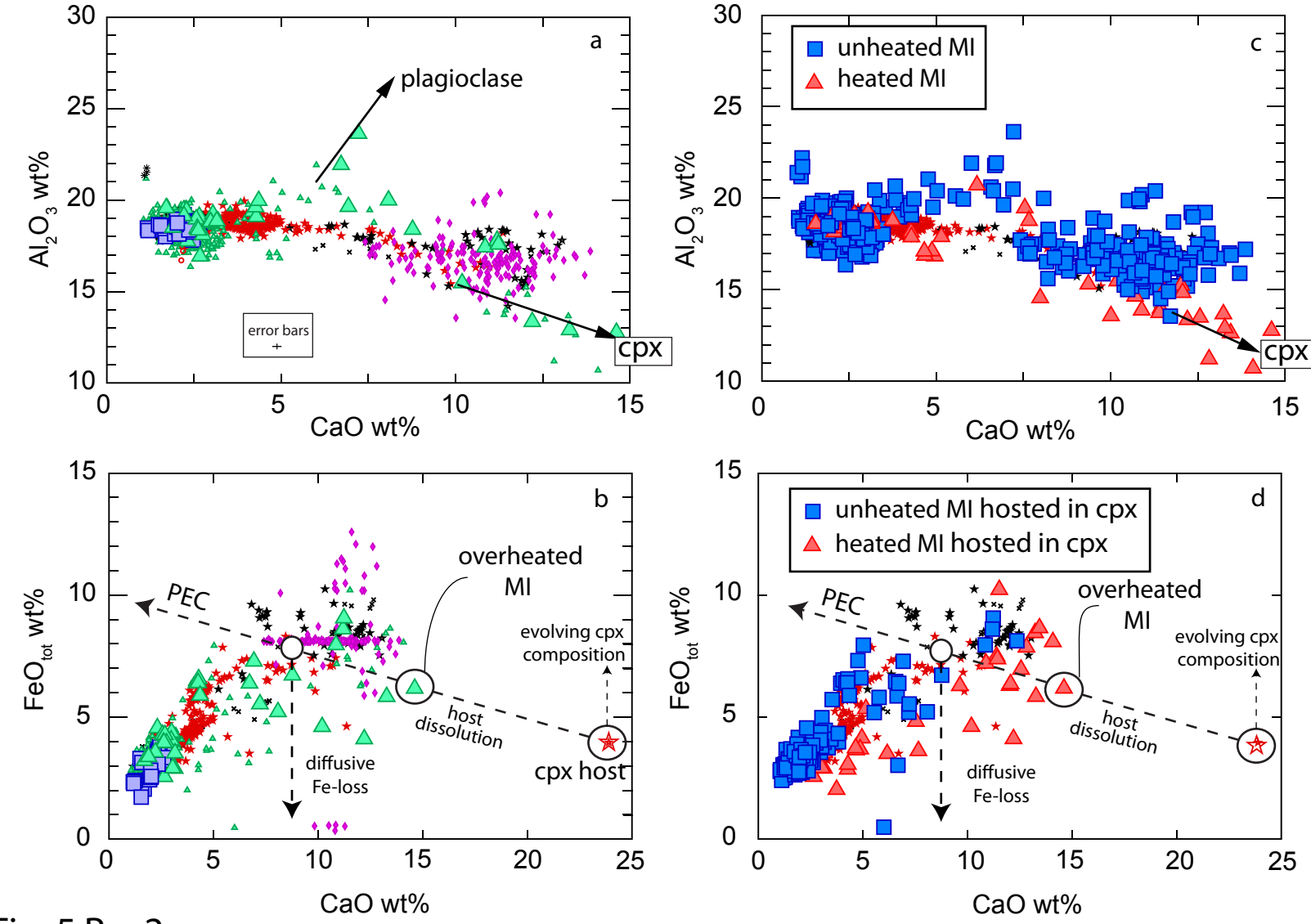


Fig. 5 Rev2

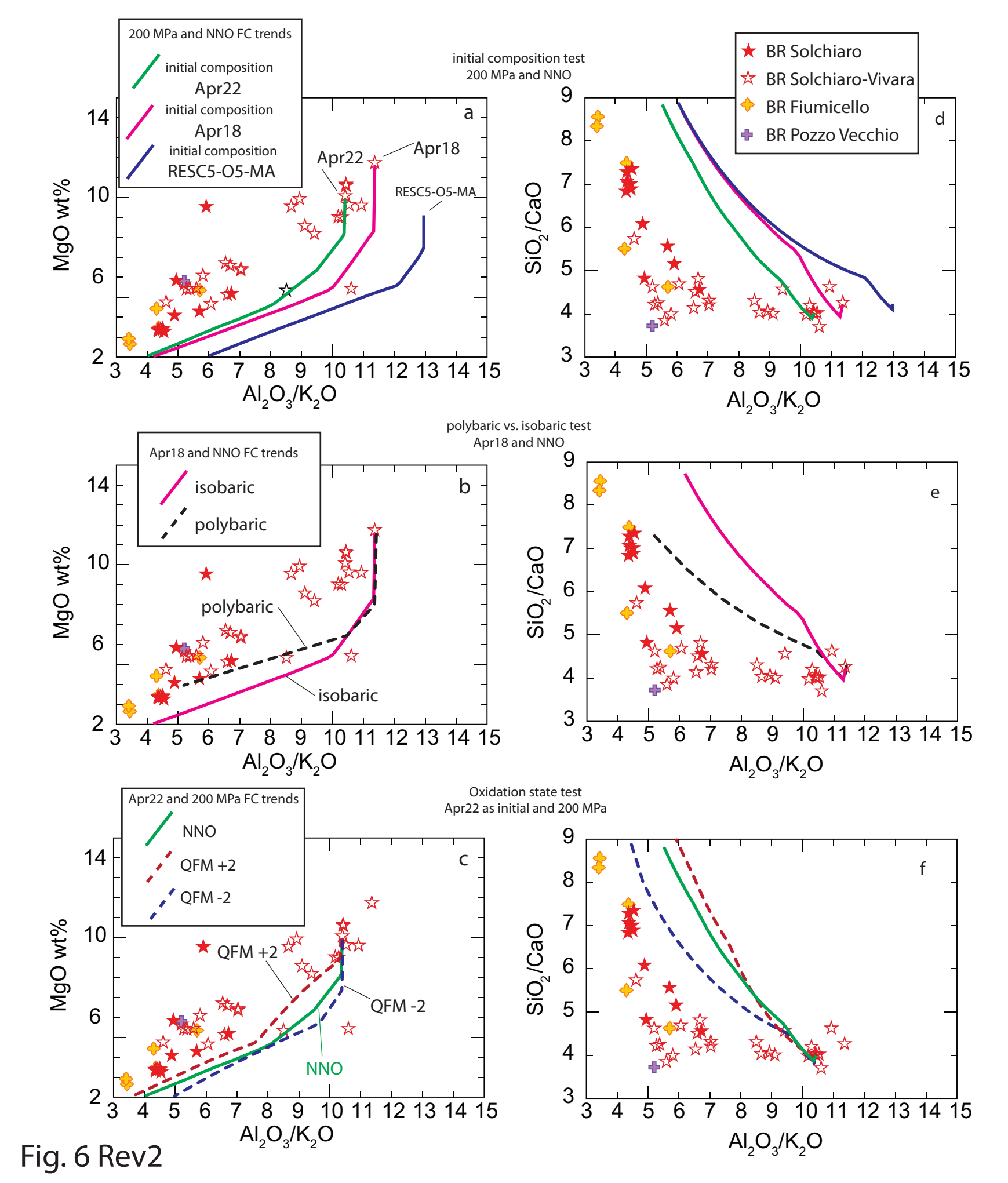


Fig. 7 Rev2

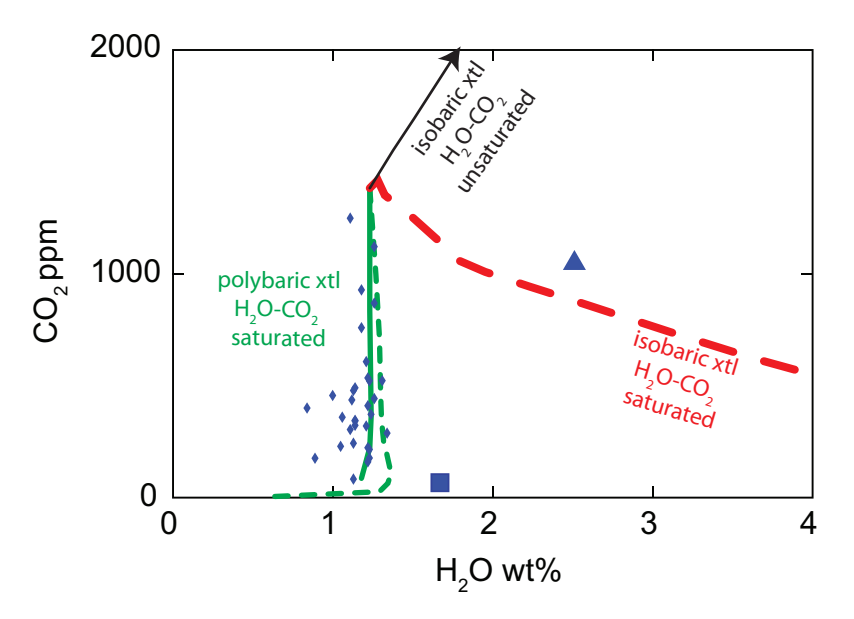


Fig. 8 Rev2

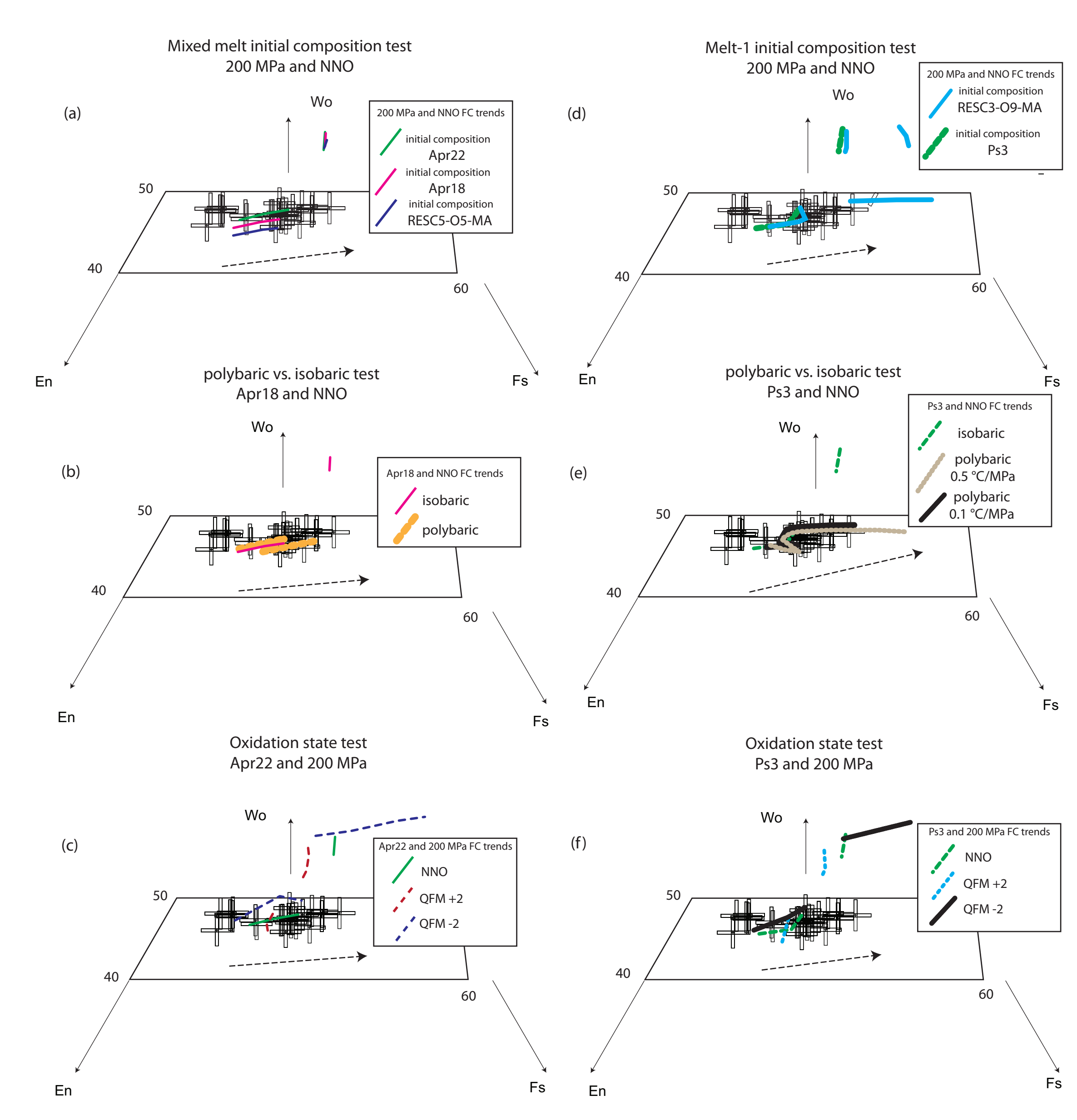
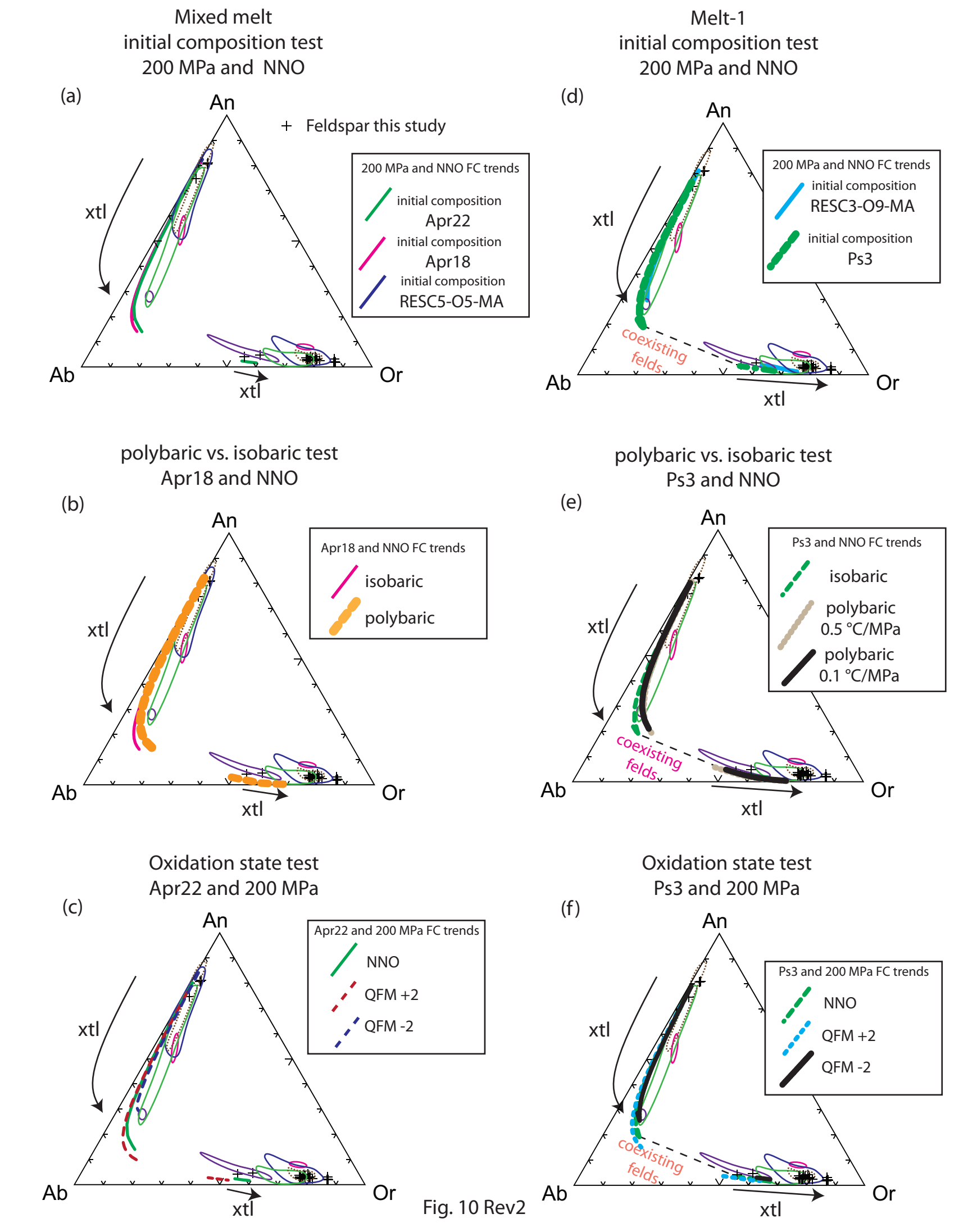


Fig. 9 Rev2



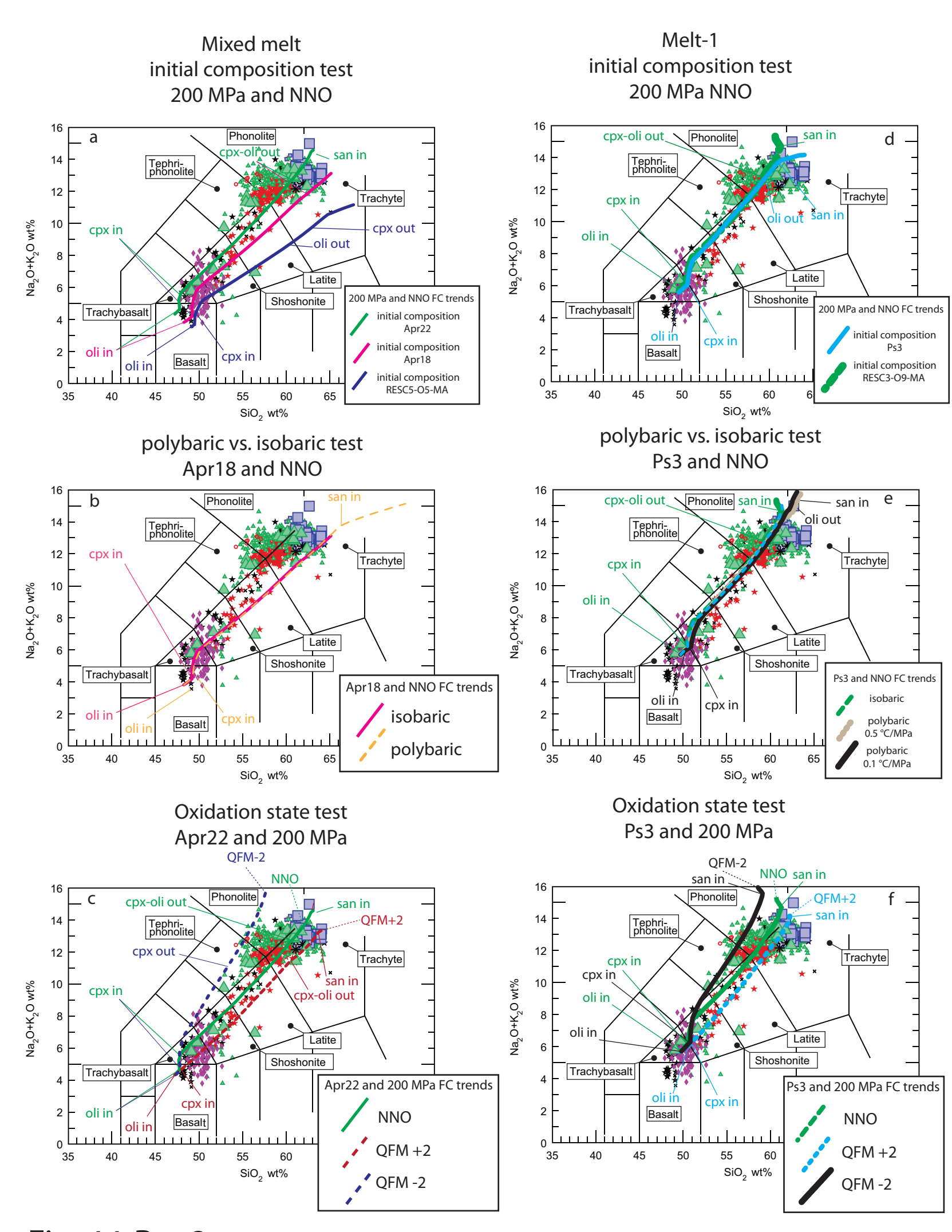


Fig. 11 Rev2

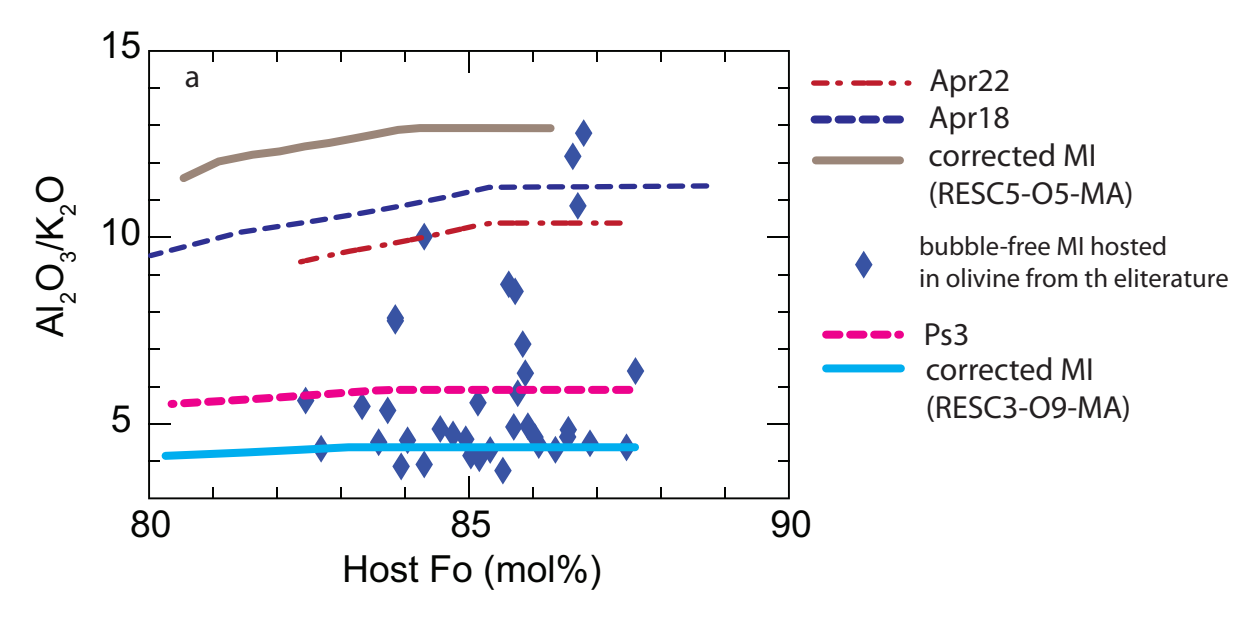
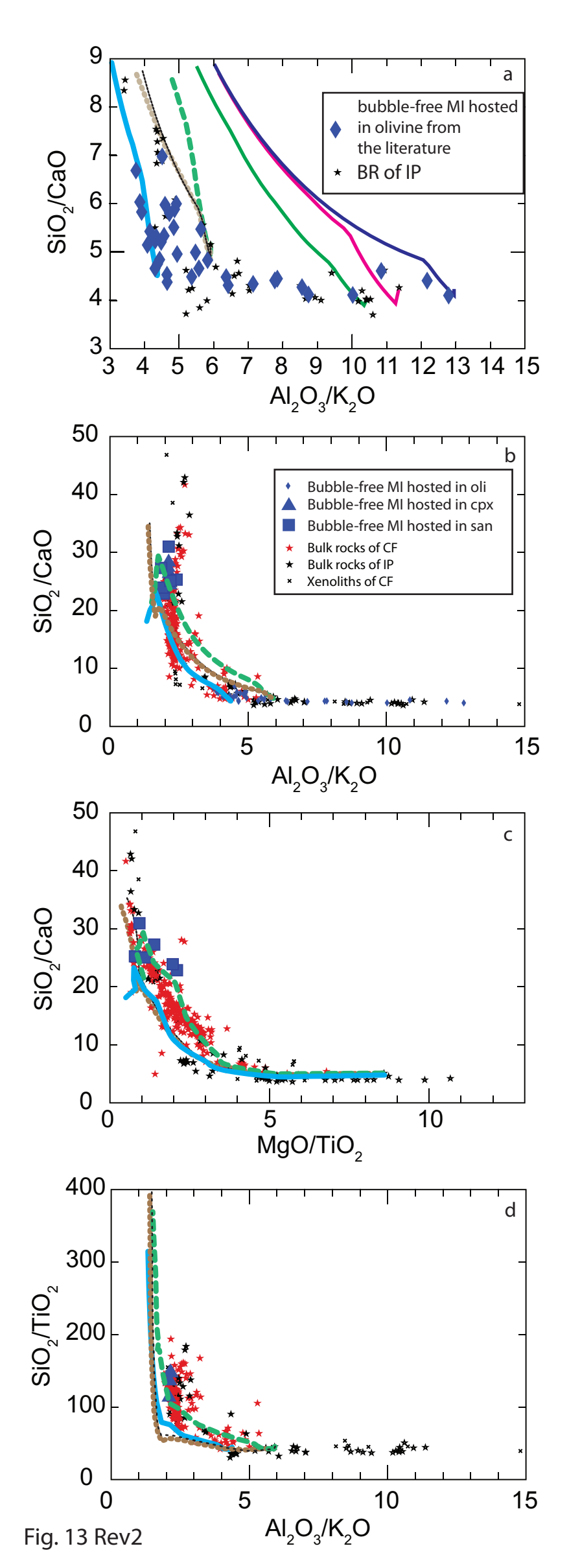


Fig. 12 Rev2



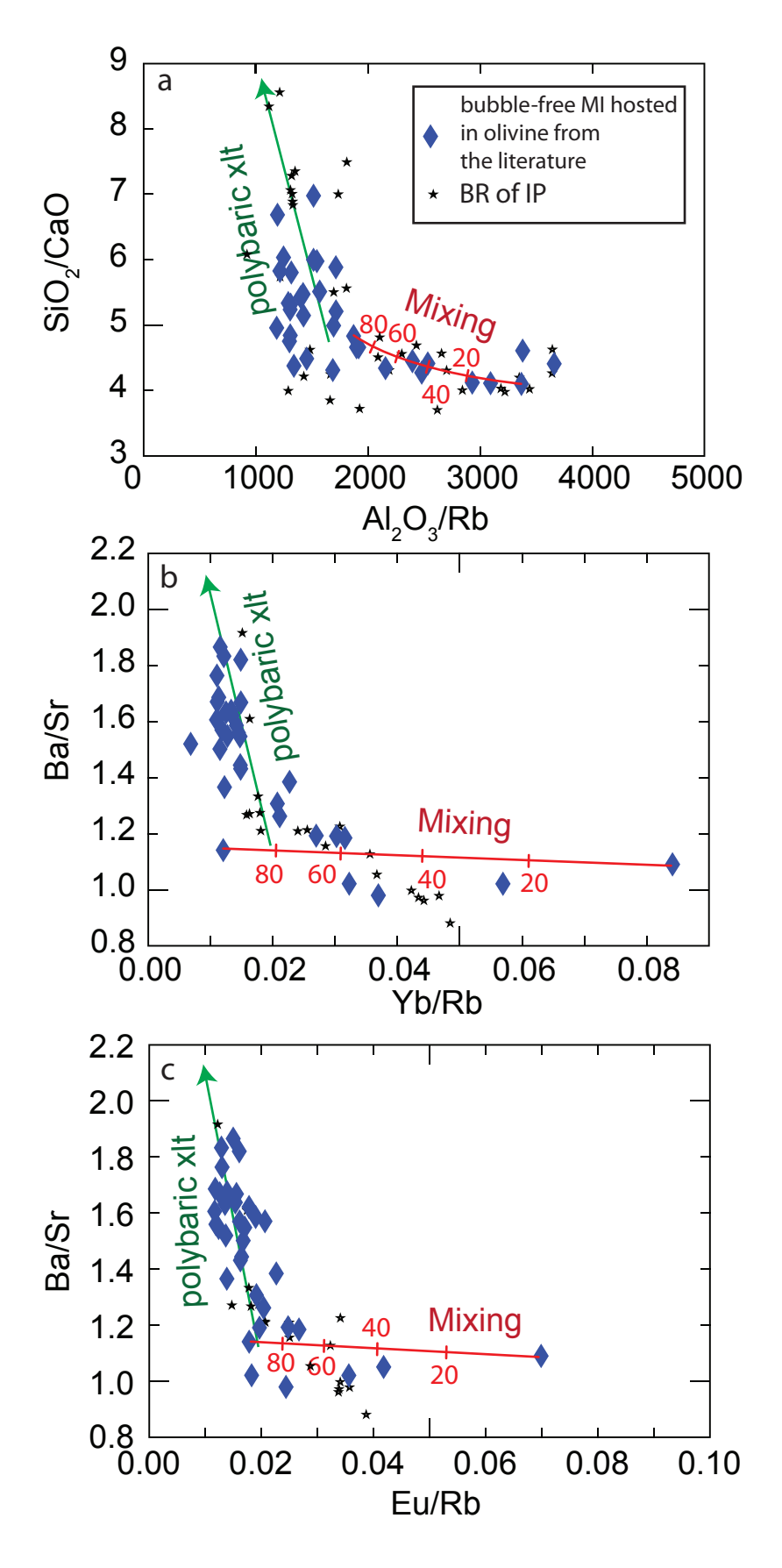


Fig. 14 Rev2

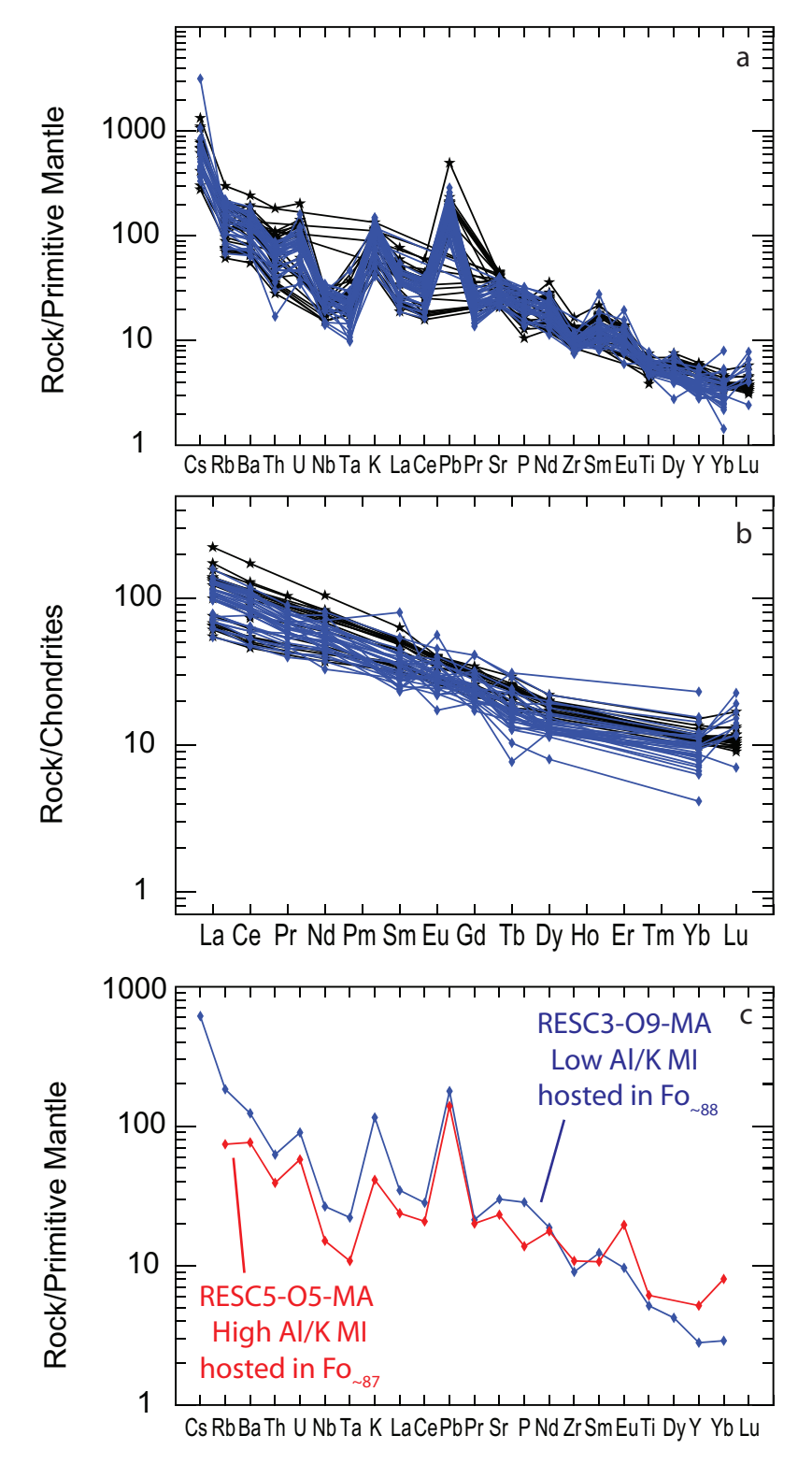
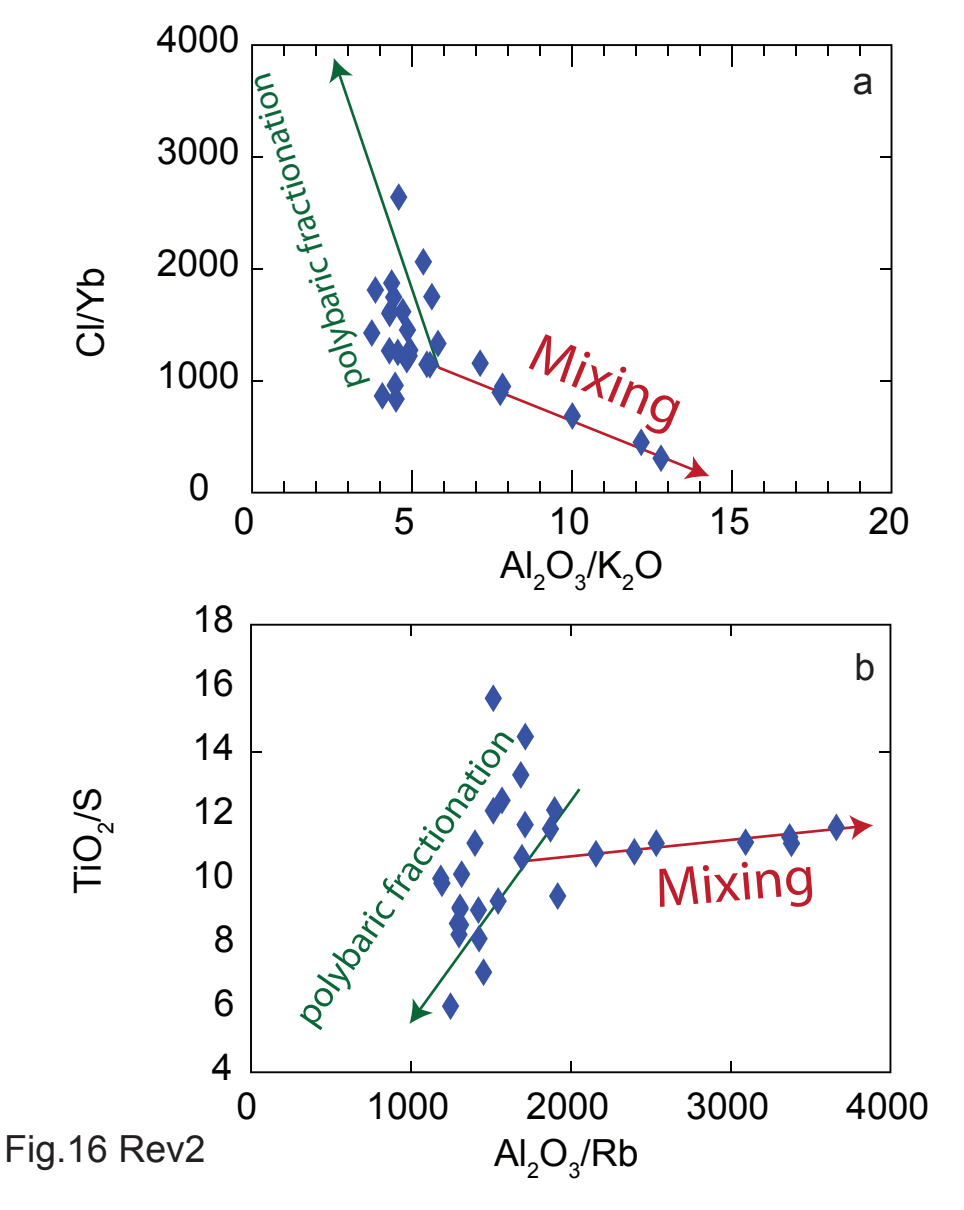


Fig. 15 Rev2



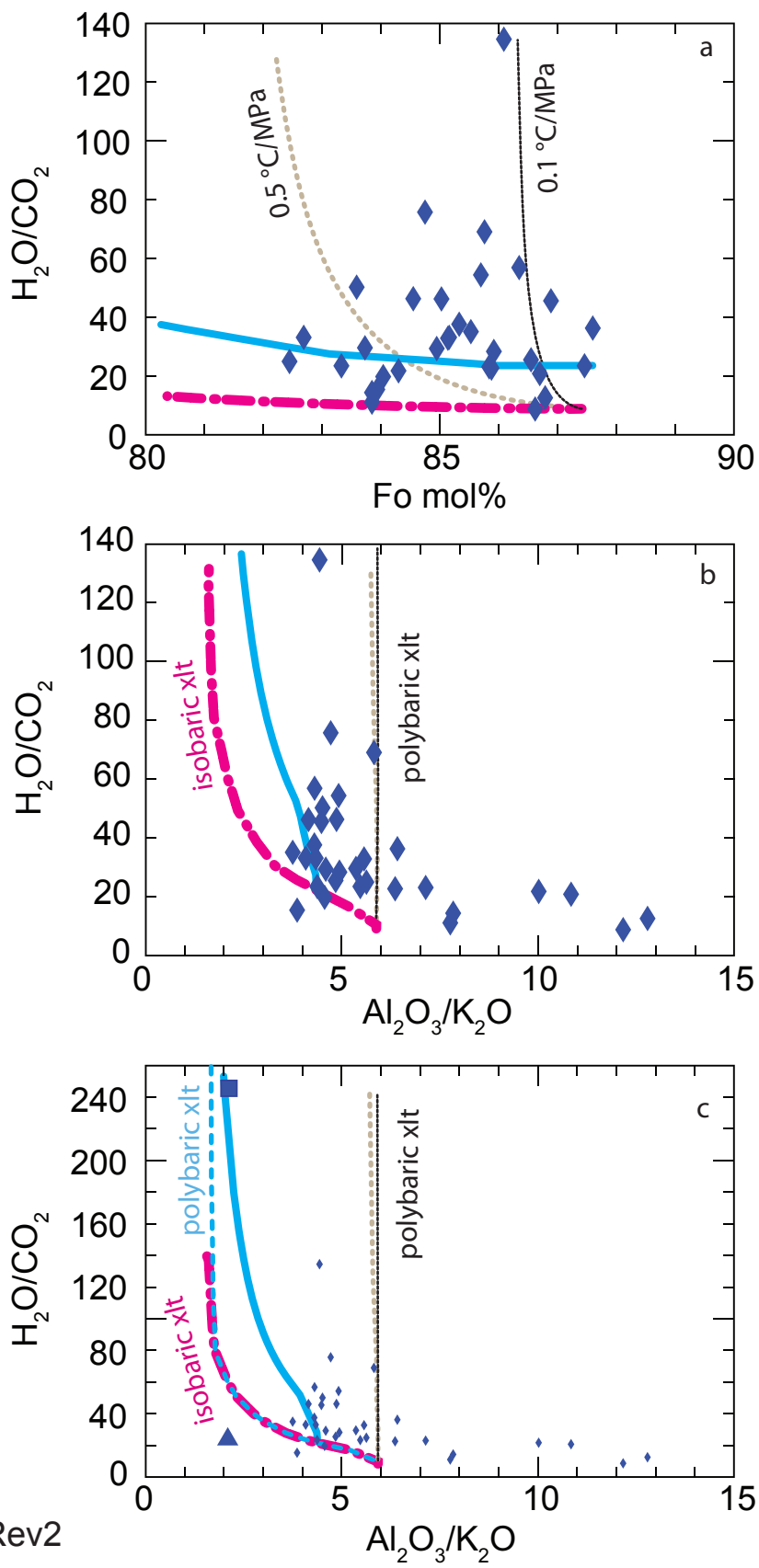


Fig.17 Rev2

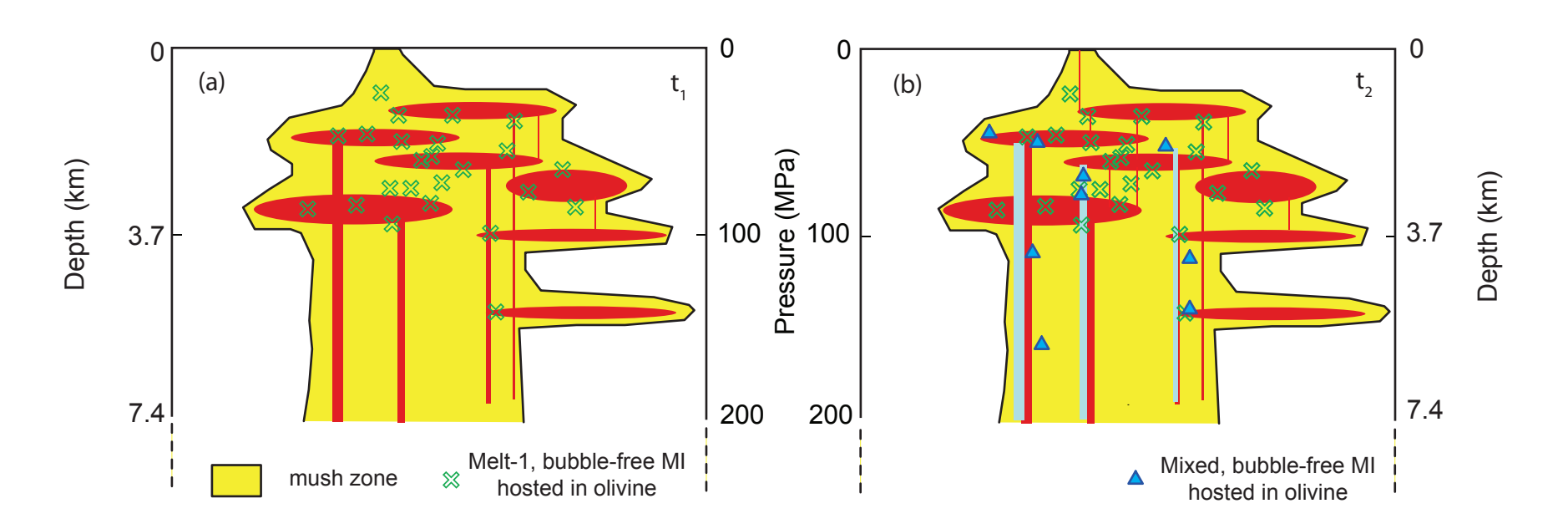


Fig. 18 Rev2

Figure captions for supplementary figures

Supplementary Figure 1. Bulk rock compositions from CF and IP.

(a) TAS diagram (LeBas et al., 1986) showing the CF and IP bulk rock (Na₂O+K₂O) versus SIO₂ relationships. (b) Concentration of MgO (wt%) versus strontium isotopic composition (⁸⁷Sr/⁸⁶Sr) of CF and IP bulk rocks. (c) The ratio of Al₂O₃/K₂O versus strontium isotopic composition (⁸⁷Sr/⁸⁶Sr) of CF and IP bulk rocks. Symbols are the same as defined in Figure 2 of the main text. Sources of bulk rock literature data are: (Albini et al., 1977; Beccaluva et al., 1991; Brocchini et al., 2001; Cannatelli et al., 2007; Capaldi et al., 1972; D'Antonio et al., 1999a; D'Antonio et al., 1999b; De Astis et al., 2004; de Vita et al., 1999; Di Girolamo et al., 1984; Di Vito et al., 2011; Ghiara et al., 1979; Mastrolorenzo and Pappalardo, 2006; Orsi et al., 1995; Orsi et al., 1992; Pappalardo et al., 2002; Piochi et al., 2005; Piochi et al., 2008; Scarpati et al., 1993; Tonarini et al., 2009; Tonarini et al., 2004; Turi et al., 1991; Villemant, 1988; Wohletz et al., 1995).

Supplementary Figure 2. Comparison MI and host mineral compositions. The plots show mineral compositions (Y-axis) versus the SiO₂ concentrations of MI (X-axis). (a) Concentration of SiO₂ in MI versus orthoclase contents of feldspar hosts. (b) Ratio of SiO₂/CaO of MI versus orthoclase contents of sanidine hosts. The negative correlation of these two variables is consistent with crystallization of late stages of crystallization (Melluso et al., 2012). (c) Concentration of SiO₂ in MI versus ferrosilite contents of clinopyroxene hosts. Note the positive correlation between the two variables is consistent with trapping of MI during fractional crystallization. Large symbols are MI and host data from this study and small symbols are MI and host data from the literature.

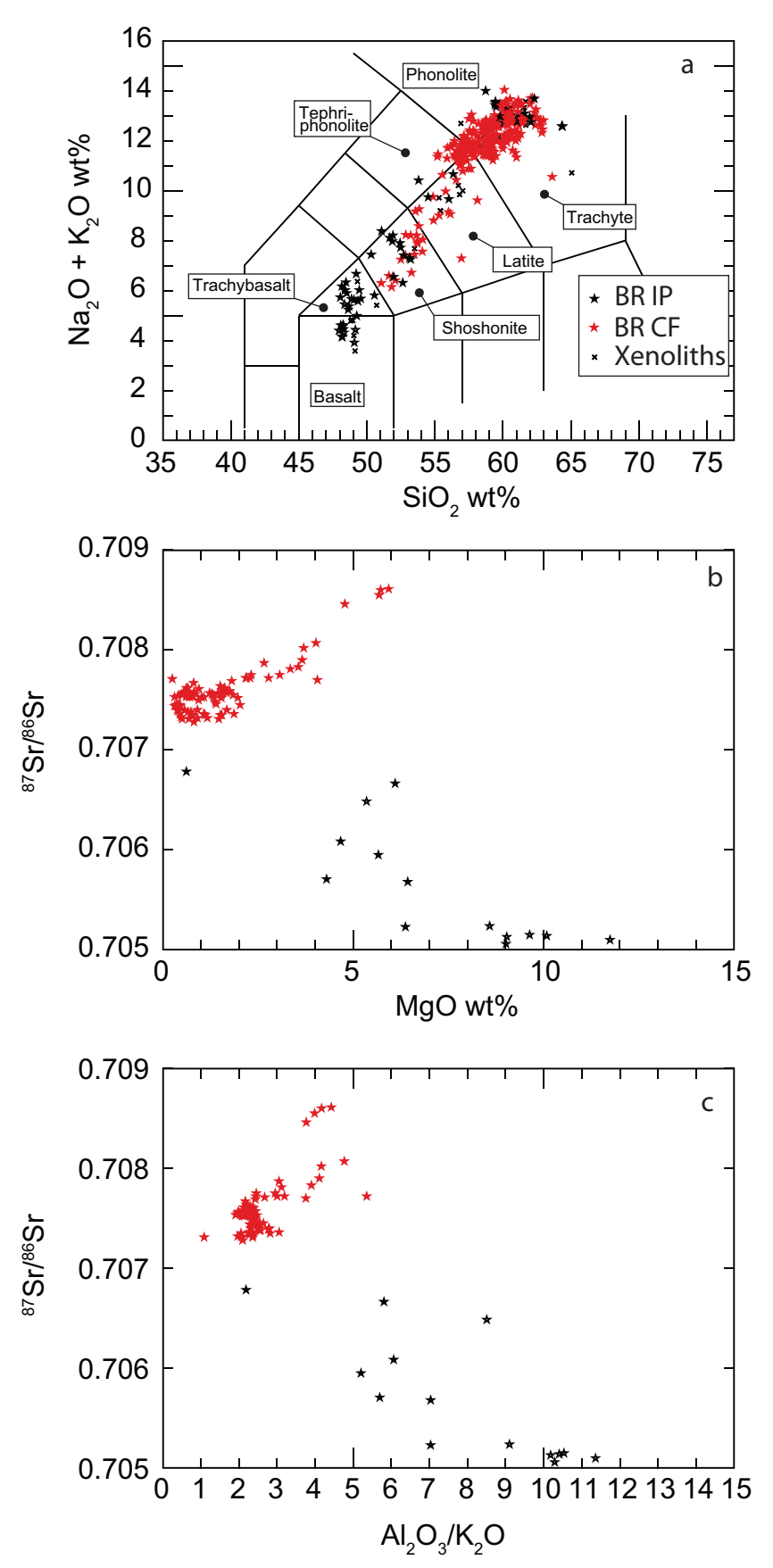
Supplementary Figure 3. Summary of various methods tested to correct compositions of anomalous MI.

(a) Concentrations of CaO vs. Al₂O₃ for anomalous MI (red circle symbols). Trajectories in CaO vs. Al₂O₃ space that result if compositions of anomalous MI hosted in clinopyroxene are corrected by incorporating (dissolving) host material into the MI to account for overheating of the MI are shown by red solid and dashed lines. Trajectories to correct the compositions for PEC are shown by blue solid and dashed lines. The correction was based on regression (black line) of bulk rock data (small symbols). (b) Concentrations of SiO₂ versus K₂O showing the trajectory in SiO₂ versus K₂O space of corrected MI. Note that the correction for host dissolution results in a significant offset of these MI away from the bulk rock trends. (c) Concentrations of SiO₂ versus FeO_{tot} resulting from dissolution and PEC corrections. Note that MI corrected for PEC still do not align to the bulk rock trend. (d) Concentrations of SiO₂ versus P₂O₅ resulting from dissolution and PEC corrections. Note that the correction predicts trends in the opposite direction from the bulk rock trend, especially for anomalous MI corrected for host dissolution (overheated MI).

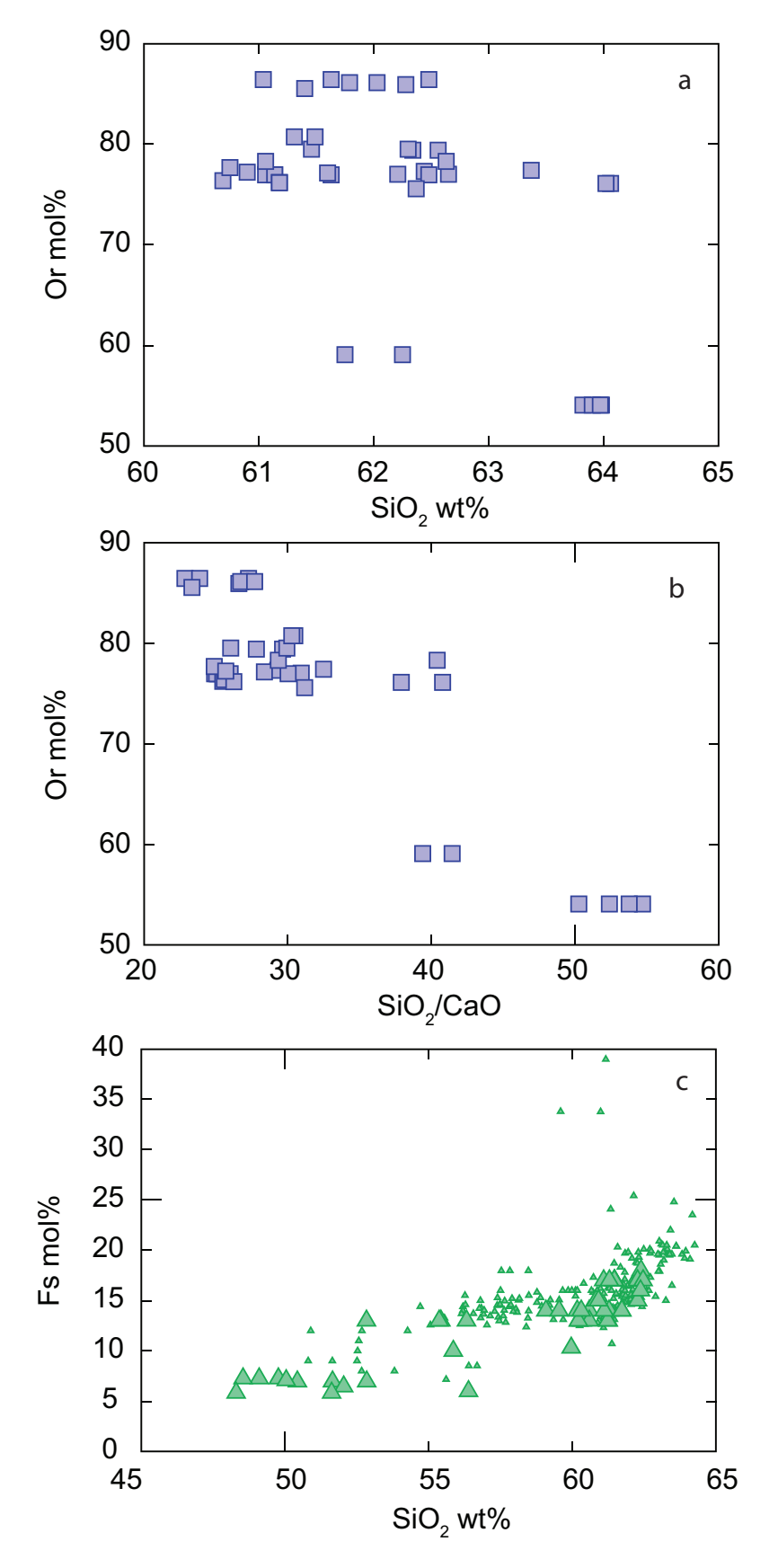
Supplementary Figure 4. Concentration of K₂O in MI versus size of MI hosted in sanidine.

Note that in general the most K₂O-rich MI are MI that were reheated in the lab, suggesting that the MI were heated to a temperature greater than the trapping

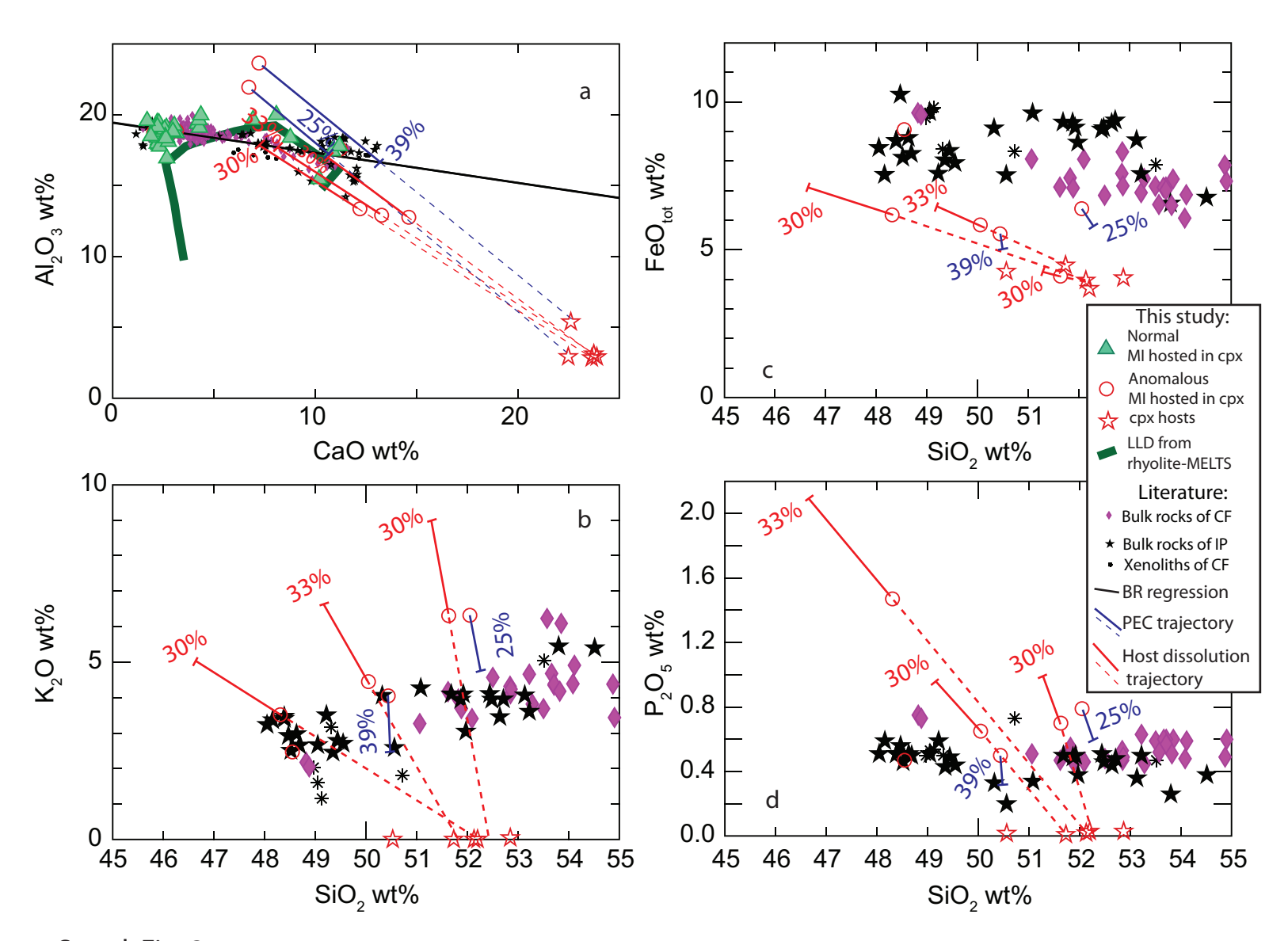
temperature. Also, no apparent correlation between these two variables is noted for the unheated MI, i.e., MI that contained only glass as found.



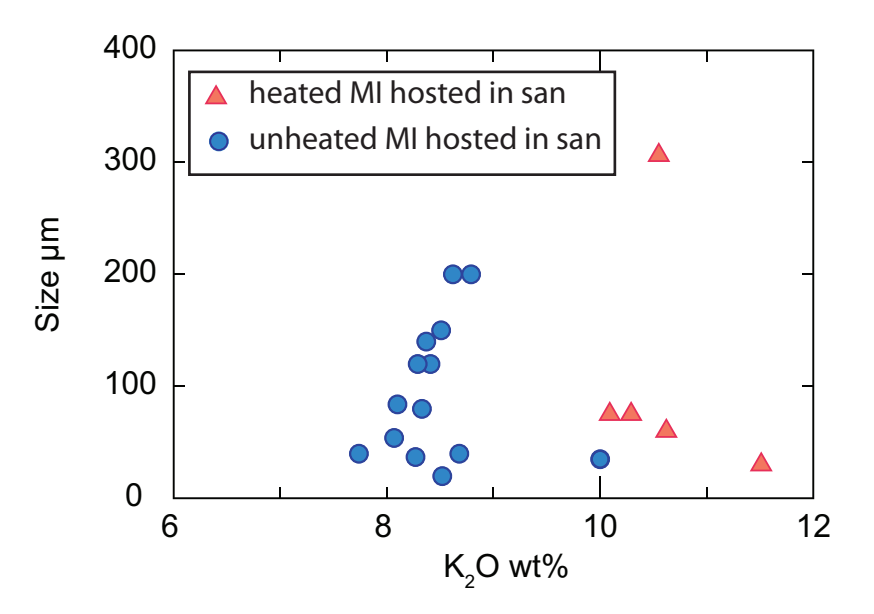
Suppl. Fig. 1



Suppl. Fig. 2



Suppl. Fig. 3



Suppl. Fig. 4